ARL-TR-77-27

Copy No. 47

(2)

SC

RESULTS OF A STUDY OF THE OCEAN BOTTOM INTERACTION OF UNDERWATER SOUND

Final Report under Contract N00039-76-C-0081

Kenneth E. Hawker et al.

DDC
RECEIVED
APR 6 1978
B

REPORT DOCUMENTATION PAGE		READ INSTRUCTIONS BEFORE COMPLETING FORM
1. REPORT NUMBER	2. GOVT ACCESSION NO.	3. RECIPIENT'S CATALOG NUMBER

4. TITLE *(and Subtitle)*	5. TYPE OF REPORT & PERIOD COVERED
RESULTS OF A STUDY OF THE OCEAN BOTTOM INTERACTION OF UNDERWATER SOUND.	final technical report, 1 Oct 75 - 31 Dec 76
	6. PERFORMING ORG. REPORT NUMBER
	ARL-TR-77-27

7. AUTHOR(s)	8. CONTRACT OR GRANT NUMBER(s)
Kenneth E. Hawker Steven R. Rutherford Karl Focke Winifred Williams Terry Foreman	N00039-76-C-0081

9. PERFORMING ORGANIZATION NAME AND ADDRESS	10. PROGRAM ELEMENT, PROJECT, TASK AREA & WORK UNIT NUMBERS
Applied Research Laboratories The University of Texas at Austin Austin, Texas 78712	

11. CONTROLLING OFFICE NAME AND ADDRESS	12. REPORT DATE
Naval Electronic Systems Command Department of the Navy Washington, D. C. 20360	25 Oct 77
	13. NUMBER OF PAGES
	178

14. MONITORING AGENCY NAME & ADDRESS*(if different from Controlling Office)*	15. SECURITY CLASS. *(of this report)*
	UNCLASSIFIED
	15a. DECLASSIFICATION/DOWNGRADING SCHEDULE N/A

16. DISTRIBUTION STATEMENT *(of this Report)*

Approved for public release; distribution unlimited.

17. DISTRIBUTION STATEMENT *(of the abstract entered in Block 20, if different from Report)*

18. SUPPLEMENTARY NOTES

19. KEY WORDS *(Continue on reverse side if necessary and identify by block number)*

bottom interaction	subbottom density gradients
reflection coefficients	bottom loss
Stoneley waves	sensitivity studies

20. ABSTRACT *(Continue on reverse side if necessary and identify by block number)*

This report describes the research results of the second year of an ongoing program to investigate the broad spectrum of problems associated with the interaction of underwater sound with the ocean bottom. The emphasis is on quantifying the nature of the acoustic bottom interaction problem, isolating key parameters, and developing useful minimal descriptions. This report considers in detail questions in the areas of the sensitivity of bottom reflection loss to variations in subbottom parameters, the sensitivity of propagation loss to changes in bottom reflection loss, and problems

DD FORM 1473 EDITION OF 1 NOV 65 IS OBSOLETE

20. cont'd.

(U) associated with range changing bathymetry. Additional topics considered include a review of acoustic methods for obtaining bottom sediment sound velocities, as well as various modeling problems.

ACCESSION for		
NTIS	White Section	✓
DDC	Buff Section	☐
UNANNOUNCED		☐
JUSTIFICATION		
BY		
DISTRIBUTION/AVAILABILITY CODES		
Dist.	AVAIL. and/or SPECIAL	
A		

TABLE OF CONTENTS

LIST OF FIGURES

LIST OF TABLES

I. INTRODUCTION AND SUMMARY

This report describes the results obtained during the second year of
a three year study of the ocean bottom interaction of underwater sound.
The work reported here is, for the most part, still in progress; thus,
this report portrays an ongoing investigation, not the results of a com-
pleted study.

For this reason, among others, this report is focused on the scientific
problem of acoustic bottom interaction itself and not on the intended
applications. Beginning in the third year of this study these results,
as well as the results obtained earlier, will be brought to bear on
questions oriented to specific applications.

The results appearing herein include material which has not yet
been reported elsewhere, as well as brief summaries of work which have
already appeared in specialized technical reports, papers, and oral
presentations. This appearance of original material, as well as the
necessity for documenting certain aspects of this research program,
accounts for the rather high level of detail and completeness of this
report.

A. Background: The Acoustic Bottom Interaction Problem

Until comparatively recently, interest in the interaction of underwater
sound with the ocean bottom was confined to shallow water, high frequency
bottom reflection loss studies by acousticians and short range deep
acoustic probing of the ocean floor by seismologists. As the attention
of acousticians has been drawn toward low frequency (below 1 kHz) long
range propagation problems, the necessity has grown to better understand
and describe the details of sound propagation in and near the ocean floor,
especially the deep ocean basins and their defining slopes and ridges. At
the same time, the surge of interest and effort in the area of plate
tectonics has begun to make available increasingly detailed information

-1-

concerning the subbottom structure of these areas.

The acoustic bottom interaction problem can be broadly defined as quantifying the importance of the ocean bottom substructure in determining the characteristics of propagated sound fields, regions in the water column of comparative insensitivity to bottom interaction, the exploitability of bottom traveling energy, etc. The range of such problems, considering the variability of ocean bottom substructure, acoustic frequencies, source-receiver geometries, etc., is considerable and it is clear that one immediate problem is to define a series of specific questions which can be usefully addressed.

The simplest subset of problems which still has a significant bearing on the overall problem and importance to the applications is obtained by assuming a horizontally stratified subbottom structure and using the associated plane wave reflection coefficient (bottom loss) as an investigative tool. Such bottom loss studies constitute an integral part of this research program. Questions concerning the depth to which any subbottom information is required (hidden depth problem), the importance of shear waves as a loss mechanism, the accuracy with which various parameters must be specified, etc., may be investigated without the additional complications of specifying source-receiver geometry, (water) sound speed profile, and bathymetry.

There are, of course, many important questions which do involve these variables in an integral way, such as those involving isolating regions in the water column of relative insensitivity to bottom interaction, the interplay between the refractive effects of the water sound speed structure and bottom interaction, the source-receiver range dependence of the partitioning of propagated energy between bottom interacting and purely waterborne paths, etc. These questions, as well as others, can be usefully addressed, in an approximate fashion, by assuming, again, horizontal stratification and ignoring, for the moment, the effects of range variable bathymetry and sound speed structure. A variety of problems of this type, some of which are discussed in this report, are under

investigation as part of this research program.

A third level of detail involves problems associated with range changing bathymetry, propagation over continental slopes, sea mounts, ridges, etc., as well as the associated problems of interface roughness. These problems are among the most difficult in this entire area and must themselves be addressed piecemeal. It is useful, for example, to ignore subbottom structure and employ a phenomenological bottom reflection loss within a ray trace model. This can then be used to investigate questions concerning the importance of bottom reflectivity in multipath conversion process associated with propagation over continental slopes (e.g., slope enhancement).

Another class of problems in this area concerns the sensitivity of propagation characteristics to bottom roughness, either water-sediment interface roughness or, perhaps more importantly, subbottom (basement) roughness. One possibility for investigating such questions could be to employ the results of rough surface scattering research to estimate the scattering loss. Such an approach, if applicable, would in fact be an extension of the bottom loss studies discussed earlier. A second approach would be to include the roughness directly in the propagation problem, such as by the addition of an appropriate bottom impedance modification. Both of these approaches, as well as others, have been considered and are being pursued.

The preceding breakdown of the bottom interaction problem has involved a consideration of single sources and point receivers. Some of the methods used in these studies can be extended to include consideration of multiple sources and receivers. The objectives of such an extension are twofold, to investigate the bottom interaction effects on more complex acoustic fields, such as ambient noise (or a combination of signal and noise fields), as well as to consider questions of spatial coherence and how it is affected by bottom substructure, bathymetry changes, etc. Both of these topics constitute important areas of concern and, although

not considered in this report, constitute active aspects of ongoing and future research.

B.   Structure of the ARL:UT Bottom Interaction Research Program

The breakdown of the general bottom interaction problem into more specific components, each designed for the investigation of certain physical mechanisms, was in fact the most important outgrowth of the first year of this research program. Much of the first year's effort (already reported) went into the planning and outlining of a series of problems which could be addressed in a practical way and the sum total of which would constitute the solution of an important and applicable segment of the bottom interaction problem.

During the first year's effort the major lines of investigation were begun and preliminary results were obtained, primarily via model studies using existing models obtained from other laboratories. During the course of those investigations it became clear that more specialized calculational techniques, appropriate to the then defined range of problems, would be required. Development of these methods, chiefly ray trace methods, a normal mode model, and a bottom reflection loss model, was begun.

During the subsequent year, the period reported here, this developmental effort was completed and extensive application of these tools was under-taken. Continued use was made of existing models, although in some cases considerable modification was required.

During the first two years of this program, the second of which is reported here, the emphasis has been primarily on the scientific bottom interaction problem itself, with only general guidance providing the link to applications. During the third year a major component of the study will be to assemble the individual components to form an integrated series of recommendations and results oriented toward specific applications. With this plan in mind, little attention is paid in this report to these matters.

-4-

Accompanying the theoretical parameter studies using models has been an effort to employ the results of data analysis and interpretation to these problems. This effort began during the first year of this program and has continued throughout. Applied Research Laboratories, The University of Texas at Austin (ARL:UT) acoustic data archives were initially composed only of data acquired from LRAPP sponsored exercises, and more recently expanded to include data from exercises sponsored by Naval Electronic Systems Command (NAVELEX), Code PME-124, as well as newly acquired LRAPP data. These data, together with a modeling capability specifically suited to the investigation of bottom interaction problems, constitute the primary investigative resources of this program.

The processing, analysis, and intrepretation of both existing data and newly acquired data form an integral element of various ARL:UT ongoing research programs, the spinoff from which has served as an important source of guidance and direction for the bottom interaction program, sponsored by NAVELEX, Code 320. These additional programs include ambient noise (NAVELEX, Code 320, and NORDA/LRAPP, Code 600), sensor performance, RDSS (NAVELEX, Code PME-124), multipath analysis and bottom limited propagation (NAVELEX, Code PME-124 and NORDA/LRAPP, Code 600), and in situ sediments properties (NORDA, Code 480).

C.   Contents of the Report

The technical portion of this report is divided into five additional chapters, the first three of which, Chapters II through IV, are concerned with the major research areas of this program.

Chapter II considers a variety of bottom interaction questions addressable by using the bottom reflection loss as a measure of the importance of variations in subbottom description. The first section of this chapter considers the importance of the presence of a (basalt) substrate, or basement, to the bottom reflection loss. In particular, the existence of a solid substrate under the fluid sediment layers introduces the possibility of a boundary, or interface wave, called a Stoneley wave which

can act as an additional loss mechanism. The second and third sections
of Chapter II consider the importance of depth variations (gradients) of
attenuation and density within sediments. The final section considers
the topics of hidden depths and the variation of bottom reflection loss
with changes in sediment type. The general thrust of all of the work
reported in this chapter is to determine the importance of various sub-
bottom parameters and to work toward a useful description of the sub-
bottom which requires minimal information.

Chapter III considers the sensitivity of propagation loss to variations
in bottom reflection loss using a single parameter phenomenological bottom
loss. Several existing propagation loss models have been used in this
study. Major questions which are addressed by this study include the
delineation of regions of sensitivity and insensitivity to bottom reflec-
tion loss, as well as the way this separation is affected by source depth
and profile type.

Chapter IV considers two aspects of the range variable bathymetry
problem, slope enhancement during propagation over a continental slope
and the rough interface problem. The first of these is addressed by
considering the results of the analysis of acoustic data taken from a
recent exercise as well as the results of model studies. The range of
bottom irregularities which fall into the category of bottom roughness is
considered as well as various approaches to accounting for the associated
acoustical effects.

Chapter V considers various techniques for extracting information
about subbottom sediment structure, particularly velocity gradients, from
profiling data. This chapter constitutes a particularly concise and use-
ful review of work which has been reported and is not well known in the
acoustics community.

Chapter VI serves to document the work carried out during this
reporting period on the development of normal mode, bottom loss, and ray

trace models which have been designed with a view toward the solution of bottom interaction problems.

In Chapters II through VI, figures, tables, equations, and references are numbered sequentially within each chapter. References are listed at the end of each chapter.

D. Summary of the Principal Results

This section contains a brief listing of the major results obtained during the course of this year's research. For convenience, these results are itemized according to the chapters of this report in which the associated research is described.

There are two points concerning these results which are important to appreciate: (1) all conclusions were obtained and are applicable only over some range of conditions and under circumstances which cannot be detailed in this section, and (2) they represent only the results of the research discussed in this report and are not conclusions of this total (ongoing) research program. The second of these restrictions is one that will be removed in time, whereas the first simply reflects the fact that results taken out of context can be misleading.

1. Bottom Loss Studies

The presence of a basalt basement under relatively thin clay sediments containing an appreciable sound speed gradient can lead to unexpectedly large increases in bottom loss over a narrow angular range. This loss is due to the presence of Stoneley waves.

The Stoneley wave loss peak occurs at the low grazing angles which are crucial in determining long range propagation.

Attenuation gradients within the subbottom can be important in

determining bottom loss. Ignoring attenuation gradients can lead to errors of several decibels in computed bottom loss.

Density gradients within the subbottom have only small effects over the low grazing angle regime of concern to long range propagation.

The effects of density gradients can be almost wholly accounted for by simply using the local density values at each interface and ignoring the continuous changes.

The sound speed gradient within the subbottom is the controlling parameter in determining the hidden depth.

The hidden depth is found to be several sound wavelengths below the ray turning depth. This result is, for practical purposes, independent of the precise definition of hidden depth so long as it is defined in terms of a fractional change in bottom loss.

The sensitivity of bottom loss to changes in sediment type is best studied via the parameterization of density, sound speed, and attenuation by porosity.

This parameterization, the results of which have been used in this study, has been carried out in the literature. It will be important to extend the existing parameterization, developed only for surficial sediments, to depth in the sediment.

2.   Propagation Loss Sensitivity Studies

Bottom interaction effects on propagation loss divide the water column into three regions based on source and source conjugate depths. Propagation loss has a regular dependence on critical angle in the central region.

Outside this region of regularity (near the boundaries), bottom

influence is strongly dependent on receiver depth and is more sensitive to bottom loss the nearer the receiver is to the surface.

3. Effects of a Range Variable Environment

For a shallow source, both data and theoretical calculations show that slope enhancement is sensitive to receiver depth, at least for North Atlantic, double minimum type profiles.

When slope enhancement is potentially present geometrically, it will be quite sensitive to the bottom loss near the upper lip of the continental slope.

The absence of enhancement for a deep receiver and a shallow source located over the continental shelf is associated with multipath conversion process which severely constrains the coupling between source and receiver for this geometry.

The definition of the scope of the rough surface problem, considering the length and height scales for which roughness will be important, as well as probable methods for obtaining information about ocean bottom roughness, is quite sensitive to frequency and will disappear entirely in the very low frequency (VLF) region submerging itself in the (deterministic) sloping bottom problem.

The most promising method for accounting for roughness effects on propagation is the smoothed boundary condition approach.

Rough surface scattering theory will be useful primarily for obtaining estimates for the amount of scattering loss the coherent field will suffer per bounce, but not for actually carrying out quantitative propagation calculations.

II.   BOTTOM LOSS STUDIES

This chapter consists of four independent sections devoted to different
aspects of the problem of the sensitivity of bottom loss to variations
of subbottom composition. This approach is part of a consistent pattern
of attacking the bottom interaction problem both from a propagation view-
point with certain classes of sound speed profile, sensor geometries, etc.,
and from a more local viewpoint using bottom reflection loss as a measure
of the effects of subbottom variations.

The first section deals with the effects of a solid substrate (basalt
basement) on bottom loss. This work, the beginnings of which were noted
in the final report from the first year's work in this program (Hawker et
al.[1]), deals with a loss mechanism which can significantly affect low angle
bottom loss.

The second and third sections of this chapter concern, respectively,
the sensitivity of bottom loss to the variation of attenuation and density
with depth in the sediment. These studies are directed toward establish-
ing the minimum amount of information concerning subbottom makeup which is
required for accurate prediction of either propagation loss or bottom loss.

The fourth section of this chapter concerns the problems of hidden
depths (the depth of significant acoustic penetration) and sensitivity to
variations in sediment type. The work in this section has already been
reported under this contract (Hawker, Focke, and Anderson[2]); thus, only
a brief synopsis of it is given here.

A.   The Influence of Stoneley Waves on Bottom Reflection Loss

This section considers the effects of a particular type of interface,
or surface, wave known as a Stoneley wave on bottom reflection loss. These
waves can exist at a solid-solid boundary as well as at a fluid-solid
boundary. The particular interface of concern here is the one that divides

sediments (fluids) from the basement or substrate (solid), usually taken to be basalt.

Typical values for the compressional and shear wave speeds in basalt are 5700 m/sec and 2700 m/sec, respectively. Such values will result in compressional and shear critical angles of approximately 74° and 55°, respectively. Given the constraints on grazing angles imposed by the range of propagation geometries of interest, it is clear that even the shear wave critical angle will not constitute an important effect to long range propagation.

At first sight, then, it would appear that the relevant effects of the basement would be limited to a slight increase in bottom loss (relative to a perfect reflector) due to absorption (nonperfect reflection below the shear wave critical angle). This is, in fact, the situation for the case of a solid such as basalt directly underlying the water column. However, when a sediment layer, either a high porosity material such as clay or silt, intervenes with a positive velocity gradient or a low porosity material such as sand, it becomes possible to excite Stoneley waves at the sediment-basalt interface. These waves (when absorption is present) add a new loss mechanism which can result in large increases in bottom loss even at very low angles.

The effects of a solid substrate (basalt) on bottom reflection loss and the examination of the various wave mechanisms will be presented in the next two sections.

All bottom loss calculations displayed in this chapter were made using the ARL:UT developed bottom loss model BOTLOSS, described in detail by Hawker and Foreman.[3]

1.   The Effects of a Solid Substrate on Bottom Reflection Loss

Figure II-1 shows schematically the bottom model to be considered.
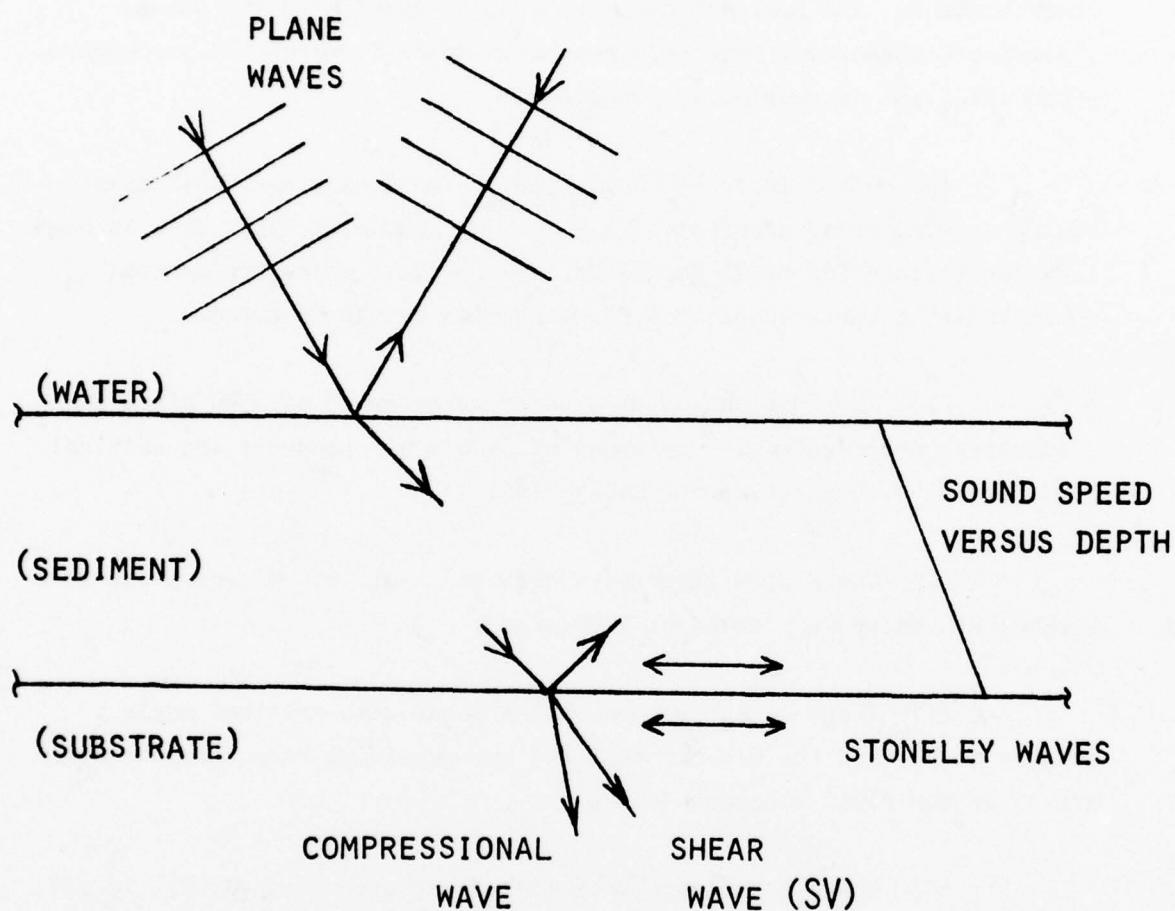
FIGURE II-1
SCHEMATIC ILLUSTRATION OF THE WAVE STRUCTURE FOR A
SINGLE FLUID SEDIMENT LAYER OVERLYING A SOLID SUBSTRATE

AS-77-308

The water is a isovelocity fluid supporting incoming and outgoing plane waves, the amplitudes of which are related by the complex reflection coefficient R. The sediment can have a sound speed gradient but is otherwise homogeneous. The substrate half-space is permitted to support shear waves and is completely homogeneous.

The bottom loss, $-10 \log_{10} (RR^*)$, for a clay sediment layer having a sound speed gradient of $1.2 \ \text{sec}^{-1}$ is shown in Figs. II-2 through II-4 for frequencies of 25 Hz, 50 Hz, and 100 Hz. There are several characteristic features of these curves which should be noted.

(1) The combination of a water sound speed of 1540 m/sec and a substrate compressional wave speed of 5700 m/sec produces the critical angle effect evident at approximately 74°.

(2) There is a shear wave critical angle at 55° resulting from a substrate shear wave speed of 2700 m/sec.

(3) There is an absence of the shear wave critical angle feature at 55° and the retention of the compressional wave critical angle effect in the fluid substrate cases.

(4) There is a large peak in loss at approximately 17° in all three cases.

(5) The absence of the low angle peak in the fluid substrate cases.

(6) The angular location of the low angle peak is nearly frequency independent.

Of these six items, (1) through (3) are well understood and present no difficulties of interpretation. The very existence of a large bottom loss peak at low angles, (4), well removed from the shear

-14-

ID: 1550, 1551

MATERIAL: CLAY
SOUND SPEED GRADIENT: 1.2 sec^{-1}
FLUID SUBSTRATE ------
SOLID SUBSTRATE ———
FREQUENCY: 25 Hz

GRAZING ANGLE – deg
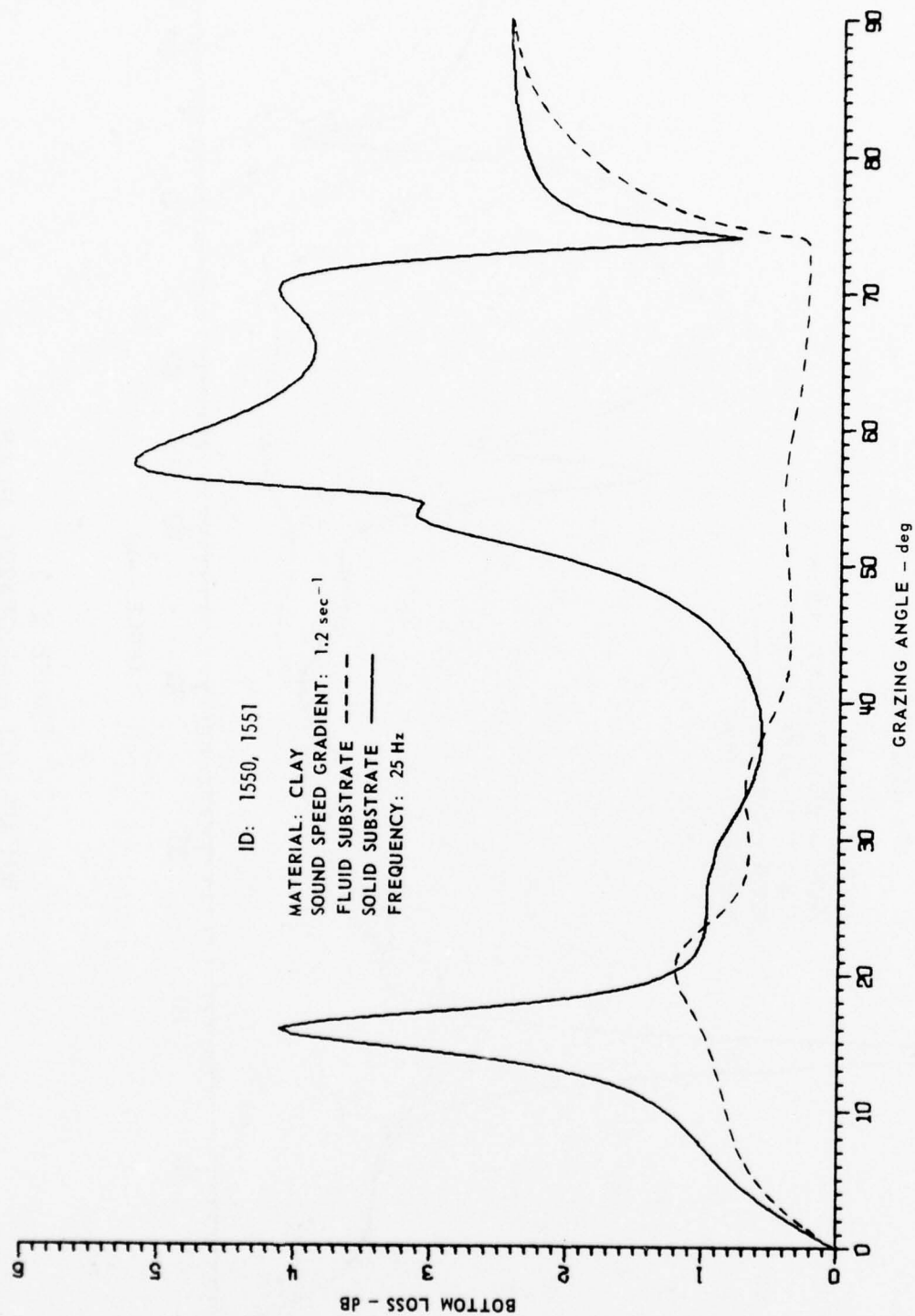
BOTTOM LOSS – dB

FIGURE II-2

BOTTOM LOSS versus GRAZING ANGLE
FOR A 100 m CLAY LAYER AT 25 Hz

ARL - UT
AS-76-205
KEH - DR
2 - 27 - 76

15

ID: 1552, 1553

MATERIAL: CLAY
SOUND SPEED GRADIENT: 1.2 sec^{-1}
FLUID SUBSTRATE - - - -
SOLID SUBSTRATE ———
FREQUENCY: 50 Hz

BOTTOM LOSS – dB

ANGLE – deg
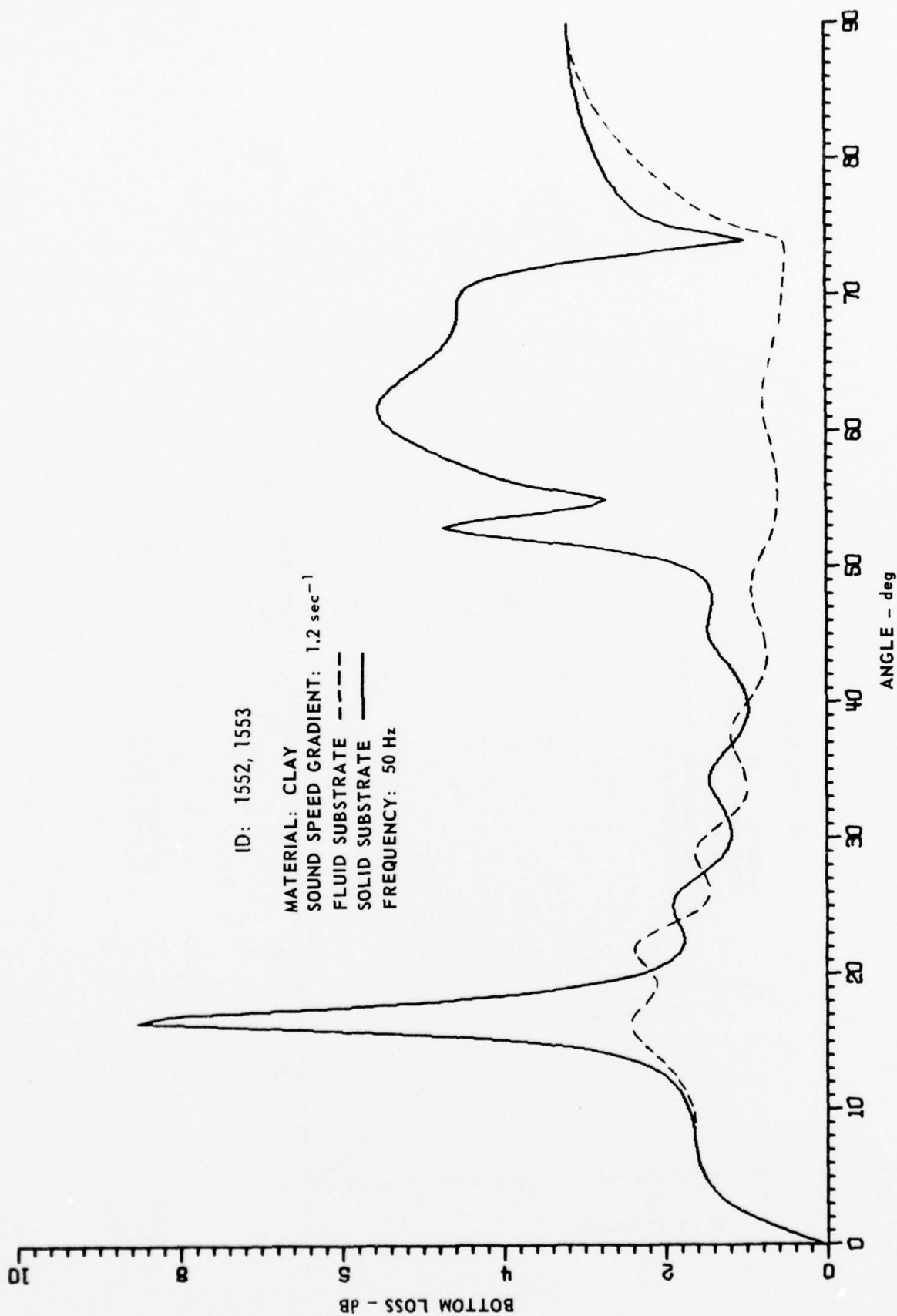
FIGURE II - 3

BOTTOM LOSS versus GRAZING ANGLE
FOR A 100 m CLAY LAYER AT 50 Hz

ARL - UT
AS-76-206
KEH - DR
2 - 27 - 76

16

ID: 1554, 1555

MATERIAL: CLAY
SOUND SPEED GRADIENT: 1.2 sec^{-1}
FLUID SUBSTRATE ———
SOLID SUBSTRATE ———
FREQUENCY: 100 Hz
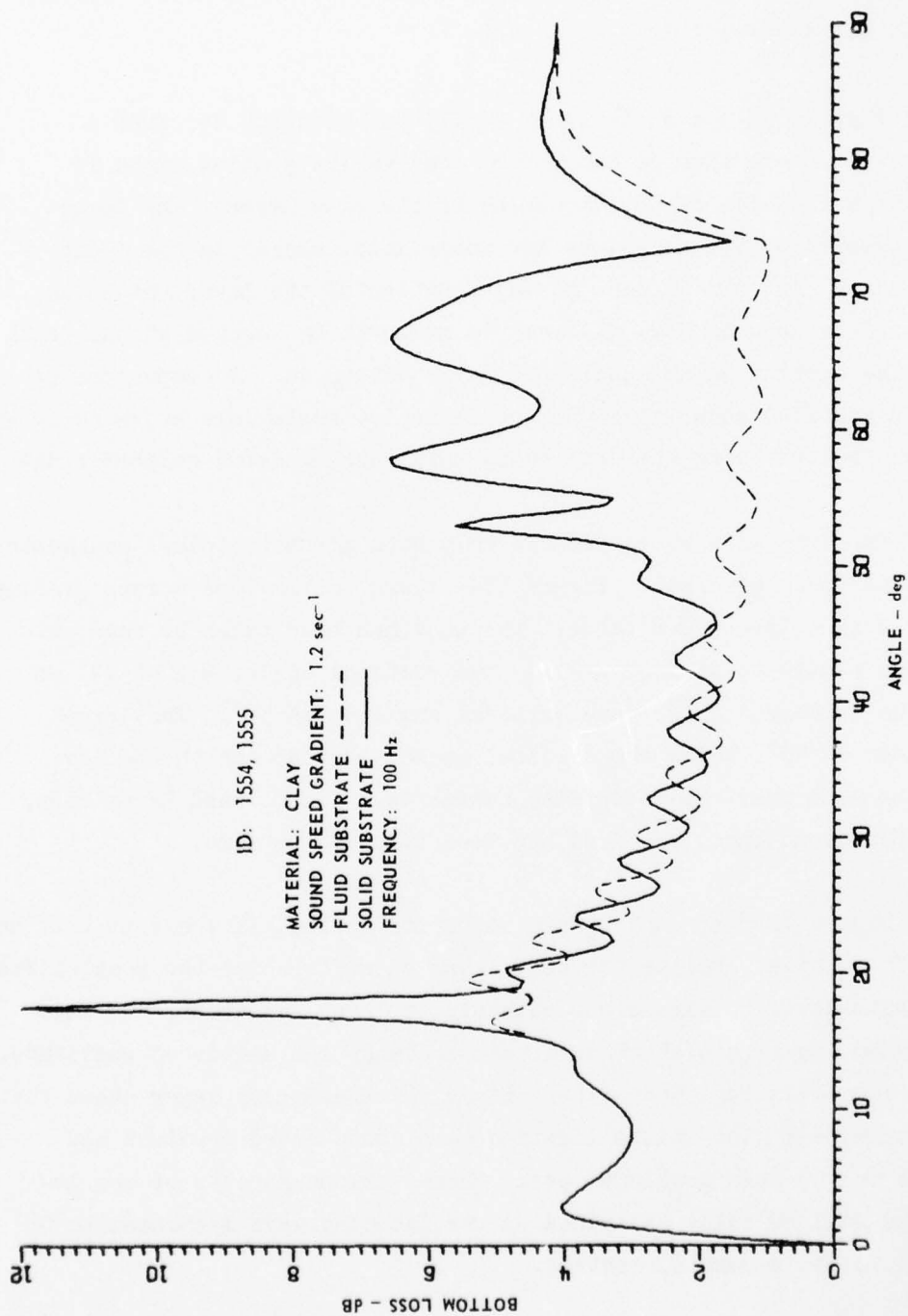
FIGURE II-4

BOTTOM LOSS versus GRAZING ANGLE
FOR A 100 m CLAY LAYER AT 100 Hz

17

wave critical angle and clearly related to the solid aspects of the substrate, (5), not to mention the frequency independence, (6), is evidence of some additional and different loss mechanism.

Figures II-5 and II-6 show additional evidence for such a mechanism. In these figures the bottom loss versus grazing angle is depicted as a function of the thickness of the clay layer. The large "ridge" composed of the anomalous low angle loss, absent in the fluid substrate case, is seen to be a strong function of the layer thickness. The minor ridge seen in Fig. II-6 can be shown to be located at the depth at which the turning depth equals the layer thickness. A comparison of Figs. II-5 and II-6 shows that the anomalous low angle loss peaks occur at depths just below the depths defined by this turning depth related ridge.

Thus far we have considered only high porosity (clay) sediments with a sound speed gradient. Figure II-7 shows bottom loss versus grazing angle for a sand layer 50 m thick. The sand has been taken to have zero attenuation simply to display vividly the critical angle, θ_c, at 24° as well as the substrate shear wave critical angle θ_s at 57°. The large peak in loss at 20°, below the critical angle, corresponds to the low angle peaks seen previously for clay sediments. In the sand layer case, however, the sound speed gradient has been taken to be zero.

Figure II-8 shows the same situation as Fig. II-7 except that the layer is 75 m thick. Unlike the clay layer case for which the peak shifts location with layer thickness but maintains a large amplitude, the iso-velocity sand layer case shows no location change but a reduced amplitude. A series of calculations made with a fixed thickness clay layer shows that the low angle peak also shifts location with sound speed gradient and disappears in the zero gradient case. These various aspects of the low angle peaks will be fully explained by the Stoneley wave mechanism to be introduced in the second subsection.

Finally, we consider a sequence of sediment types having a
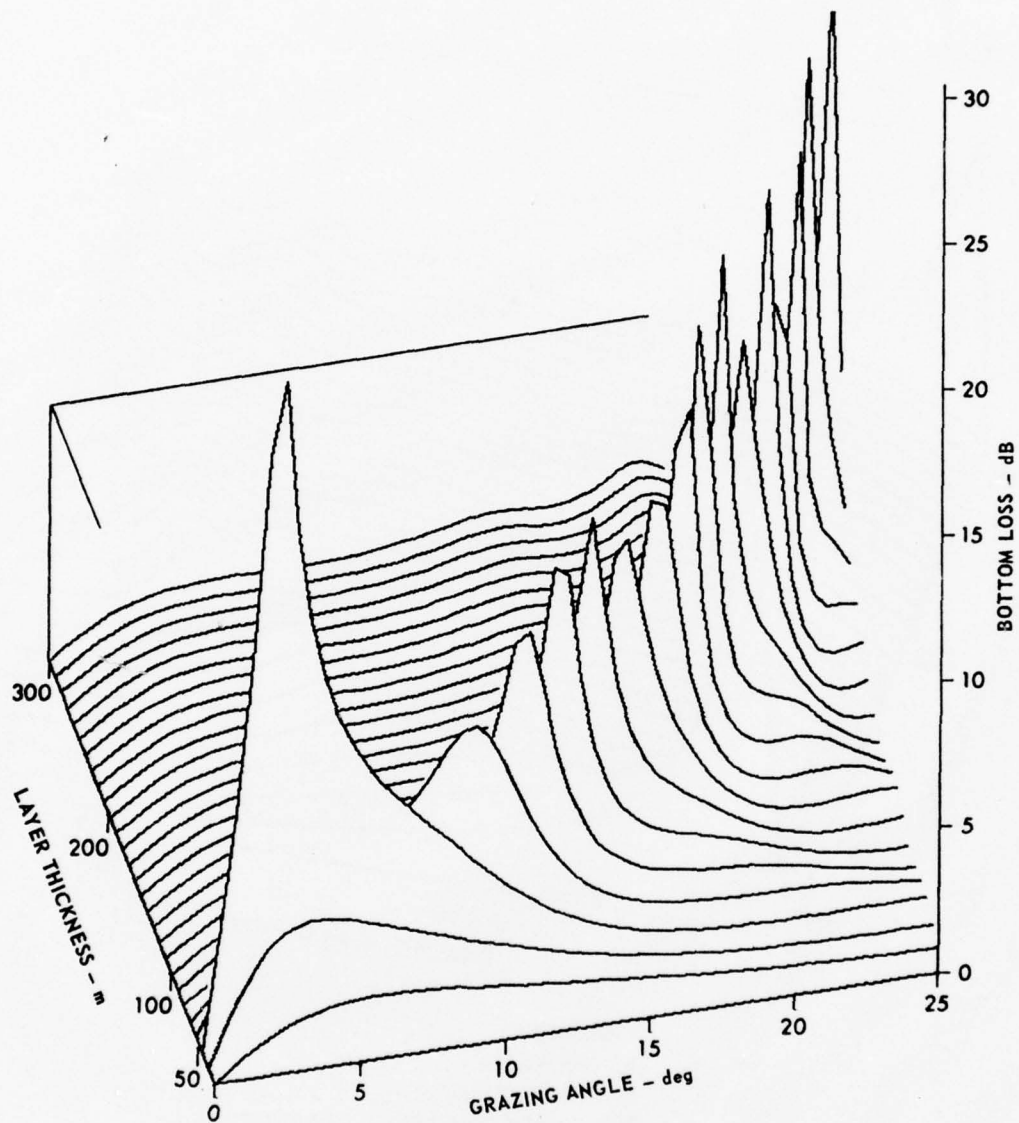
FREQUENCY: 50 Hz
LAYER MATERIAL: CLAY
SOUND SPEED GRADIENT: 1.0 sec^{-1}
SUBSTRATE: SOLID

FIGURE II-5
BOTTOM LOSS versus GRAZING ANGLE
versus LAYER THICKNESS FOR A CLAY LAYER
OVERLYING A SOLID SUBSTRATE

ARL - UT
AS-76-685
KEH - RFO
6 - 28 - 76

19
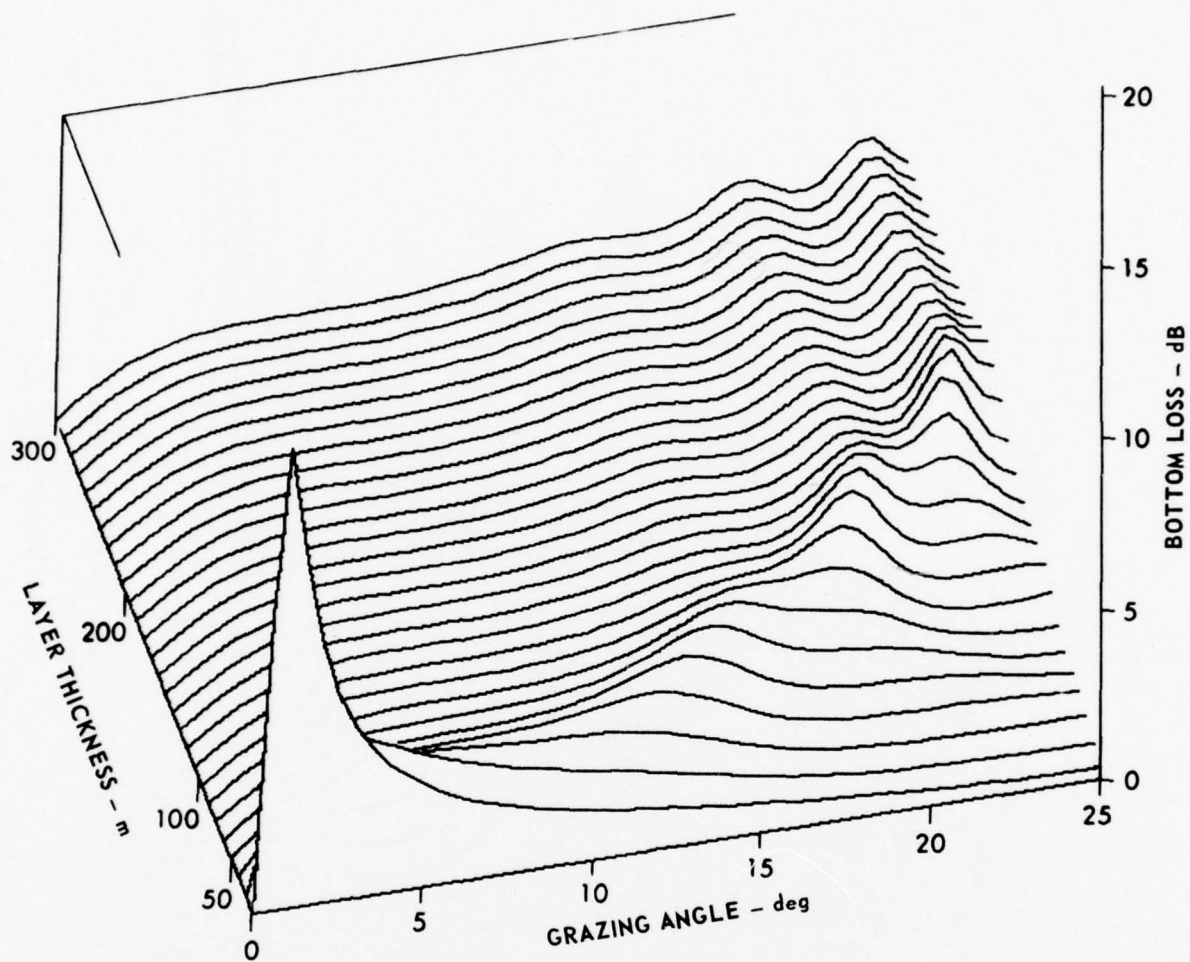
FREQUENCY: 50 Hz
LAYER MATERIAL: CLAY
SOUND SPEED GRADIENT: 1.0 sec^{-1}
SUBSTRATE: PERFECT REFLECTOR

FIGURE II-6
BOTTOM LOSS versus GRAZING ANGLE
versus LAYER THICKNESS FOR A CLAY LAYER
OVERLYING A PERFECT REFLECTOR

FREQUENCY: 50 Hz
SEDIMENT: SAND WITH ZERO ATTENUATION
SUBSTRATE: BASALT
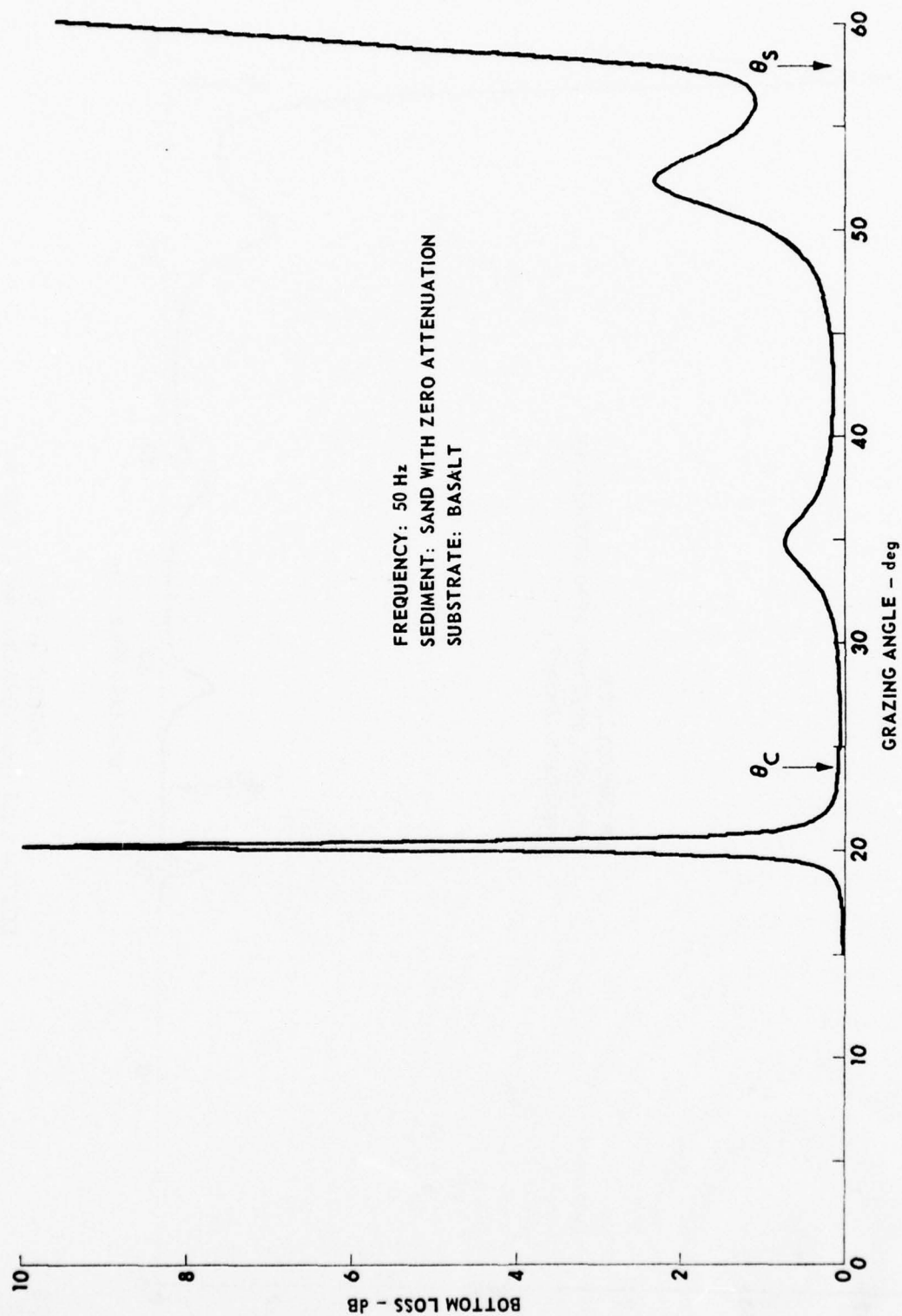
FIGURE II-7
BOTTOM LOSS versus GRAZING ANGLE FOR AN
IDEAL 50 m ISOVELOCITY SAND LAYER AT 50 Hz

ARL - UT
AS-77-331
KEH - DR
4 - 19 - 77

21

FREQUENCY: 50 Hz

SEDIMENT: SAND WITH ZERO ATTENUATION

SUBSTRATE: BASALT
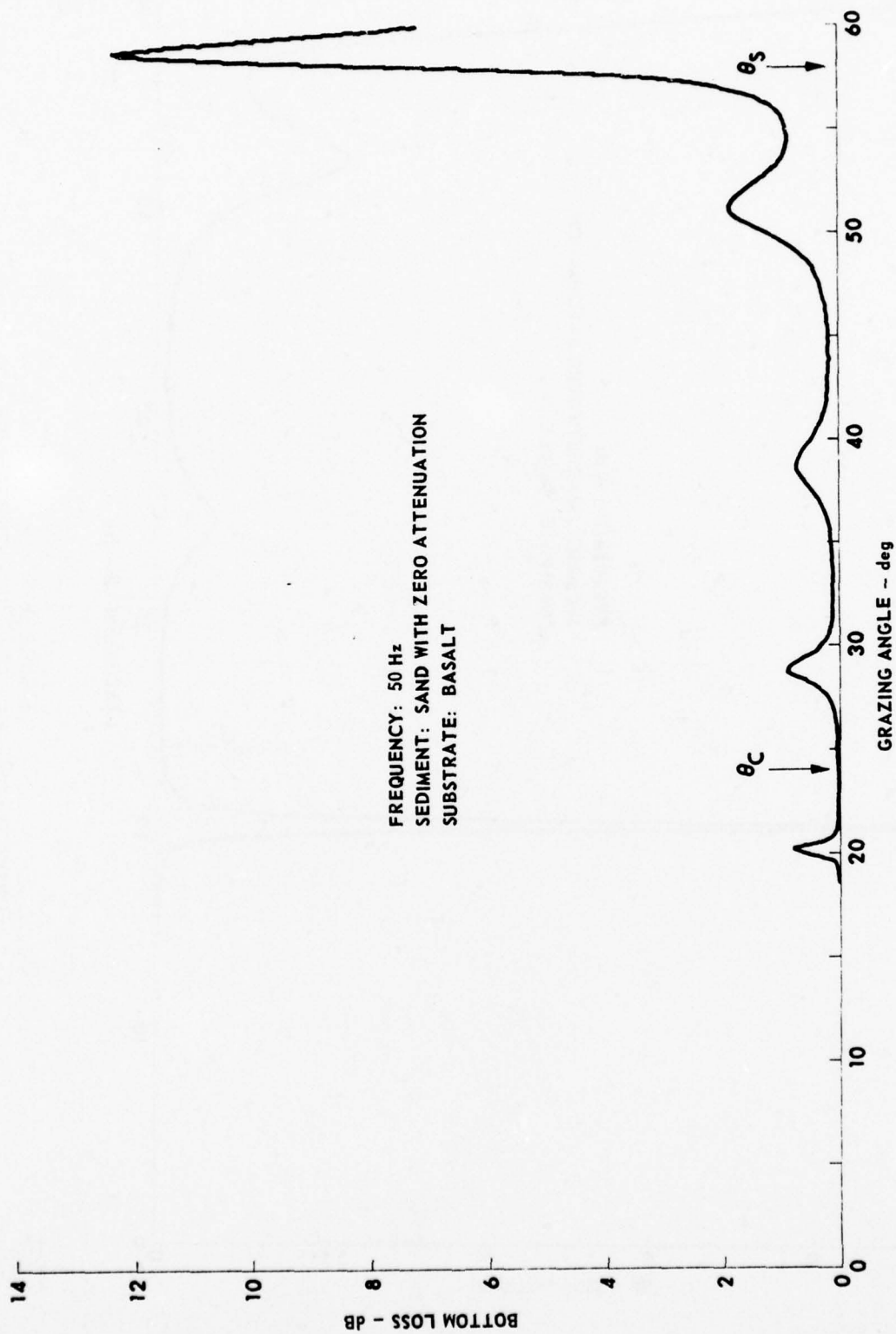
FIGURE II - 8

BOTTOM LOSS versus GRAZING ANGLE FOR AN
IDEAL 75 m ISOVELOCITY SAND LAYER AT 50 Hz

sound speed gradient of 1.2 $\sec^{-1}$ and a thickness of 100 m. The density, surficial sound speed, and attenuation are related to porosity by the regression equations of Hamilton[7] and the resulting parameters used to compute the bottom loss. The results are shown in Fig. II-9, which is taken from Hawker, Focke, and Anderson.[2]

The curving ridge of bottom loss peaks between 15° and 25° shows the effect on the low angle loss peak of varying the sediment type. As would be expected on the basis of Figs. II-7 and II-8, the sand sediments (porosity ≅ 36% to 50%) do not show an anomalous peak for a layer of this thickness. The peaks are most pronounced for the high porosity sediments, silts, and clays.

2.   Stoneley Waves and Bottom Reflection Loss

Before entering into a discussion of the nature of Stoneley waves at a fluid-solid interface, it will be useful to carry forward the heuristic studies of the previous subsection in order to further understand the characteristics of the loss mechanism.

Figure II-10 shows the same situation as in Fig. II-3 except that, in the present case, the sediment (clay) attenuation as well as the substrate compressional attenuation have been set to zero. The 17° bottom loss peak is still evident in Fig. II-10; however, below the neighborhood of this peak, there is perfect reflection (zero loss). Although examples are not shown here, essentially the same thing occurs if any two of the three relevant attenuations are set to zero with the remaining attenuation (the substrate shear attenuation in the present case) nonzero.

Figure II-11 shows the result of setting all three attenuations to zero. As expected, there is no loss below the shear critical angle (55°) whereupon the loss increases and remains nonzero up to 90°. The results shown in Figs. II-10 and II-11 show that the mechanism responsible for the low angle peaks is dependent on at least one medium composing
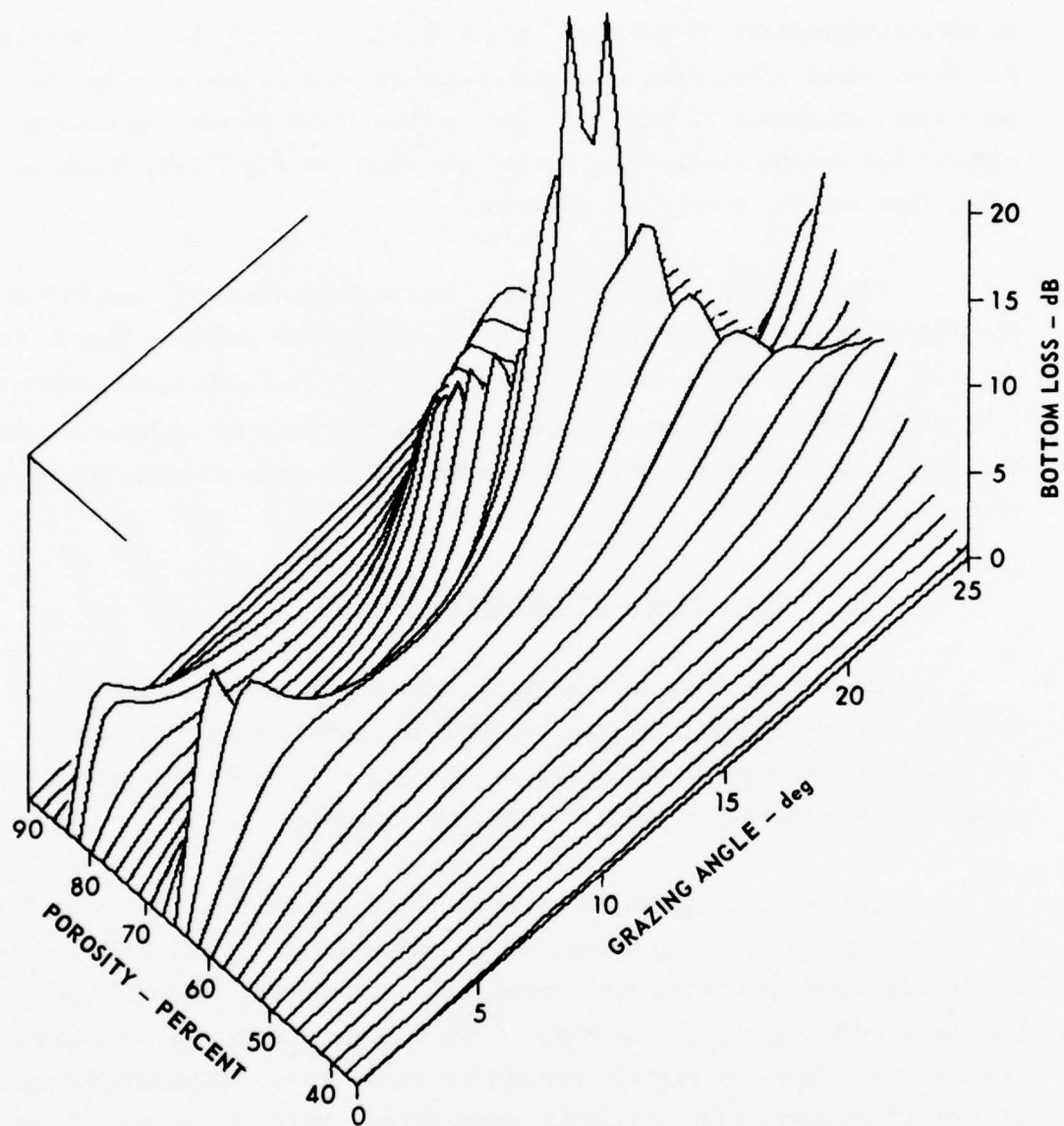
FREQUENCY: 50 Hz
LAYER THICKNESS: 100 m
SOUND SPEED GRADIENT: 1.2 sec^{-1}

FIGURE II-9
BOTTOM LOSS versus GRAZING ANGLE
versus POROSITY FOR A 100 m LAYER
OVERLYING A SOLID SUBSTRATE

ARL - UT
AS-76-687
KEH - RFO
6 - 28 - 76

24

FREQUENCY: 50 Hz
LAYER THICKNESS: 100 m
LAYER MATERIAL: CLAY
GRADIENT: 1.2 sec⁻¹

GRAZING ANGLE – deg
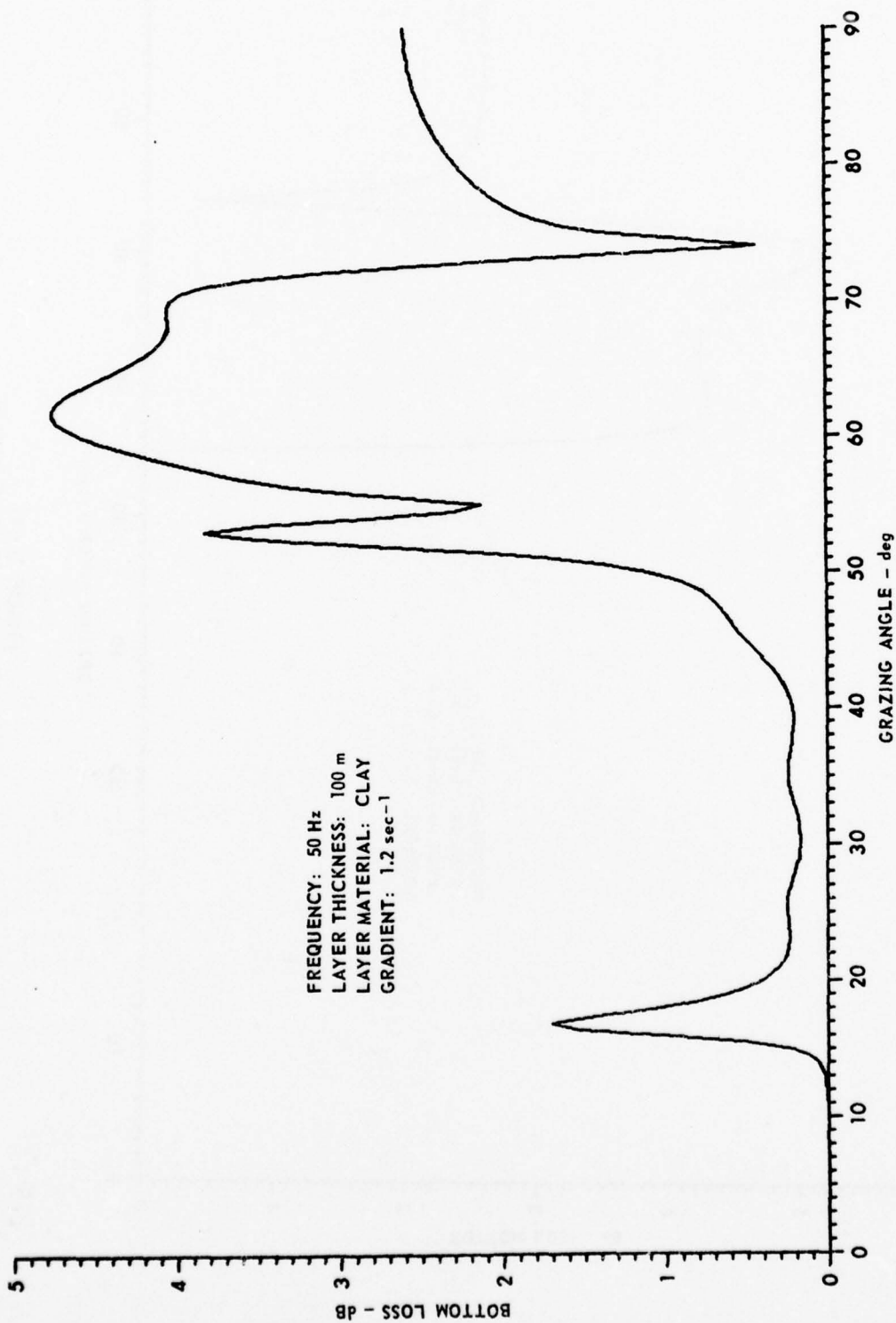
BOTTOM LOSS – dB

FIGURE II - 10
BOTTOM LOSS versus GRAZING ANGLE WITH ONLY
THE SUBSTRATE SHEAR ATTENUATION NONZERO

ARL - UT
AS-76-641
KEH - DR
6 - 14 - 76

25

FREQUENCY: 50 Hz
LAYER THICKNESS: 10 m
LAYER MATERIAL: CLAY
GRADIENT: 1.2 sec^{-1}
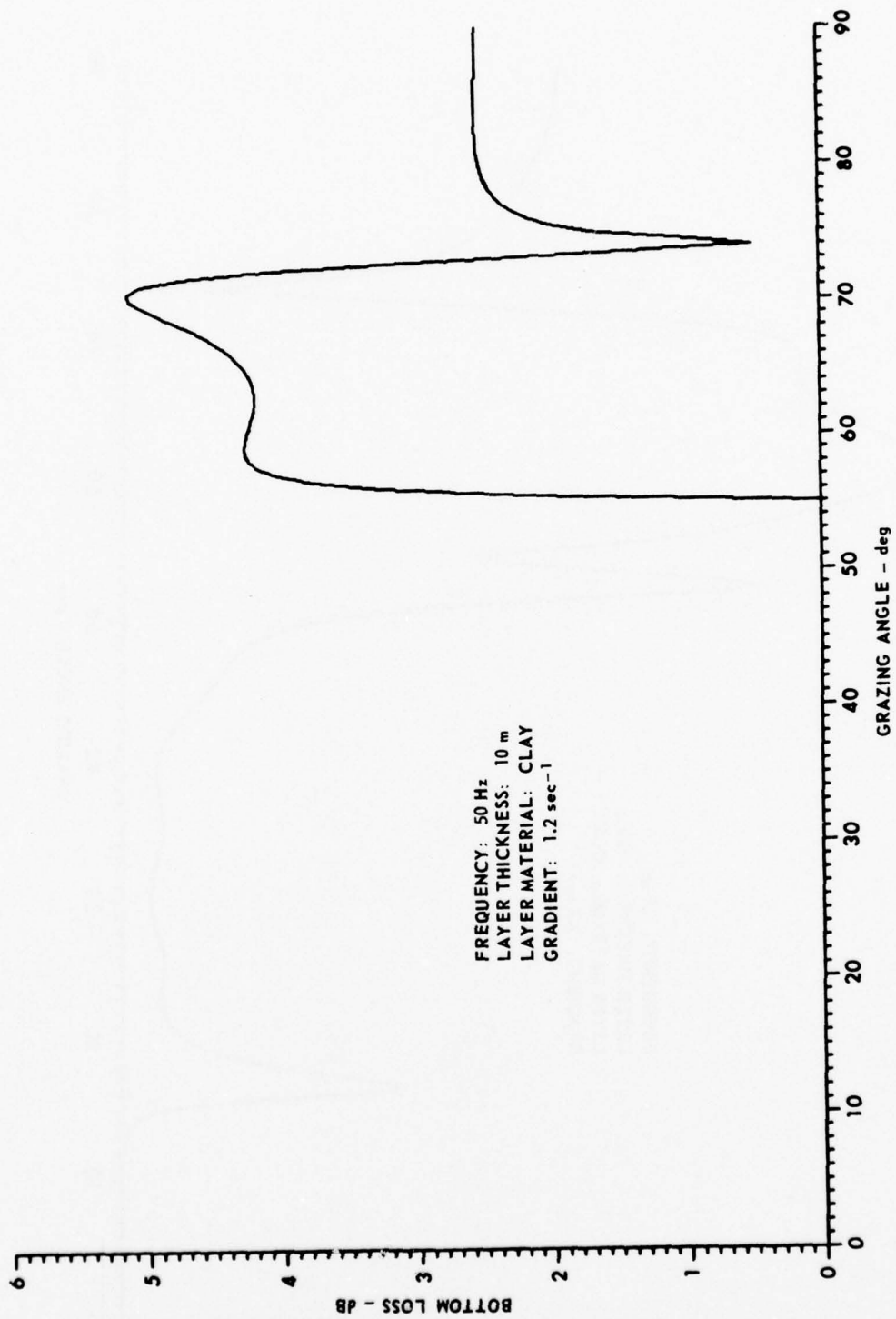
FIGURE II-11
BOTTOM LOSS versus GRAZING ANGLE
WITH ALL ATTENUATIONS ZERO

ARL - UT
AS-76-648
KEH - DR
6 - 14 - 76

the interface being lossy. These peaks are not simply due to energy being propagated away, which is the mechanism responsible for the loss shown in Fig. II-11.

Figures II-12 and II-13 show the phase of the reflection coefficient for the same situation used in Figs. II-3, II-10, and II-11; for a solid substrate, Fig. II-12; and a fluid substrate, Fig. II-13. It will be observed that in the neighborhood of the 17° loss peak (denoted by a cross on Fig. II-12) the phase is rapidly changing and goes through an entire extra cycle of variation relative to the fluid case.

Figure II-14 shows the pressure amplitude versus depth within the same 100 m clay layer for a plane wave incident at 16.5°, for both fluid and solid substrates. The fluid case displays the expected behavior, oscillatory above the turning depth, Z_T, and quasiexponentially decaying below Z_T. The solid substrate case is similar except the field shows a growing amplitude with depth very near the surface. Figure II-15 is the same situation as Fig. II-14 except that the grazing angle is 17.5°, the angle at which the peak in loss occurs. The fluid substrate case is essentially unchanged (the turning depth is slightly deeper); however, the solid case is substantially different. The field now displays a sharp increase in amplitude as the interface is approached, with a near constant behavior above Z_T.

Of course, since the substrate is taken to be homogeneous, the shear and compressional fields are purely linear combinations of exponential solutions. For angles below the shear and compressional critical angles, the shear and compressional wave potential are respectively

$$\psi = A_s \, e^{i(k_o x\cos\theta - \omega t)} \, e^{-\kappa_s Z} \quad ,$$

$$\Phi = A_p \, e^{i(k_o x\cos\theta - \omega t)} \, e^{-\kappa_p Z} \quad ,$$

where
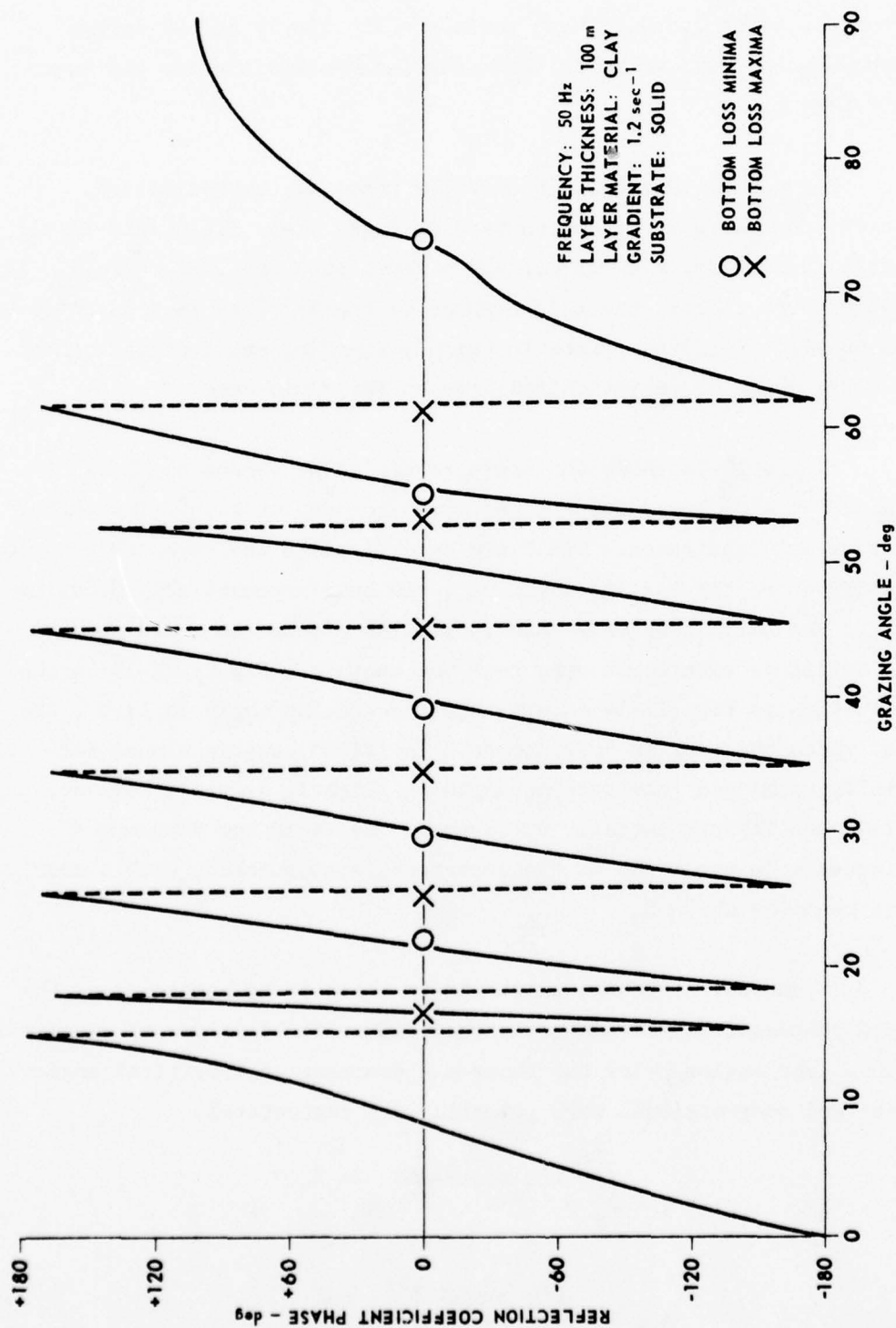
FIGURE II-12

REFLECTION COEFFICIENT PHASE *versus* GRAZING ANGLE
FOR A SOLID SUBSTRATE

FREQUENCY: 50 Hz
LAYER THICKNESS: 100 m
LAYER MATERIAL: CLAY
GRADIENT: 1.2 sec^{-1}
SUBSTRATE: SOLID

O BOTTOM LOSS MINIMA
X BOTTOM LOSS MAXIMA

GRAZING ANGLE – deg

REFLECTION COEFFICIENT PHASE – deg
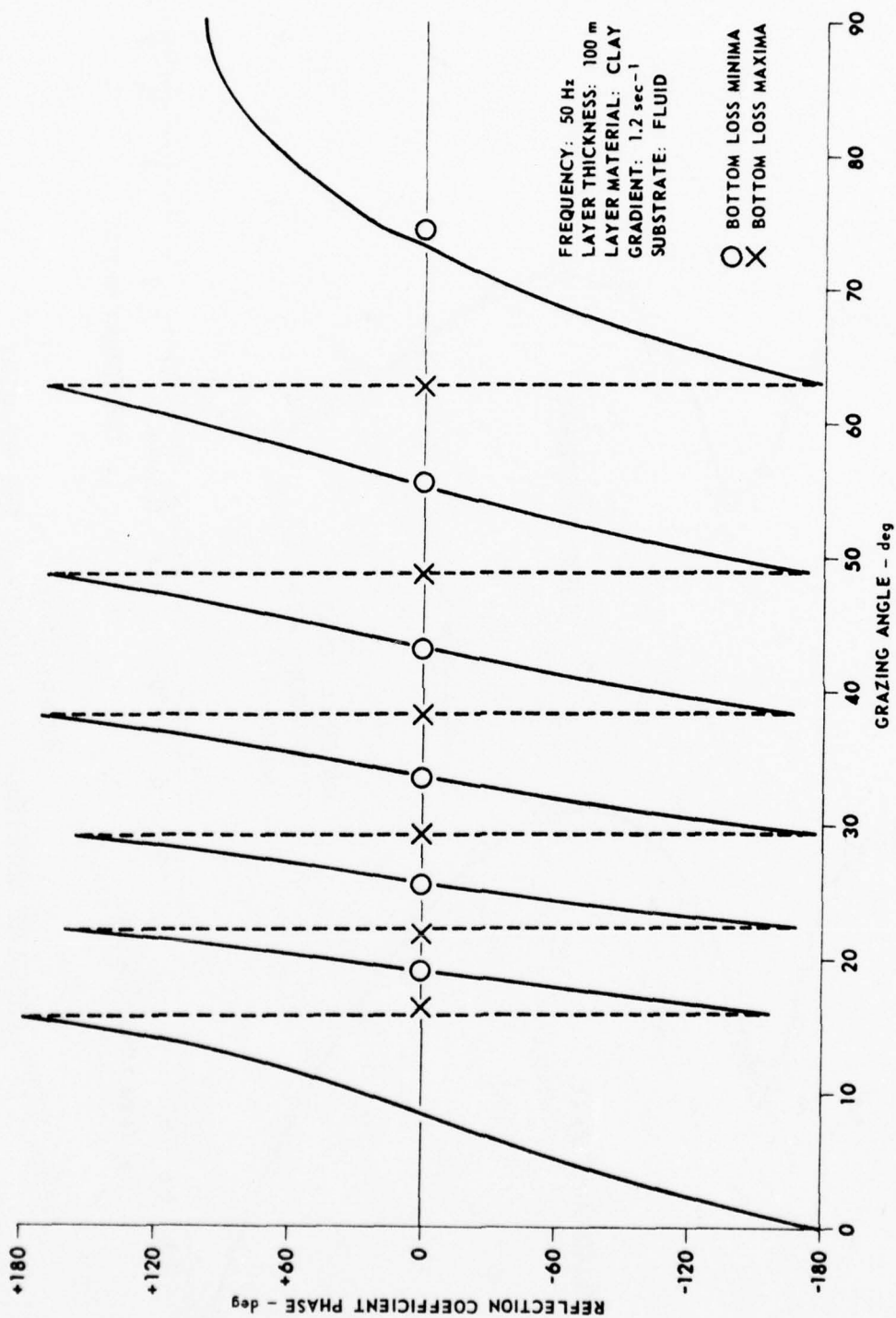
FIGURE II-13
REFLECTION COEFFICIENT PHASE versus GRAZING ANGLE
FOR A FLUID SUBSTRATE

FREQUENCY: 50 Hz
LAYER THICKNESS: 100 m
LAYER MATERIAL: CLAY
GRADIENT: 1.2 sec^{-1}
SUBSTRATE: FLUID

O BOTTOM LOSS MINIMA
X BOTTOM LOSS MAXIMA

GRAZING ANGLE – deg

REFLECTION COEFFICIENT PHASE – deg

ARL - UT
AS-76-652
KEH - DR
6 - 9 - 76

29
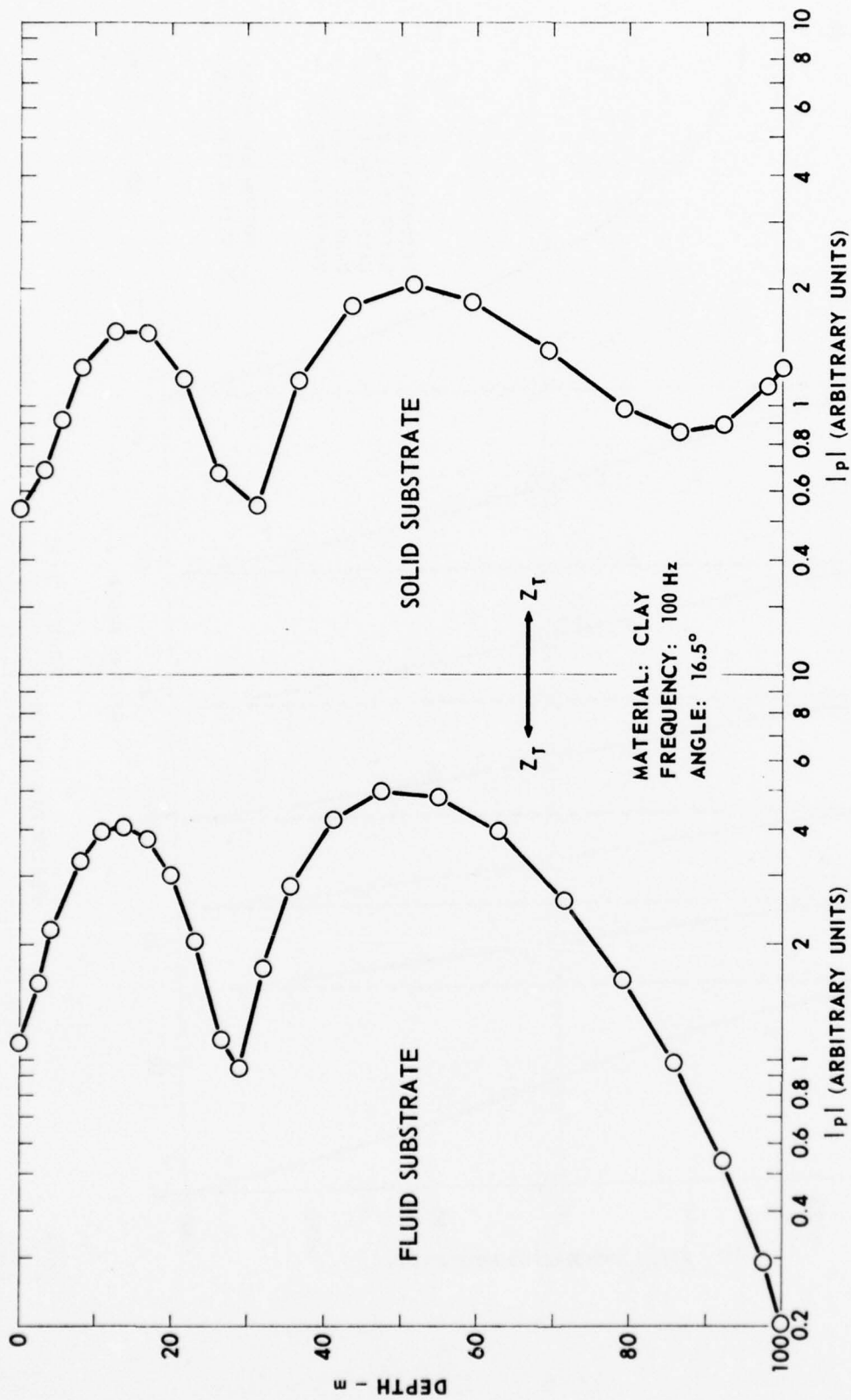
FIGURE II-14

PRESSURE AMPLITUDE versus DEPTH IN THE SEDIMENT
AT A GRAZING ANGLE OF 16.5°
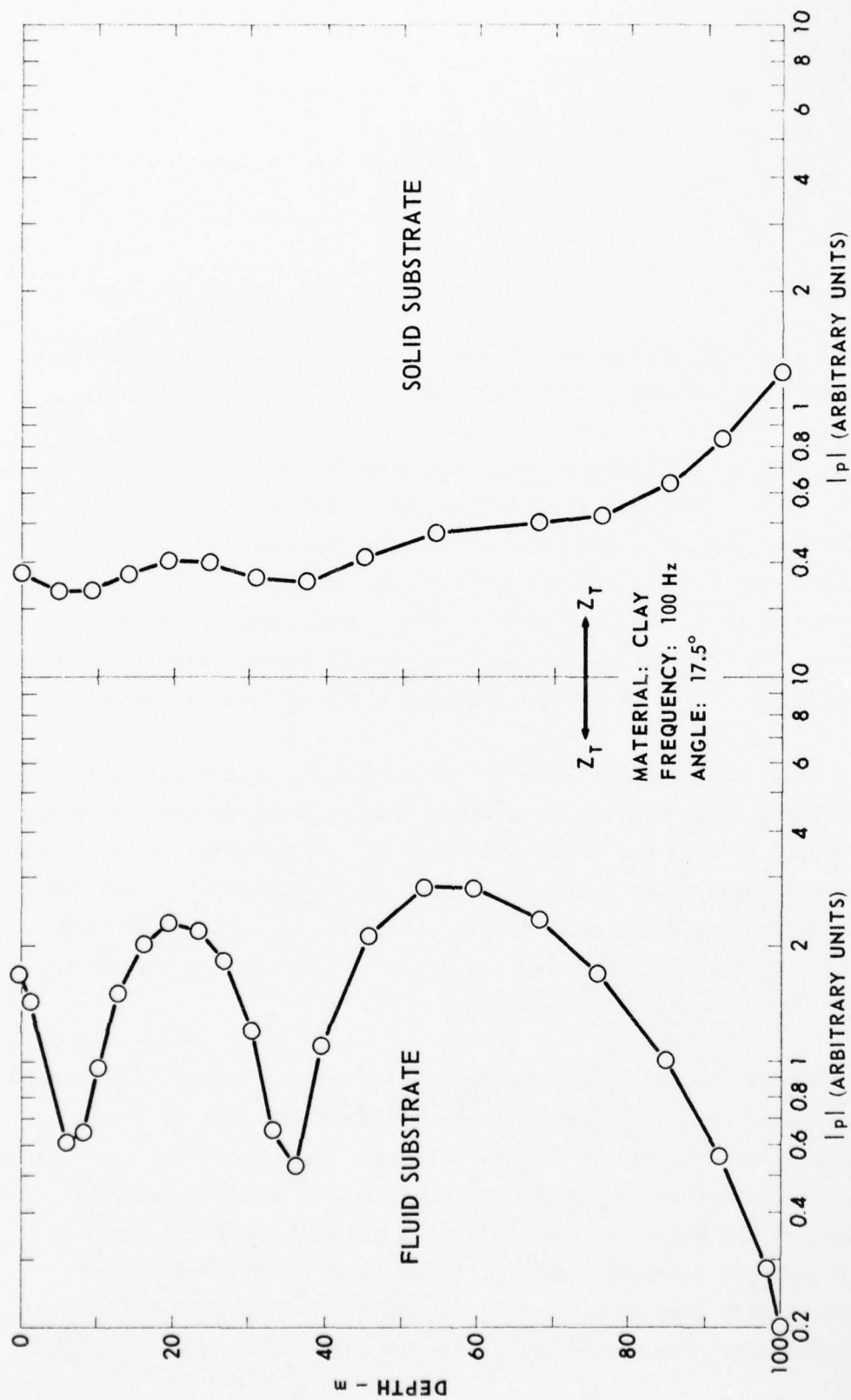
FIGURE II-15

PRESSURE AMPLITUDE versus DEPTH in THE SEDIMENT
AT A GRAZING ANGLE OF 17.5°

MATERIAL: CLAY
FREQUENCY: 100 Hz
ANGLE: 17.5°

SOLID SUBSTRATE

FLUID SUBSTRATE

31

$$\kappa_s^2 = k_o^2 \cos^2 \theta - k_s^2 \quad ,$$

$$\kappa_p^2 = k_o^2 \cos^2 \theta - k_p^2 \quad ,$$

k_o is the water wave number, and k_s and k_p are the substrate shear and compressional wave numbers. The amplitudes A_s and A_p are constants.

The fields therefore decay away from the interface in <u>both</u> directions when the grazing angle is near the angle at which the low angle loss peak occurs. This behavior is characteristic of an interface (or surface) wave and without further evidence can be taken to prove that a Stoneley wave is present. This point is discussed in detail by Tolstoy and Clay[4] for two joined isovelocity half-spaces which lead to a dispersion equation for the unique phase velocity of Stoneley waves.

If we ignore for the moment the complexity introduced by the layered inhomogeneous configuration being treated here, we can understand how there must be a unique angle associated with the excitation of Stoneley waves. Since these waves can have only one phase velocity, v_s, and this is in the direction, x, parallel to the interface, they can exist only when the plane waves have an equal x component. That is, $c_o/\cos \theta$ must equal v_s, thus defining an angle θ.

A sufficiently accurate model which contains the basic physical processes can be obtained by considering a fluid half-space overlying a solid half-space. The fluid is taken to have a sound speed which decreases away from the interface, while the solid is assumed to be isovelocity. The neglect of the water-sediment interface bounding the fluid layer is based, in part, on the fact that Fig. II-15 shows the field decaying quasiexponentially away from the sediment-substrate interface for several sound wavelengths. The nature of the field in the region near this lower

interface will thus be effectively isolated from the presence of the upper interface which may therefore be removed.

The z-axis is taken to be increasing positively downward (into the solid) with the fluid-solid interface located at z=0. With the fluid velocity potential denoted by Φ_1 and the compressional and shear potentials in the solid denoted by Φ_2 and ψ_2, we have the usual fluid-solid relations,

$$
\begin{cases}
\rho_1 \Phi_1 = \rho_2 \Phi_2 - \dfrac{2\rho_2}{k_s^2} \left[\dfrac{\partial^2 \psi_2}{\partial x \partial z} - \dfrac{\partial^2 \Phi_2}{\partial x^2} \right] \\[20pt]
\dfrac{\partial \psi_1}{\partial z} = \dfrac{\partial \Phi_2}{\partial z} + \dfrac{\partial \psi_2}{\partial x} \\[20pt]
0 = 2\dfrac{\partial^2 \Phi_2}{\partial x \partial z} + \dfrac{\partial^2 \psi_2}{\partial x^2} - \dfrac{\partial^2 \psi_2}{\partial z^2}
\end{cases}
$$

(see, for example, Brekhovskikh).

The fields are now assumed to be of the forms

$$\Phi_1 = A_1 f(z)\, e^{i(\alpha x - \omega t)} \quad ,$$

$$\Phi_2 = A_2\, e^{-\kappa_p z}\, e^{i(\alpha x - \omega t)}$$

$$\psi_2 = B_2\, e^{-\kappa_s z}\, e^{i(\alpha x - \omega t)} \quad ,$$

where $\kappa_p^2 - \alpha^2 + \omega^2/c_p^2 = 0$, $\kappa_s^2 - \alpha^2 + \omega^2/c_s^2 = 0$ and the amplitudes A_1, A_2, B_2 are unknown. The depth function $f(z)$ in the fluid $(0 \geq z \geq -\infty)$ is determined by the sound speed profile $c_1(z)$ and a radiation condition.

If a combination of amplitudes can be found for some horizontal

wavenumber α such that the continuity conditions can be satisfied, then solutions of the type proposed here can exist. Substitution of the assumed forms for Φ_1, Φ_2, and ψ_2 into the continuity conditions clearly leads to three simultaneous homogeneous linear algebraic equations for A_1, A_2, and B_2. These equations have a nontrivial solution only if their determinant vanishes. Upon requiring this, a single (dispersion) equation is obtained for the horizontal wave number α, or the associated phase velocity v

$$(2 - \frac{v^2}{c_s^2})^2 - 4 \sqrt{1 - \frac{v^2}{c_s^2}} \sqrt{1 - \frac{v^2}{c_p^2}} + \frac{\rho_1}{\rho_2} \frac{\omega v^3 f(0)}{c_s^4 f'(0)} \sqrt{1 - \frac{v^2}{c_p^2}} = 0 \quad .$$

This equation can be rewritten in a slightly more perspicacious form by introducing the fluid sound speed at the interface $c_1(z=0)=c_1$ and the function $e(v)=\omega f(0)/(vf'(0))\sqrt{1-v^2/c_1^2}$, to obtain

$$(2 - \frac{v^2}{c_s^2})^2 - 4 \sqrt{1 - \frac{v^2}{c_s^2}} \sqrt{1 - \frac{v^2}{c_p^2}} + \frac{\rho_1}{\rho_2} \frac{v^4}{c_s^4} e(v) \sqrt{\frac{1 - \frac{v^2}{c_p^2}}{1 - \frac{v^2}{c_1^2}}} = 0 \quad .$$

In the case $e(v)=1$, this equation becomes identical with the classical result for the phase velocity of Stoneley waves at the interface between two isovelocity media, as given by Tolstoy and Clay.[4]

Before discussing solutions to this equation, it is worth recapitulating the situation thus far. Solutions of a particular type, defined by the forms assumed for Φ_1, Φ_2, and ψ_2 can exist in the two media if, and only if, the phase velocity, v, obeys the dispersion equation above.

If the function, $e(v)$, itself contains an arbitrary constant, such as that relating incoming and outgoing plane waves when $c_1(z)$ is

constant, then a solution for this equation is obviously possible for all values of v. Thus, for the plane wave reflection case, no restriction is imposed by the dispersion equation and waves can exist for all phase velocities (wave numbers). However, when a single solution, $f(z)$, is sought, no arbitrariness remains and only discrete values of v are possible.

Since we have already assumed that only the sediment properties near the fluid-solid interface are of importance, it is perfectly consistent to approximate the linear sound speed profile used in the bottom loss calculations of subsection 1 by the pseudolinear profile $c_1(z) \sim c_1(0)/(1-\beta z)$. This form leads to the differential equation,

$$f'' + (k_1^2 - \alpha^2 - k_1^2 \beta z)f = 0 \quad ,$$

for f in the region $0 \geq z$. The value of β is taken to be $2g/c_1(0)$ where g is the desired sound speed gradient at the interface. The solutions to this equation are the Airy functions $Ai(u)$ and $Bi(u)$ with $u = (\alpha^2 - k_1^2)(k_1^2\beta)^{-2/3} + (k_1^2\beta)^{1/3} z$. Since we wish to investigate the possibility of solutions which decrease in amplitude away from the interface, we choose the solution $f = Bi(u)$.

The resulting equation has been solved numerically for the phase velocity v given the parameters $\{g, c_1, c_p, c_s, \omega, \rho_1/\rho_2\}$. Since in the plane wave, layered reflection problem that is being approximated here, the x dependence was given by $\exp(ik_0 x \cos\theta)$, we must have $\alpha = k_0 \cos\theta = \omega/v = \omega \cos\theta/c_0$. The angle θ thus defined will be the angle at which a boundary wave can exist.

The results of such numerical calculations are given in Figs. II-16 through II-18, which show the predicted Stoneley wave excitation angle (solid line) and the angles at which direct bottom loss calculations show the low angle anomalous peak (circles). Figure II-16 shows these two quantities plotted versus layer thickness for a clay layer having a sound speed gradient of 1.2 sec^{-1}, whereas Fig. II-17 employs the sound speed

-35-
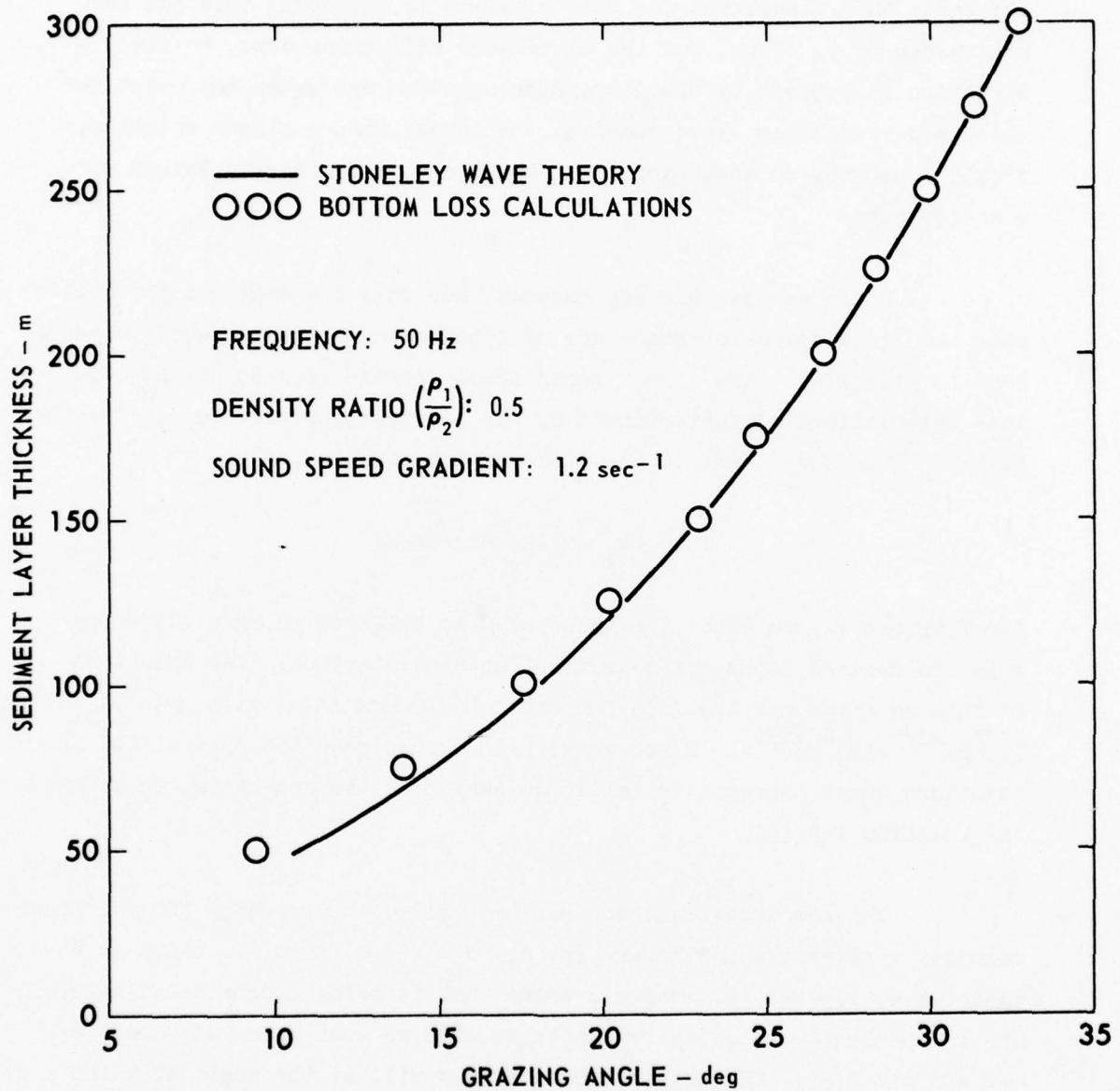
FIGURE II-16

LOCATION OF THE LOW ANGLE BOTTOM LOSS
PEAK versus SEDIMENT LAYER THICKNESS
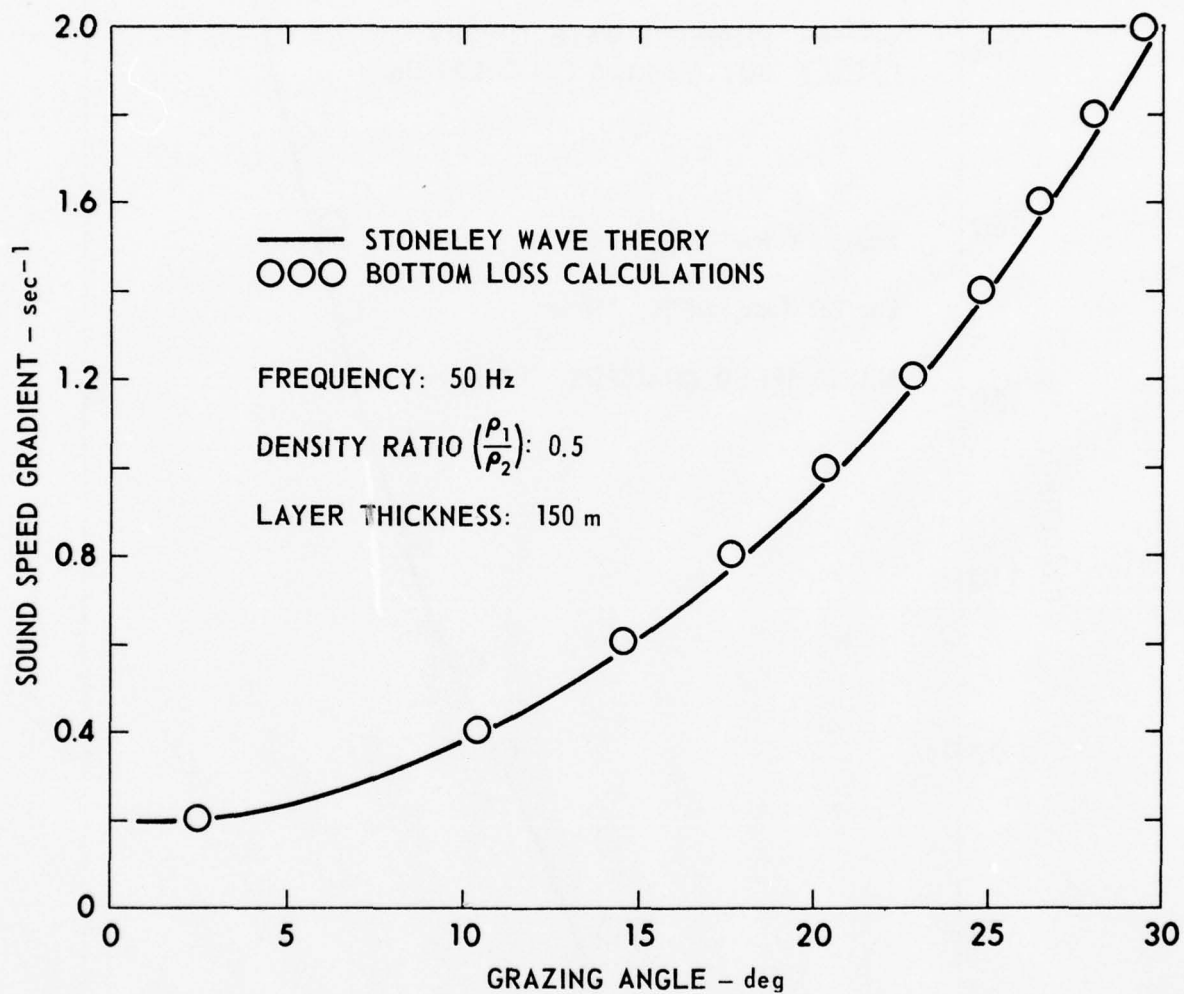
FIGURE II-17

LOCATION OF THE LOW ANGLE BOTTOM LOSS
PEAK versus SOUND SPEED GRADIENT
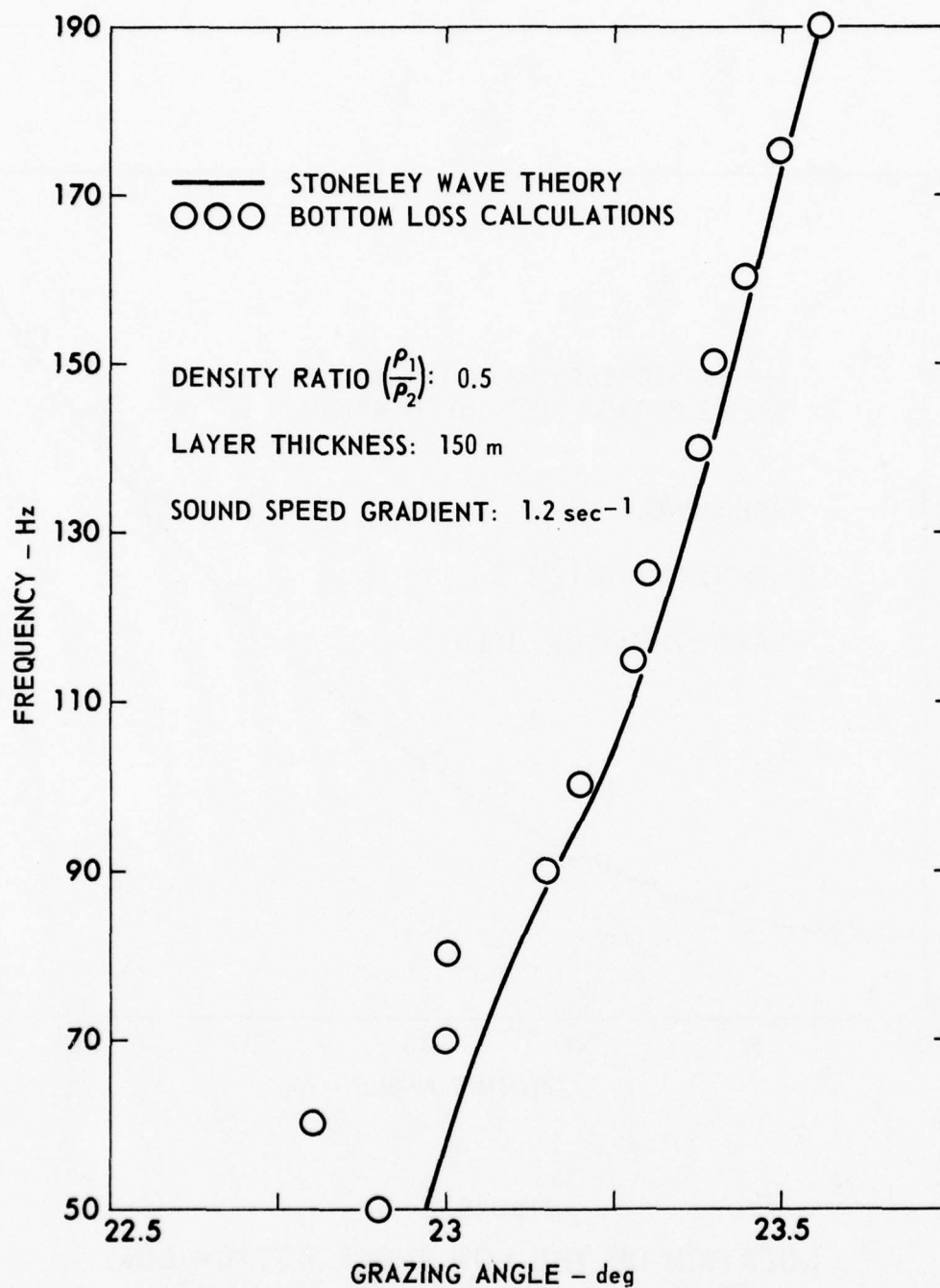
FIGURE II-18

LOCATION OF THE LOW ANGLE BOTTOM
LOSS PEAK versus FREQUENCY

gradient (with fixed layer thickness) as the independent variable. Agreement is found to be excellent in both cases.

The slight frequency dependence shown in Fig. II-18 shows that the very small shift of the loss peak with frequency shown in Figs. II-2 through II-4 is also accounted for with this theory.

These calculations provide clear evidence that the low angle bottom loss peak discussed in the first subsection of this chapter is indeed due to Stoneley waves. Several additional qualitative features are also accounted for by this mechanism. For instance, the requirement for at least one nonvanishing absorption, as evidenced by Figs. II-3, II-10, and II-11, is now understood. Since the Stoneley wave propagates along the interface, it can carry away no energy when it is excited by a plane wave. However, when absorption is present, dissipation occurs along the propagation path and loss results. Other features such as the density dependence of the location of the peak can also be explained by the Stoneley wave mechanism.

3. Practical Implications

The basic mechanism causing the anomalous low angle bottom loss peaks has been explained and understood. It is now meaningful to turn our attention to the question of the practical implications of this loss mechanism.

There are several factors evident in the work reported here which tend to increase the potential importance of this loss mechanism to propagation problems:

(1) the presence of a large loss peak in the low angle regime, 0° to 25°,

(2) the possibility of exciting Stoneley waves even for fairly thick sediment overburdens, especially in case of clay sediments, and

(3) the apparent broadening of the peak width with decreasing frequency.

There are, on the other hand, factors whose impact on the Stoneley wave loss peaks are at present unknown and are the subject of continuing investigation:

(1) the influence of shear waves in the sediments themselves,

(2) the effects of lateral variations in sediment properties and layer thickness, and

(3) the effects of interface irregularities and density inhomogenities.

In an open ocean measurement of bottom loss, data scatter is frequently so great as to preclude direct determination of the presence or absence of relatively narrow bottom loss peaks. Nevertheless, such peaks could manifest themselves in the data. In particular, a large though comparatively narrow loss peak at a low grazing angle, not directly resolvable, could result in a general increase in measured bottom loss. It is plausible that measurements showing high bottom loss (>5 dB) at low angles ($<10°$) for clay sediments are influenced by such loss peaks.

B.   Sensitivity of Bottom Loss to the Depth Variation of Attenuation

In this section, the effects of various treatments of attenuation on bottom loss curves are demonstrated. The program BOTLOSS, described in Chapter V, was used to compute all the bottom loss curves in this chapter.

The shape of the bottom loss curve is determined primarily by the sound speed profile. Attenuation increases bottom loss for angles where compressional waves enter the bottom. An attenuation gradient increases the bottom loss even more. This effect will be examined for a clay bottom. Some preliminary judgments concerning the validity of current attenuation treatments will be made using the best current attenuation

data for comparison.

In situ measurements of attenuation versus depth have recently been reviewed by Hamilton,[5] who discusses basic sand and clay bottom types and variations in the behavior of attenuation with depth. Figure II-19 illustrates the conclusions of his review. Hamilton's collected data for clay bottoms cover primarily the upper 200 m. At depths greater than 400 m, all sediments seem to have the same attenuation profile. Shirley[6] has suggested the form of the silt-clay attenuation profile between 200 and 400 m.

Clay bottoms are characterized by low reflectivities and moderate velocity gradients (1.0 to 1.5 sec^{-1}). Attenuation increases with depth to between 200 and 400 m. The velocity at the sediment-water interface is low. with

$$0.90 \lesssim \frac{C \text{ (sediment)}}{C \text{ (water)}} \lesssim 1.05$$

Table II-1 presents the input parameters used for the bottom loss curves in this chapter.

The results for an isovelocity, isodensity layer 300 m thick are shown in Fig. II-20. With no attenuation, no bottom loss occurs until the substrate shear critical angle at 62° is reached. A constant attenuation leads to nonzero bottom loss below 62° and a small increase in loss above 62°. Attenuation linearly increasing with depth causes an additional increase in bottom loss beyond the constant attenuation core. The attenuation gradient exaggerates the high loss areas of the curve.

Figure II-21 shows the results for a 300 m layer with linearly increasing velocity and density. Note that the change in sound speed treatment from constant to linearly increasing greatly alters the shape of the curve. The comments for Fig. II-20 concerning attenuation effects
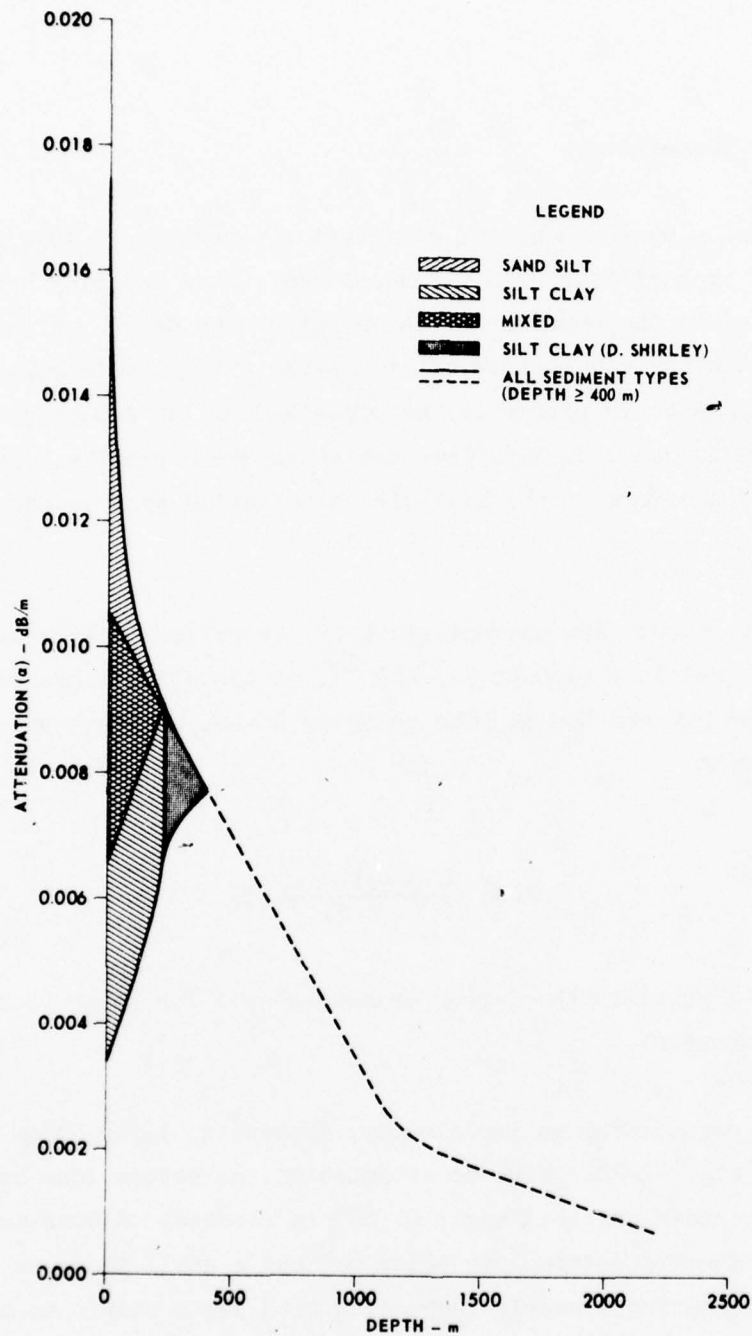
FIGURE II-19
ATTENUATION versus DEPTH, f = 50 Hz

[Taken from Hamilton, JASA 59, 528-535 (1976), p. 530]

42

TABLE II-1

PARAMETERS FOR ATTENUATION STUDY, $f = 50$ Hz

Layer	c_o (m/sec)	d_o (kg/m³)	a_o^1 (dB/m)	g_c^1 (sec⁻¹)	g_d^1 (kg/m³)/m	g_a^1 (dB/m)/m	a_{as}^1 (dB/m)
water	1515.0	1044.02	0.000	-	-	-	-
clay²	1500.0	1380.0	0.004	1.00	1.00	$+1.4 \times 10^{-5}$	0.008
substrate³ V_p	5940.0	2975.0	0.0	-	-	-	-
substrate³ V_s	3270.0		0.0	-	-	-	-

(1.) These quantities used as mathematically required.

(2.) $\dfrac{C\,(\text{clay})}{C\,(\text{water})} = 0.990$, according to Hamilton (1971).

(3.) Basalt substrate with properties taken from Hyndman and Drury (1976).

FIGURE II-20

BOTTOM LOSS CURVES FOR A SEDIMENT LAYER WITH CONSTANT SOUND SPEED AND DENSITY
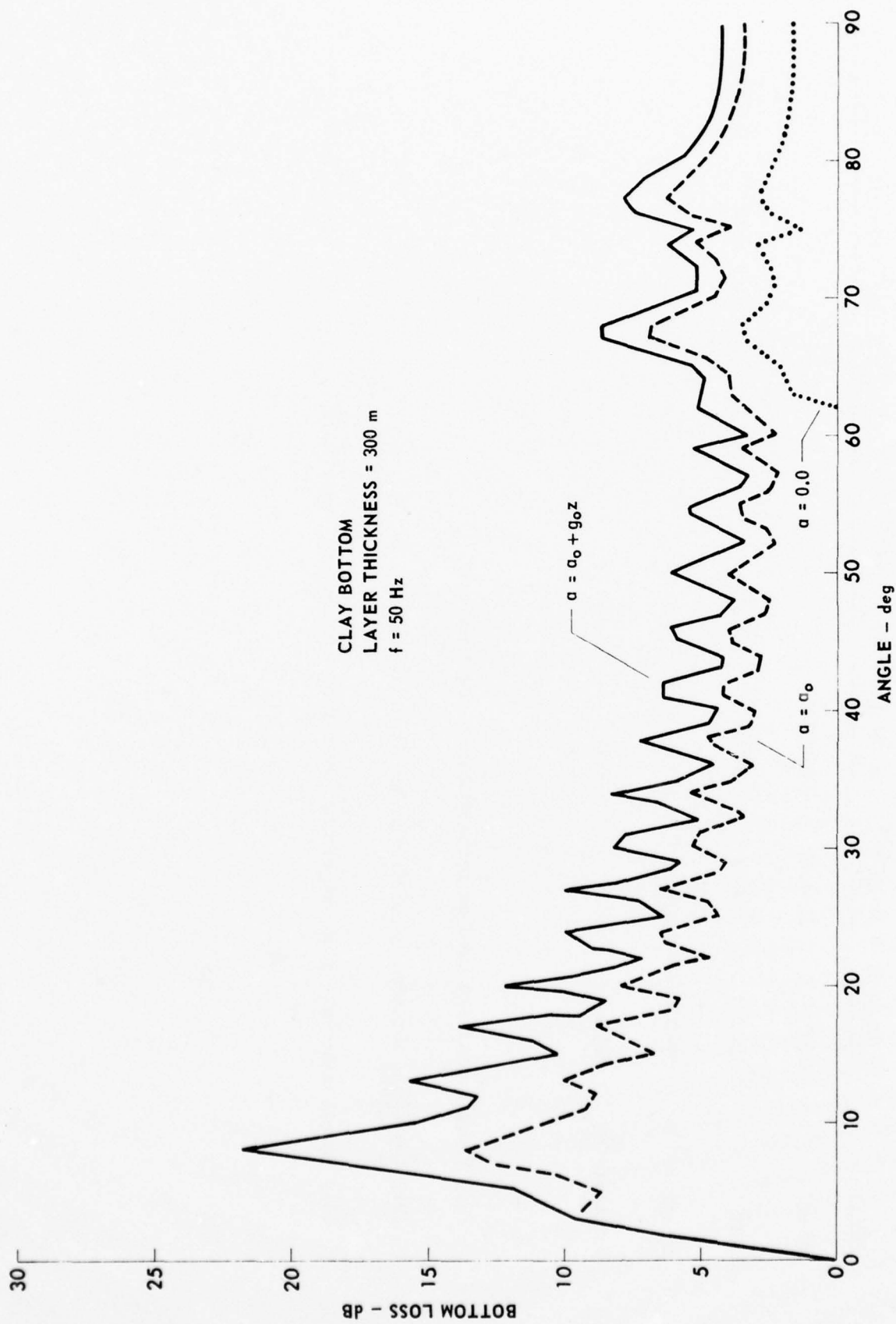
($\alpha \equiv$ ATTENUATION)

ARL - UT
AS -77 -126
WEW - DR
2 - 8 - 77
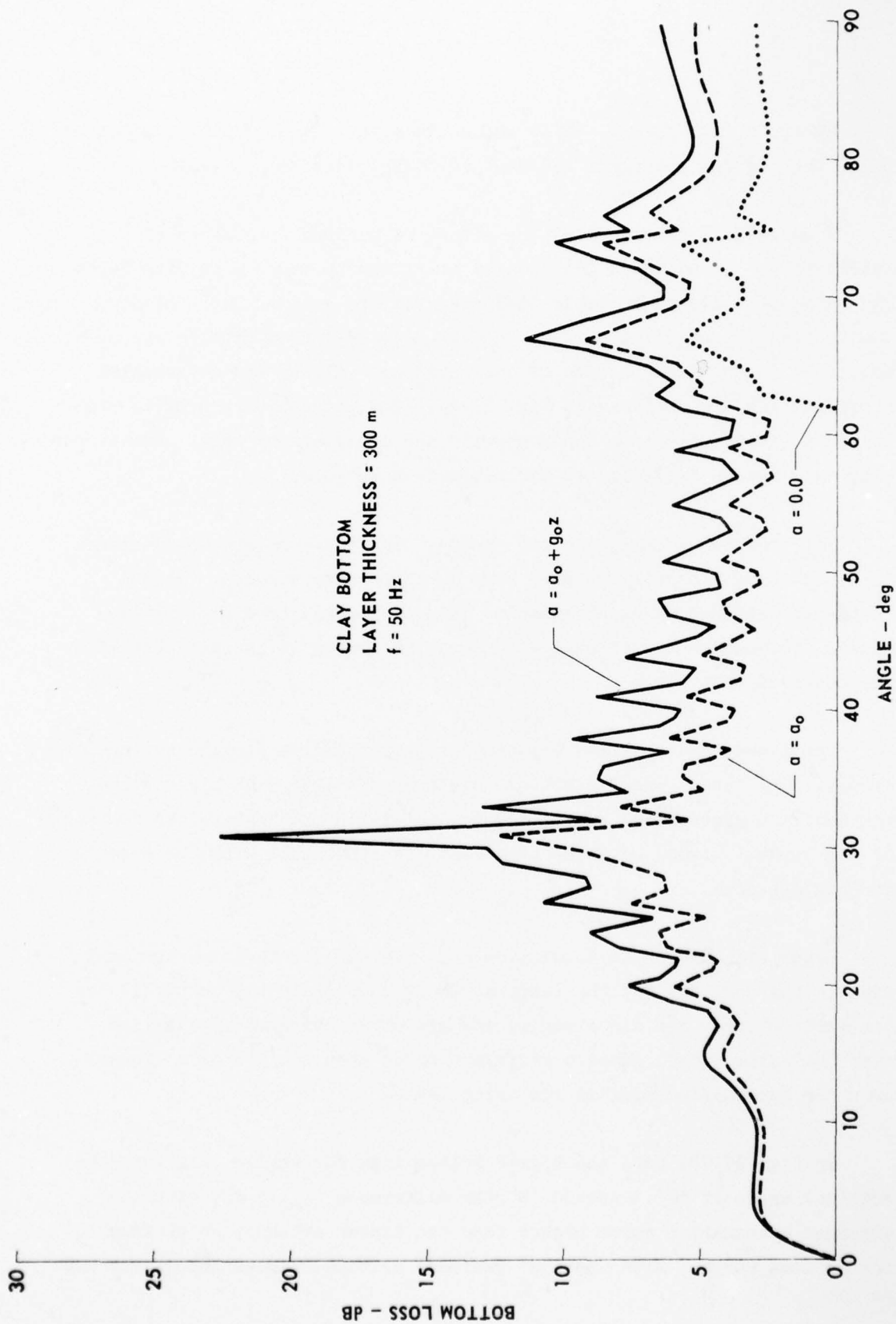
FIGURE II-21

BOTTOM LOSS CURVES FOR A SEDIMENT LAYER WITH INCREASING SOUND SPEED AND DENSITY

($\alpha \equiv$ ATTENUATION)

also apply to Fig. II-21. It is unfortunate that sound speed profiles below the top few meters of sediment are very often poorly known.

Figure II-22 demonstrates the effect of various treatments of attenuation. Sound speed and density are linearly increasing with depth. The parameters listed in Table II-1 are used for a layer depth of 300 m. The modified exponential profile and sound-speed-linked profile are described in the last section of this chapter. All of the attenuation profiles used are sketched in Fig. II-23. The pseudolinear profile contained a singularity at a shallow depth and could not be used. Hamilton's clay data region is indicated for comparison purposes.

The treatments fall into two groups. The constant and sound-speed-linked attenuation profiles give very much the same results. In the sound-speed-linked case, attenuation is proportional to c_o/c_z. This causes attenuation to decrease with depth and makes it inconsistent with the observed behavior.

The linear and modified exponential profiles give similar bottom loss curves. The linear profile bottom loss curve is 1 to 3 dB higher than the modified exponential profile curve, mainly in the higher loss regions of the curve. Either of these treatments is consistent with the current attenuation data.

Since attenuation is cumulative over the path of the compressional wave in the sediment and the penetration of waves into the bottom is determined by their incidence angle, the use of an averaged attenuation over the entire layer gives a different curve than the use of a linear or other attenuation profile for thick layers.

In Fig. II-24, note the higher bottom loss for angles less than the critical angle at 32°. Around 10° the difference is 1.5 dB, with the averaged attenuation curve higher than the linear attenuation profile bottom loss curve. After the 32° sediment critical angle, the linear and

-46-
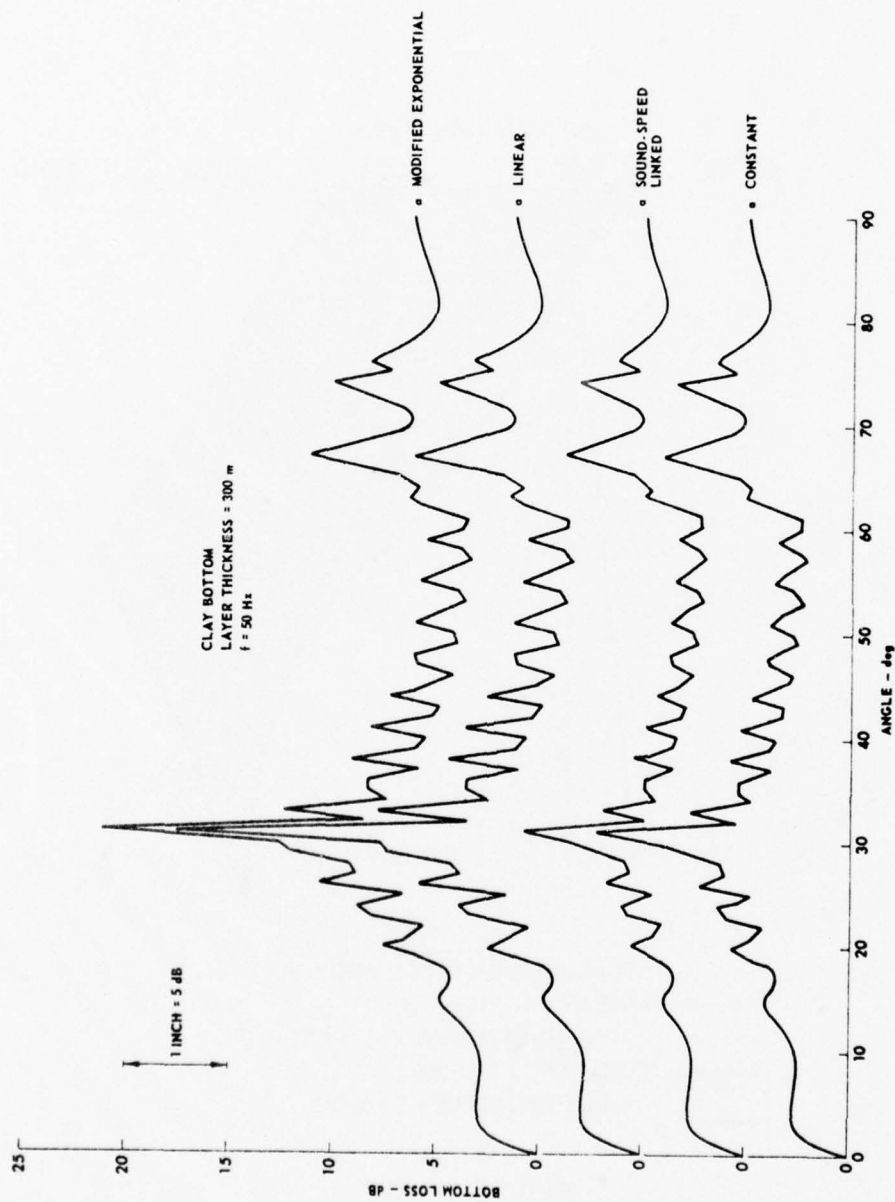
FIGURE II-22

COMPARISON OF BOTTOM LOSS CURVES FOR VARIOUS ATTENUATION PROFILES

(α = ATTENUATION)

CLAY BOTTOM
LAYER THICKNESS = 300 m
f = 50 Hz

ARL - UT
BS-77-128
WEW - DR
2 - 8 - 77
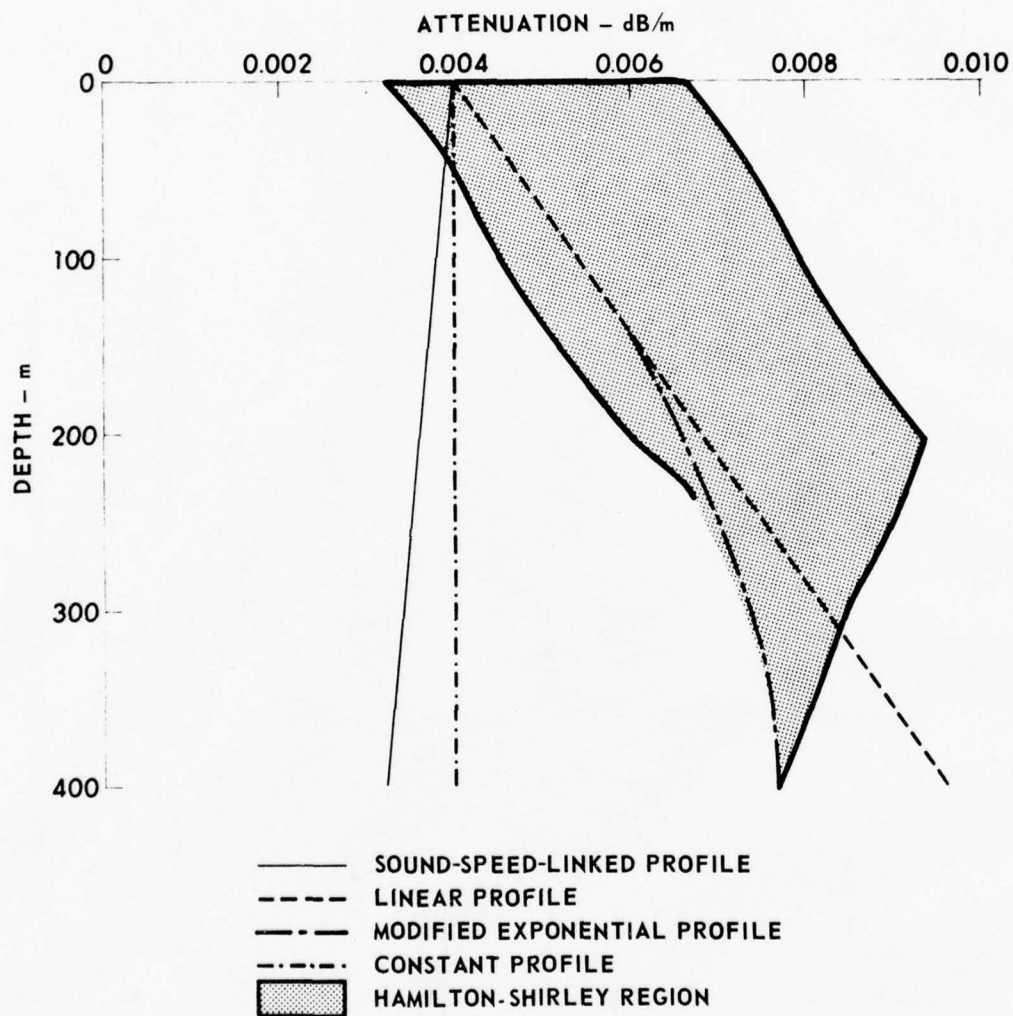
FIGURE II - 23
CLAY ATTENUATION PROFILES

CLAY BOTTOM
LAYER THICKNESS = 300 m
f = 50 Hz

$\alpha = \alpha_0 + g_0 z$

$\alpha = \alpha_0 = 0.04$

$\alpha = \dfrac{[\alpha(300) - \alpha_0]}{2}$

$= 0.0061$

ANGLE – deg
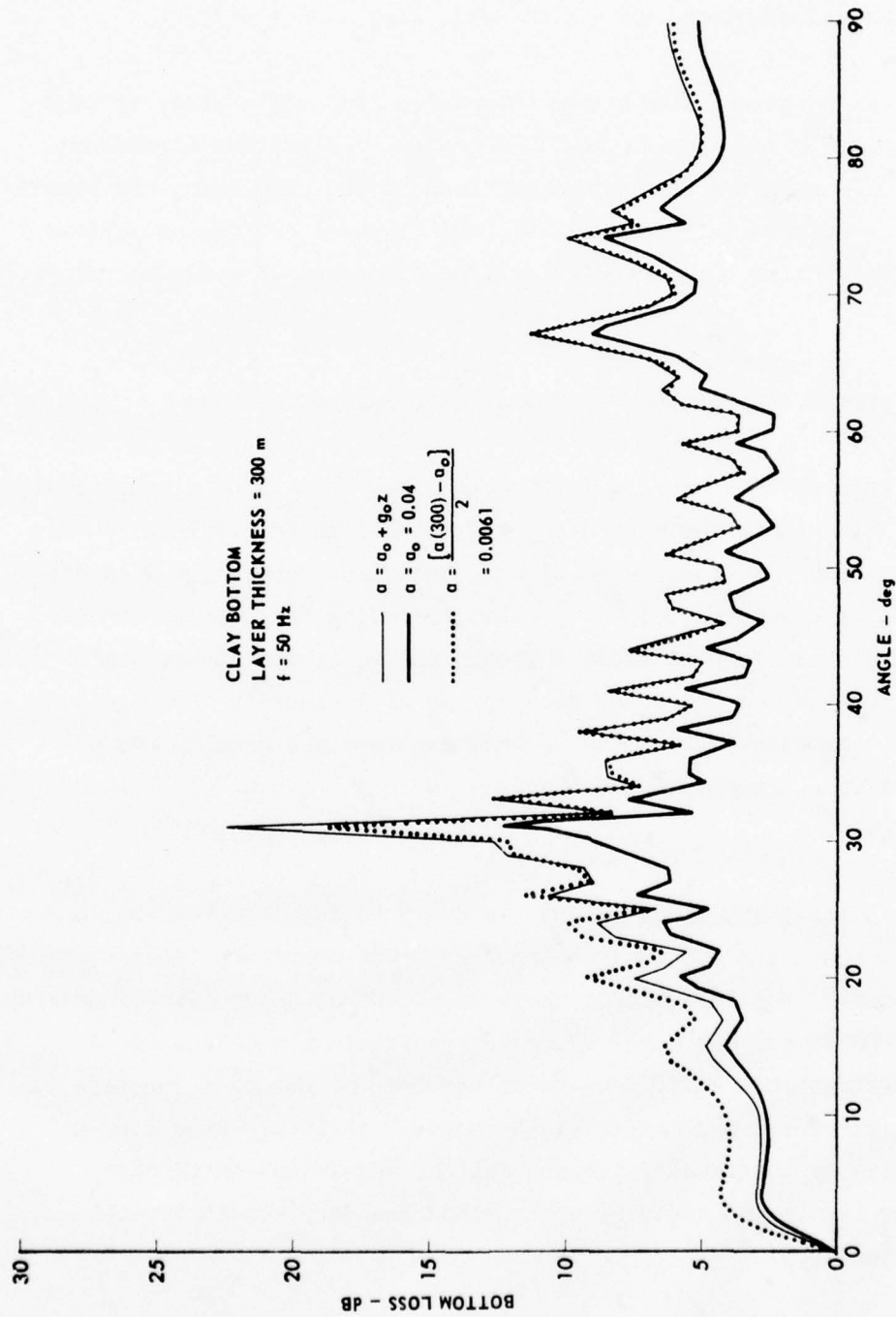
BOTTOM LOSS – dB

FIGURE II-24

COMPARISON OF BOTTOM LOSS CURVES FOR TWO CONSTANT ATTENUATION VALUES
AND A LINEARLY INCREASING ATTENUATION PROFILE

($\alpha \equiv$ ATTENUATION)

ARL - UT
AS - 77 - 130
WEW - DR
2 - 8 - 77

49

averaged attenuation profiles are nearly identical. The sound speed and
density values and gradients are as in Table II-1.

Further attenuation studies now in progress include a study of sand
bottoms, a study of the effects that the change of attenuation gradient
from positive to negative have on bottom loss in the clay case, and studies
of attenuation effects in more realistic multilayered bottoms of various
types. The results of these studies will be discussed in a future report.

C.   Sensitivity of Bottom Loss to Subbottom Density Gradients

The purpose of this section is to report the results of a sensitivity
study on the effects of sediment density gradients on bottom loss.   This
section is divided into four subsections. The first subsection will dis-
cuss theoretical treatments of the problem including the results obtained
from bottom loss models to support the conclusions of the theoretical
treatments. The second and third subsections will classify the magnitude
of the density gradient effects as to sediment type and grazing angle
regimes. The fourth subsection summarizes the results and conclusions
of this study.

In this sensitivity study it was necessary to adopt two models, one being
a bottom loss model and the other being a sediment structure (geoacoustic)
model. The model used to evaluate the bottom loss as a function of grazing
angle was BOTLOSS, a plane wave reflection coefficient model based on
numerical integration. BOTLOSS computes the bottom loss as a function
of grazing angle for a multilayer fluid sediment structure overlying a
solid substrate by numerically integrating the wave equation through
the different layers and applying appropriate boundary conditions at
the layer interfaces.

1.   Background

The wave equation in the jth subbottom layer when a density
gradient in the vertical direction is present is

$$\left[\nabla^2 + \Gamma_j(z) \; \frac{\partial}{\partial z} \right] P_j(x,y,z,t) = \frac{1}{c_j^2(z)} \frac{\partial^2}{\partial t^2} \; P_j(x,y,z,t),$$

where

$$\Gamma_j(z) = - \frac{d}{dz} \{ \ln \rho_j(z) \} \quad .$$

If $P_j(xzt)$ is expressed as

$$P_j(x,z,t) = e^{-i\omega t} \; e^{ik_o \cos\theta x} \; p_j(z) \quad ,$$

the following equation for $p_j(z)$ is obtained

$$\frac{d^2 p_j}{dz^2} \; (z) + \Gamma_j(z)\frac{dp_j}{dz} + \left[k_j^2(z) - k_o^2 \cos^2 \theta \right] p_j(z) = 0 \quad . \qquad (1)$$

The angle θ is the grazing angle at the boundary between the water and subbottom layers and k_o is the wave number in the water.

A useful form of Eq. (1) is obtained by reducing it to normal form. This is accomplished by writing $p_j(z)$ as

$$p_j(z) = \chi_j(z) \exp\left\{ -\frac{1}{2} \int_{z_o}^{z} \Gamma_j(z')dz' \right\} \quad ,$$

where z_o is an arbitrary reference depth.

If this equation is used in Eq. (1), the following differential equation for $\chi_j(z)$ is obtained,

$$\frac{d^2}{dz^2} \chi_j(z) + \left\{ k_j^2(z) - k_o^2 \cos^2 \theta - \frac{1}{4} \Gamma_j^2(z) - \frac{1}{2} \Gamma_j'(z) \right\} \chi_j(z) = 0 \quad ,$$

$$(2)$$

-51-

with

$$p_j(z) = \left[\frac{\rho_j(z)}{\rho_j(z_o)}\right]^{1/2} \chi_j(z) \quad . \tag{3}$$

An expression for the reflection coefficient in terms of the wave equation in the first subbottom layer, $p_1(z)$, may be obtained by an application of the continuity conditions at the water-sediment interface. This procedure yields

$$R = \frac{i\kappa_o - (\rho_o/\rho_1)(p'_1/p_1)_o}{i\kappa_o + (\rho_o/\rho_1)(p'_1/p_1)_o} \quad , \tag{4}$$

where $\kappa_o = k_o \sin\theta$, ρ_o is the water density, and ρ_1 is the density of the first subbottom layer at the water-sediment interface, i.e., z=0. Equations (2) through (4) will be used in the upcoming theoretical discussion. For details concerning the actual numerical solution of the wave equations and the boundary conditions, see Hawker and Foreman.[3]

The geoacoustic model used for the bottom in this sensitivity study is a simple one. The subbottom structure is modeled as a relatively thin fluid sediment layer (100 to 300 m) having a positive velocity gradient, overlying an isovelocity solid substrate half-space, in which the substrate is treated as a true solid supporting shear waves as well as compressional waves (see Fig. II-25). This layering structure models the abyssal plain environment reasonably well.

The examples used in this study will deal with three different sediment types: clay, silt, and sand. The acoustic parameters of the sediments that were used in BOTLOSS are listed in Table II-2.

A feeling for the effects of density gradients may be obtained by an examination of Eqs. (2) and (3).
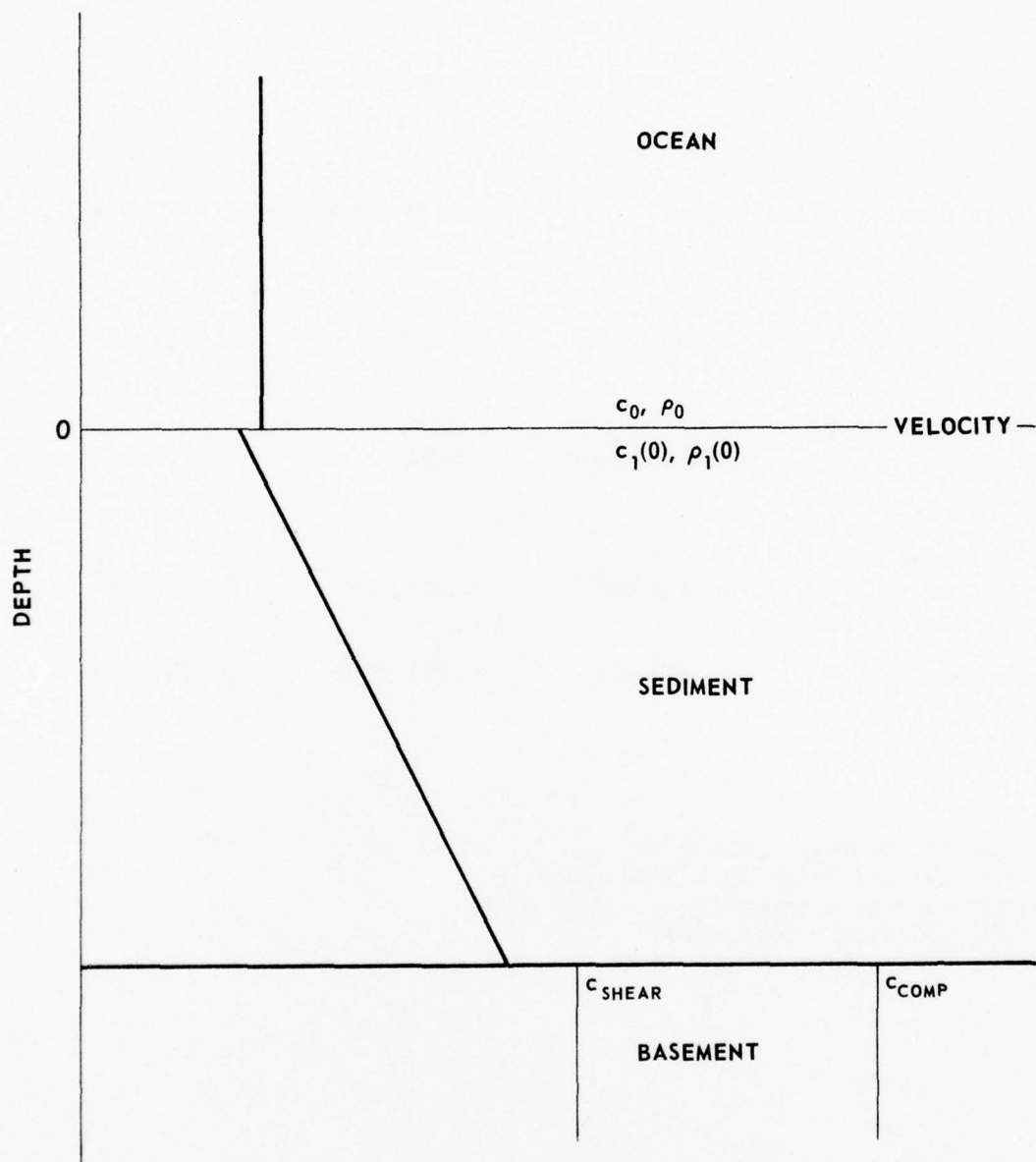
FIGURE II-25
LAYER CONFIGURATION AND VELOCITY STRUCTURE

TABLE II-2

SEDIMENT ACOUSTIC PARAMETERS

Water Density = 1.053 g/cm^3 Water Sound Velocity = 1540 m/sec

	Clay	Silt	Sand
Velocity at top of layer	1526.6 m/sec	1518.3 m/sec	1723.8 m/sec
Density at top of layer	1.27 g/cm^3	1.68 g/cm^3	2.08 g/cm^3
Attenuation	0.0029 dB/m	0.012 dB/m	0.024 dB/m

Substrate Density = 2.6 g/cm^3
Compressional Velocity = 5700 m/sec
Compressional Attenuation = 0.0015 dB/m
Shear Velocity = 2700 m/sec
Shear Attenuation = 0.01 dB/m

$$\frac{d^2}{dz^2}\kappa_j(z) + \left[\tilde{k}_j^2(z) - k_o^2 \cos^2\theta\right]\kappa_j(z) = 0$$

$$\tilde{k}_j^2(z) = k_j^2(z) - \frac{1}{4}\Gamma_j^2(z) - \frac{1}{2}\Gamma'_j(z)$$

$$p_j(z) = \left[\frac{\rho_j(z)}{\rho_j(z_o)}\right]^{1/2} \chi_j(z) \quad .$$

Equation (2) reveals that one effect of a density gradient is to alter the sound speed profile from $c_j(z)$ to $\tilde{c}_j(z)$, where

$$\tilde{c}_j(z) = \omega \left[k_j^2(z) - \frac{1}{4}\Gamma_j^2(z) - \frac{1}{2}\Gamma_j'(z)\right]^{-1/2} \quad .$$

Thus a positive density gradient causes $c_j(z)$ to increase relative to the case $\rho'_j = 0$. Hence, a positive density gradient will introduce additional refractive effects beyond those caused by a positive sound speed gradient. This modification to the sound speed profile, however, is very small for the values of ρ'/ρ expected to be encountered in the ocean.

A very simple estimate of the effect of a density gradient on the sound speed profile may be made on the basis of a model in which $c_j(z)$ is assumed constant and $\rho_j(z)=\rho(0) e^{\gamma z}$ with $\gamma>0$. In this case $\Gamma_j(z)=-\gamma$ and $\Gamma_j'(z)=0$. Hence, $\tilde{c}_j(z)=\omega[k_j^2-\gamma^2/4]^{-1/2}=c_j[1-\gamma^2/4k_j^2]^{-1/2}$. Typical values of ρ'/ρ in deep sea sediments would be on the order of 10^{-3} m^{-1} (see Hamilton[7,8]). Hence, $\gamma^2/4\,k_j^2=(\gamma c/4\pi f)^2 \leq 1.5\times10^{-2}/f^2$. Therefore, for frequencies above 10 Hz, $\gamma^2/4k_j^2 \ll 1$; this implies that such a modification would be negligible.

A higher order density gradient effect is seen in Eq. II-3. Equation II-3 indicates that an added modification introduced by the density gradient

-55-

is through the multiplicative factor $[\rho(z)/\rho(z_o)]^{1/2}$. This multiplicative factor represents a modification to the pressure field that increases with depth in the presence of a positive density gradient. This factor, although usually not too different from 1, does represent an effect of higher order than the modification introduced into the velocity profile.

The two modifications just discussed are due to added terms in the wave equation which are present when density gradients are considered. Another "hidden effect" arises from the boundary conditions that the pressure wave function must satisfy across layer boundaries. When the density is variable, it is only the densities at the interfaces which are used in the continuity conditions. Since the interface reflection and transmission coefficients are dependent upon the density ratios across the interface, it does not seem unlikely that this "hidden effect" can be dominant in many circumstances. Later in this section some examples will be given showing that the effect of a density gradient can be handled quite adequately by using interface densities in the boundary conditions.

Since the models used in this investigation explicitly assume positive sound speed gradients, it is convenient to consider low grazing angle and high grazing angle density effects separately. In the low angle region where refractive effects keep the incident energy away from the substrate, the density gradient effects will be mainly due to the presence of the density gradient in the wave equation. In the high angle regions where significant energy encounters the bottom, it is expected that the hidden "boundary condition effects" will become dominant.

2. Low Grazing Angle Effects

To derive an expression which is useful in the low angle region and indicates the effect of a density gradient on the magnitude of the reflection coefficient, it is necessary to adopt a tractable mathematical model. The following development will consider a two half-space problem.

The first half-space will be isovelocity and the second will be explicitly assumed to have a positive velocity gradient and an exponential density variation given by $\rho(z)=\rho(z_o) e^{\gamma z}$. The reason that this model is expected to work reasonably well for the current sediment model is that, at low angles, rays incident on the bottom have shallow turning depths due to velocity gradients. These turning depths are usually shallow enough such that the exponential density variation is essentially linear and the substrate at deeper depths is effectively absent from the problem.

Consider two half-spaces, the upper being isovelocity with a sound speed and density of c_o and ρ_o and the lower having an arbitrary positive velocity gradient and an exponential density variation $[\rho(z)=\rho(z_o) e^{\gamma z}]$. This being the case, the pressure variation with depth in the lower layer is given by

$$p_1(z) = \left[\frac{\rho_1(z)}{\rho_1(0)}\right]^{1/2} \chi_1(z) = e^{\gamma z/2} \chi_1(z) \quad , \quad (5)$$

where $\chi_1(z)$ satisfies

$$\left[\frac{d^2}{dz^2} + k_1^2(z) - k_o^2 \cos^2\theta - \frac{\gamma^2}{4}\right] \chi_1(z) = 0 \quad ,$$

with $k_1(z) = \omega/c_1(z)$ and $k_o = \omega/c_o$. From Eq. (5) it follows that

$$\frac{p_1'(z)}{p_1(z)} = \frac{\gamma}{2} + \frac{\chi_1'(z)}{\chi_1(z)} \quad . \quad (6)$$

Using Eq. (6) in Eq. (4) the reflection coefficient may be expressed as

$$R = \frac{i\kappa_o - \frac{\alpha\gamma}{2} - \alpha \left.\frac{\chi_1'}{\chi_1}\right|_{z=0}}{i\kappa_o + \frac{\alpha\gamma}{2} + \alpha \left.\frac{\chi_1'}{\chi_1}\right|_{z=0}} \quad (7)$$

with $\alpha = \rho_o/\rho_1(0)$ and $\kappa_o = k_o' \sin \theta$.

A first order treatment of Eq. (7) consists of neglecting the effect of the density variation on the velocity profile, that is,

$$R \simeq \frac{i\kappa_o - \frac{\alpha\gamma}{2} - \alpha \left. \frac{x_1'(0)}{x_1(0)} \right|_{z=0}}{i\kappa_o + \frac{\alpha\gamma}{2} + \alpha \left. \frac{x_1'(0)}{x_1(0)'} \right|_{z=0}}$$

where $x_1(0)(z)$ satisfies

$$\left[\frac{d^2}{dz^2} + k_1^2(z) - k_o^2 \cos^2 \theta \right] x_1(0)(z) = 0 \quad .$$

The expression for R may now be written as

$$R \simeq \frac{N_o - \frac{\alpha\gamma}{z}}{D_o + \frac{\alpha\gamma}{z}} \quad ,$$

where

$$N_o = i\kappa_o - \alpha \, x_1'(0)/x_1(0) \big|_{z=0} \quad .$$

The expression for R may now be written as

$$R \simeq \frac{N_o}{D_o} \frac{[1 - \frac{\alpha\gamma}{2N_o}]}{[1 + \frac{\alpha\gamma}{2D_o}]} = R_o \frac{[1 - \frac{\alpha\gamma}{2N_o}]}{[1 + \frac{\alpha\gamma}{2D_o}]} \quad , \tag{8}$$

where R_o is the reflection coefficient when $\rho_1'(z)=0$.

Since γ is in general very small, it is possible to approximate the squared

magnitude of R as follows

$$|R|^2 \simeq |R_o|^2 \left\{ \frac{1 - \dfrac{\alpha\gamma}{|N_o|^2} Re(N_o) + 0(\gamma^2)}{1 + \dfrac{\alpha\gamma}{|D_o|^2} Re(D_o) + 0(\gamma^2)} \right\}$$

$$|R|^2 \simeq |R_o|^2 \left\{ \left(1 - \frac{\alpha\gamma}{|N_o|^2} Re(N_o)\right) \left(1 - \frac{\alpha\gamma\, Re(Do)}{|D_o|^2} + 0(\gamma^2)\right) \right\}$$

$$|R|^2 \simeq |R_o|^2 \left\{ 1 - \alpha\gamma Re(N_o)\left[\frac{1}{|D_o|^2} - \frac{1}{|N_o|^2}\right] + 0(\gamma^2) \right\} \quad , \qquad (9)$$

where the last step uses

$$Re(N_o) = -Re(D_o)$$

and

$$|R_o| = \frac{|N_o|}{|D_o|} \leq 1 \quad .$$

The real part of N_o is related to the reflection coefficient R_o as follows:

$$Re(N_o) = \frac{-2\kappa_o |R_o| \sin \Phi}{[1 + |R_o|^2 + 2|R_o| \cos \Phi]} \quad ,$$

where $|R_o = |R_o| e^{i\Phi} \quad .$

Therefore,

$$|R|^2 \simeq |R_o|^2 \{1 + \beta \sin \Phi\} \quad , \qquad (10)$$

where

$$\beta = \left\{ \frac{2\alpha\gamma\kappa_o |R_o|}{1 + |R_o|^2 + 2|R_o| \cos \Phi} \right\} \left(\frac{1}{|N_o|^2} - \frac{1}{|D_o|^2}\right) > 0 \quad .$$

-59-

Equation (10) indicates that the direction of the shift in $|R|$ due to a density gradient is controlled by the sign of the phase of the reflection coefficient for $\rho'(z)=0$. To see this effect, consider a 100 m clay layer with a constant sound speed gradient of 1 sec^{-1} overlying a rock substrate. The parameters for the rock and clay are listed in Table II-2. Figure II-26 depicts bottom loss curves for this clay layer for three different values of constant density gradient, $\rho'=(0, 0.001, and 0.002)$ $(g/cm^3)/m$. Since only rays encountering the bottom at grazing angles greater than $18.78°$ will encounter the substrate, the above derived results should be valid in the small grazing angle region. Figure II-27 depicts the typical phase behavior of the reflection coefficient for a 100 m clay layer for $\rho'=0$. This figure shows that the phase approaches $-\pi$ through the third quadrant as θ goes to zero. Hence, Eq. (10) indicates that

$$|R|^2 < |R_o|^2 \text{ as } \theta \to 0 \quad .$$

Since bottom loss is defined as $BL = -20 \log |R|$, it follows that

$$BL(|R|) > BL(|R_o|) \text{ as } \theta \to 0 \quad .$$

This is precisely the behavior of Fig. II-26 for small θ. Figures II-28 and II-29 depict bottom loss curves for silt and sand layers overlying rock substrate. The phase of R_o for these sediments behave similarly to that of clay; hence as $\theta \to 0$, $BL(R) > BL(R_o)$. Although Figs. II-28 and II-29 do not clearly show it, this is actually the case. The differences are so small, however, that they could not be resolved on the plotter. Needless to say, in the absence of subbottom reflectors, the effects of a density gradient are negligibly small.

3. Boundary Condition Effects

It is important to remember that the effects just described are due to the changes in form of the wave equation itself, i.e., the presence
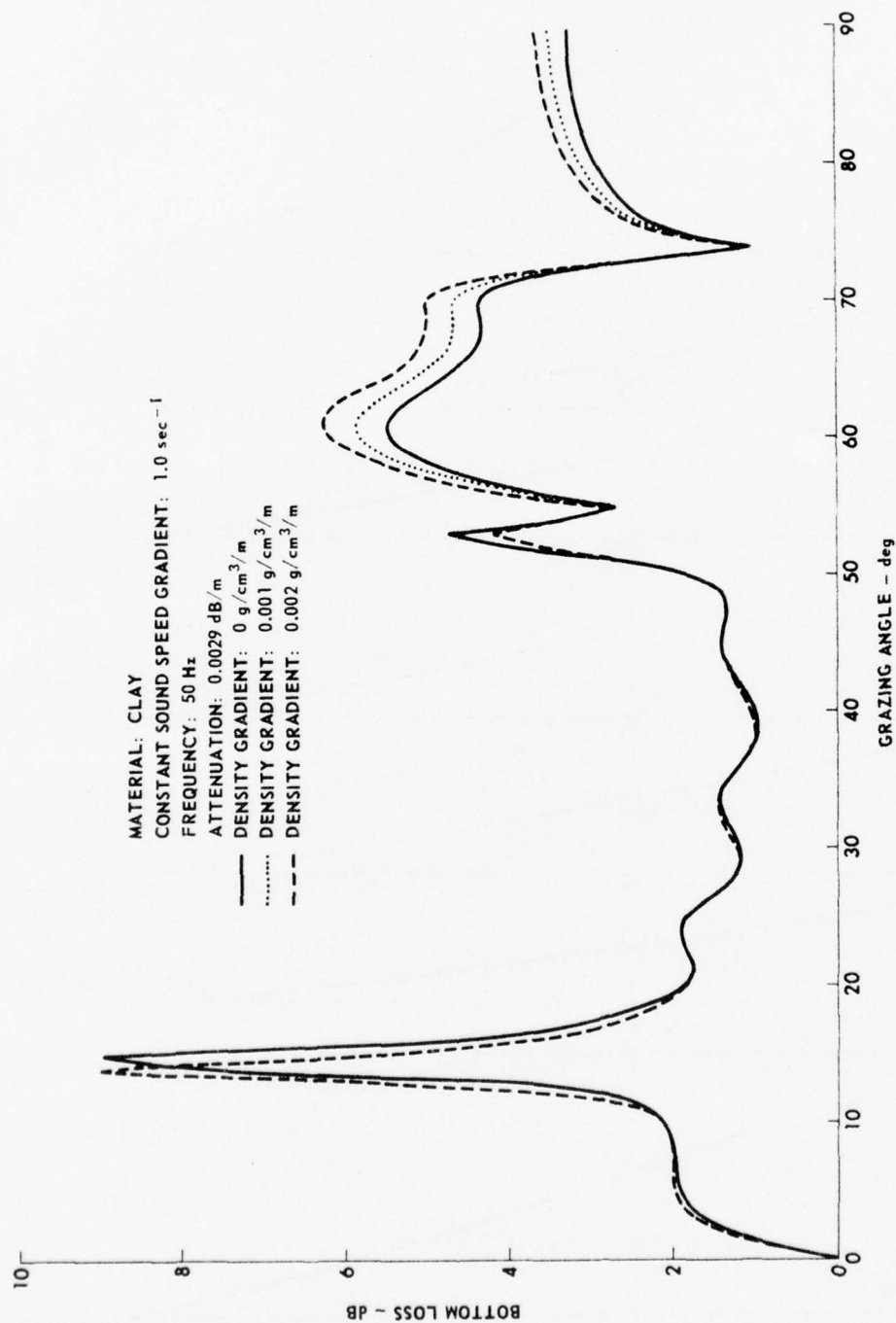
FIGURE II-26

BOTTOM LOSS versus GRAZING ANGLE FOR A 100 m CLAY
SEDIMENT LAYER OVERLYING A ROCK SUBSTRATE

MATERIAL: CLAY
CONSTANT SOUND SPEED GRADIENT: 1.0 sec^{-1}
FREQUENCY: 50 Hz
ATTENUATION: 0.0029 dB/m
DENSITY GRADIENT: 0 g/cm^3/m
DENSITY GRADIENT: 0.001 g/cm^3/m
DENSITY GRADIENT: 0.002 g/cm^3/m

ARL - UT
AS-77-25
SRR - DR
1 - 17 - 77

61
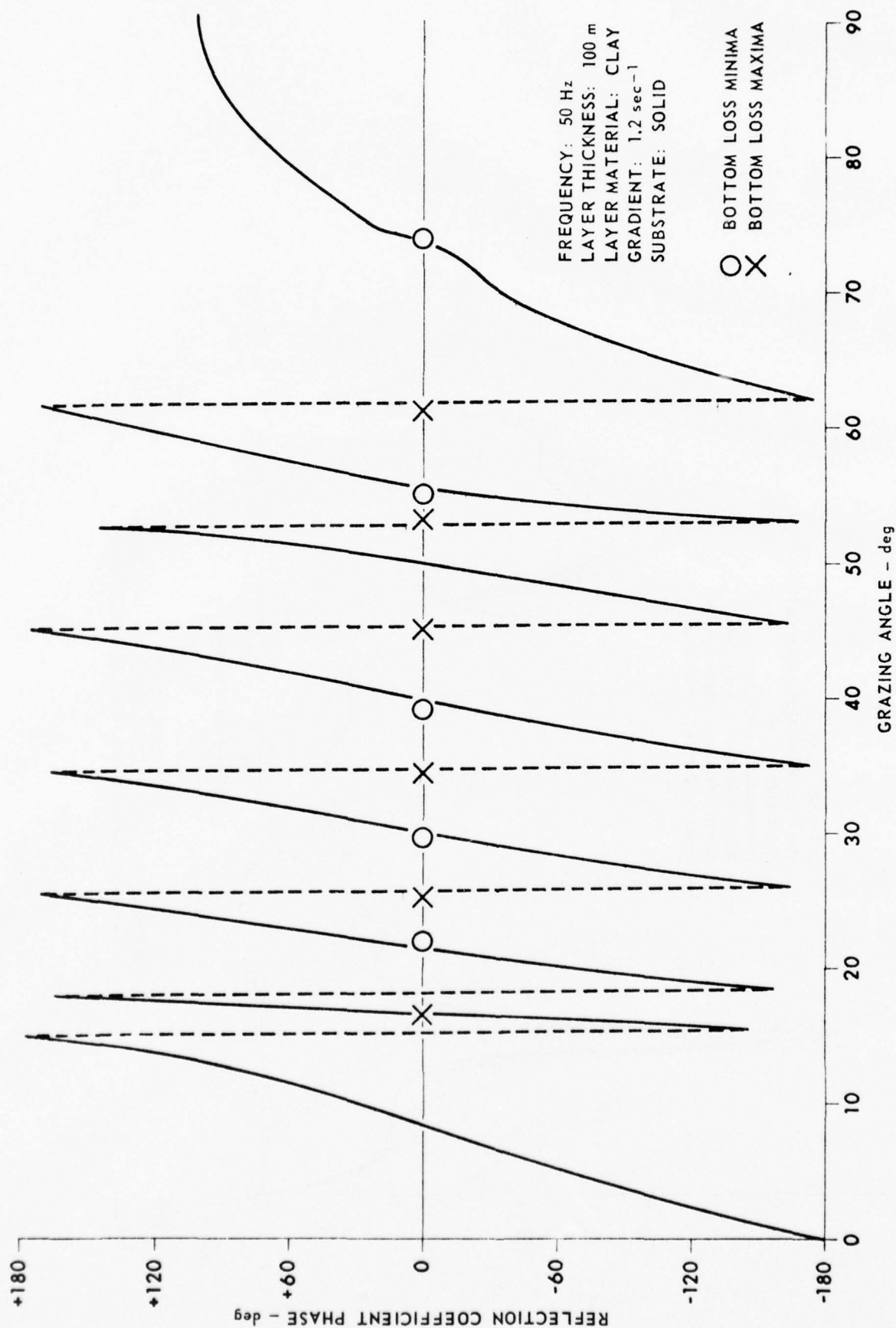
FIGURE II-27

REFLECTION COEFFICIENT PHASE versus GRAZING ANGLE
FOR A SOLID SUBSTRATE

FREQUENCY: 50 Hz
LAYER THICKNESS: 100 m
LAYER MATERIAL: CLAY
GRADIENT: 1.2 sec^{-1}
SUBSTRATE: SOLID

O BOTTOM LOSS MINIMA
X BOTTOM LOSS MAXIMA

GRAZING ANGLE – deg

REFLECTION COEFFICIENT PHASE – deg

MATERIAL: SILT
CONSTANT SOUND SPEED GRADIENT: 1.0 sec⁻¹
FREQUENCY: 50 Hz
ATTENUATION: 0.012 dB/m
DENSITY GRADIENT: 0 g/cm³/m
DENSITY GRADIENT: 0.001 g/cm³/m
DENSITY GRADIENT: 0.002 g/cm³/m
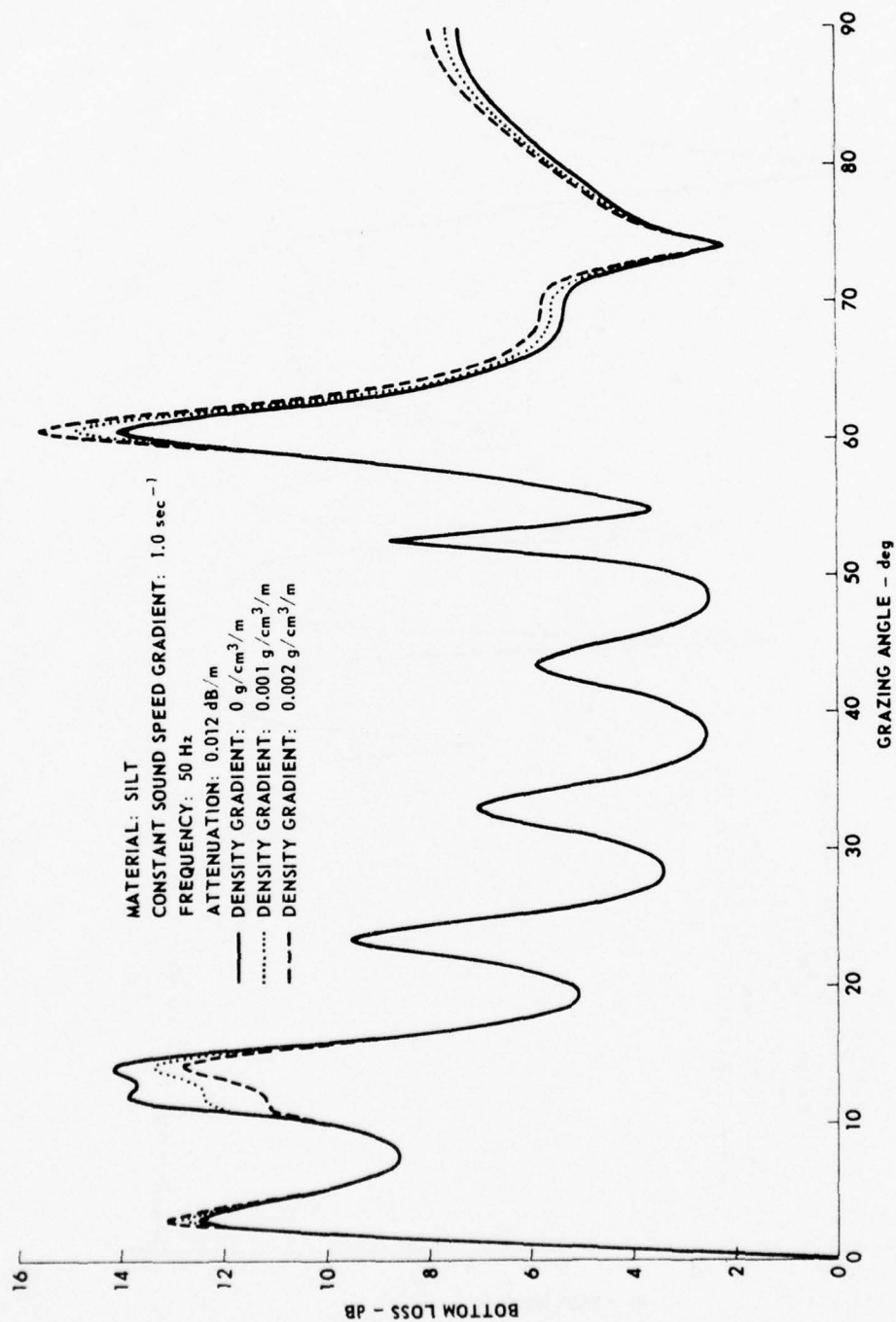
FIGURE II-28
BOTTOM LOSS versus GRAZING ANGLE FOR A 100 m SILT
SEDIMENT LAYER OVERLYING A ROCK SUBSTRATE

ARL - UT
AS - 77 - 24
SRR - DR
1 - 17 - 77

63

MATERIAL: SAND
CONSTANT SOUND SPEED GRADIENT: 1.0 sec^{-1}
FREQUENCY: 50 Hz
ATTENUATION: 0.024 dB/m
—— DENSITY GRADIENT: 0 g/cm^3/m
- - - DENSITY GRADIENT: 0.002 g/cm^3/m
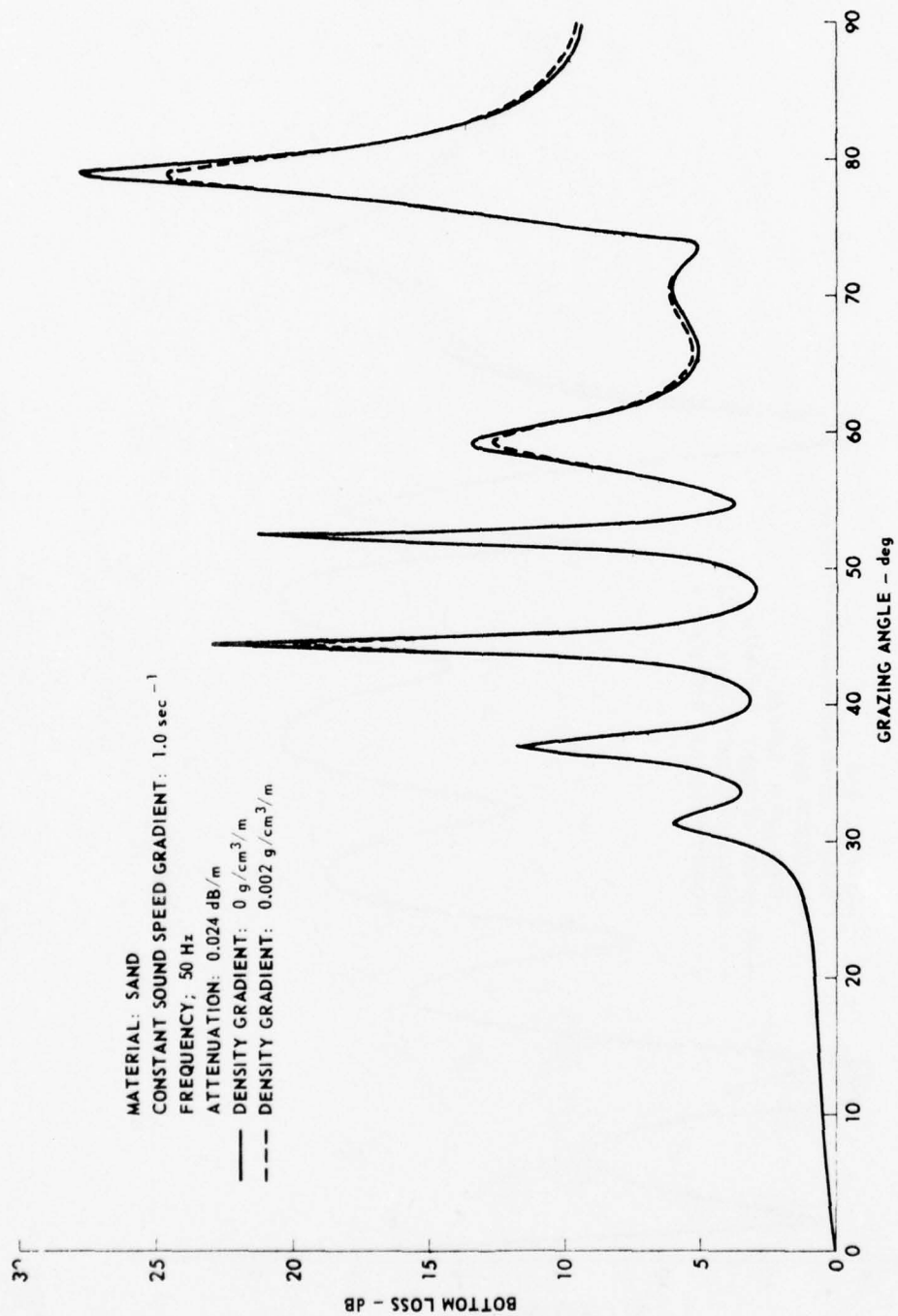
FIGURE II-29
BOTTOM LOSS versus GRAZING ANGLE FOR A 100 m SAND
SEDIMENT LAYER OVERLYING A ROCK SUBSTRATE

ARL - UT
AS - 77 - 23
SRR - DR
1 - 17 - 77

64

of terms in the wave equation involving the density gradient. The indirect effect due to altered boundary conditions is to be considered next.

How a density gradient affects the bottom loss at larger grazing angles may be understood by considering the changes of impedance at subbottom reflecting horizons, specifically the rock substrate in the cases considered here. In general, since rock density is usually higher than sediment densities, the effect of a positive density gradient is to increase the impedance matching across a sediment-rock interface. This increased impedance matching, in turn, enhances the transmission into the substrate which, in turn, increases the loss. This effect will begin when waves impinge upon the substrate at near the shear wave critical angle since, in this region, transmission into the substrate becomes non-negligible.

For the clay, silt, and sand examples being considered, the bottom angles corresponding to the shear wave critical angle and the compressional wave critical angle are 55.22° and 74.33°, respectively. Figures II-26 and II-28 show the expected results, i.e., higher bottom loss in the presence of density gradients above 55.22°.

Figure II-29 for sand shows the same general features above the shear wave critical angle with the exception of the peaked regions at about 60° and 78°. In these regions the bottom loss for $\rho' \neq 0$ is less than for $\rho'=0$. Sand is different from clay and silt in that it has higher attenuation and it is a high speed bottom exhibiting a critical angle effect. It seems possible that some coupling between the attenuation and density gradient might be responsible for the deviation around 78°.

Figure II-30 depicts the bottom loss for sand using an attenuation reduced by an order of magnitude. With the exception of the region around 60°, the effect has been reversed and is now similar to a silt or clay. The interplay between ρ' and attenuation and the nature of the reversal effect at 60° are topics for further consideration.

MATERIAL: SAND

CONSTANT SOUND SPEED GRADIENT: 1.0 sec^{-1}

FREQUENCY: 50 Hz

ATTENUATION: 0.0024 dB/m

———— DENSITY GRADIENT: 0 gr/cm^3/m

– – – – DENSITY GRADIENT: 0.002 gr/cm^3/m
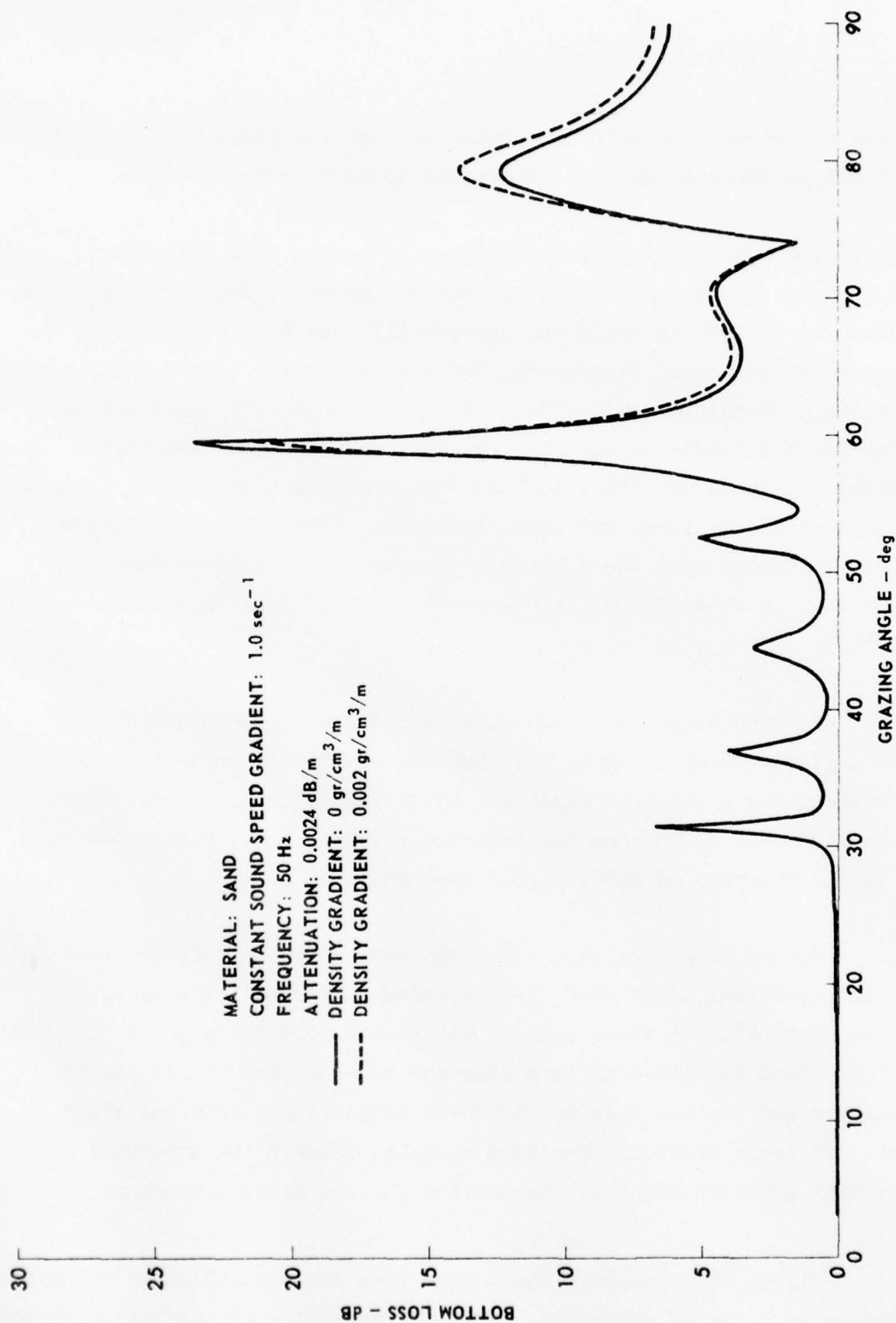
FIGURE II-30

BOTTOM LOSS versus GRAZING ANGLE FOR A 100 m, LOW ATTENUATION
SAND SEDIMENT LAYER OVERLYING A ROCK SUBSTRATE

ARL - UT
AS - 77 - 112
SRR - DR
1 - 31 - 77

66

To test the hypothesis that the density gradient can be handled
to a good approximation by considering only boundary condition effects,
the clay bottom loss was redetermined neglecting the effect of the density
gradient on the wave equation. In other words, the pressure variations
throughout the clay layer were calculated numerically as if $\rho'=0$ whereas
the boundary conditions to be satisfied were specified assuming a nonzero
density gradient. The bottom loss computed with this pressure function
was then compared to that computed with the pressure field calculated
with a full treatment of the density gradient. The results of this
comparison for $\rho'=0.002$ $(g/cm^3)/m$ were excellent. In the low angle region
($0°$ to $10°$) where boundary condition effects are expected to be unimportant,
the most deviation was noted; the average deviation in the bottom loss was
0.05 ± 0.03 dB. In the higher angle regions ($20°$ to $90°$) where the boundary
effects are important, the differences were less and were too small to be
graphically displayed. The average deviation in bottom loss was
0.01 ± 0.008 dB. The angular region from $10°$ to $20°$ was excluded because
of the anomalous behavior in this region. (The large peak at about $14°$
is due to the excitation of a Stoneley wave.)

Several dominant features are apparent in the previously
mentioned bottom loss curves, e.g., the prominent peaks at low angles
for silt and clay and the peak at about $53°$ in clay. The peak in clay
bottom loss at $53°$ is associated with the excitation of a Rayleigh wave.
A Rayleigh wave is an interface wave which exists ideally at the free
surface of a solid. The enhancement of this peak when $\rho'=0$ is consistent,
since, in this situation, the sediment density above the substrate is
lower and the substrate boundary more closely approaches a free surface.
This Rayleigh wave peak is also present in silt although its magnitude
does not show the sensitivity to ρ' that clay does. This is likely related
to the fact that silt attenuation is much higher than it is in clay.

The low angle peak at about $14°$ in clay has been previously
identified as due to excitation of a Stoneley wave (Hawker[9]). A Stoneley
wave is an interface wave excited on the surface of a solid. Figure II-26

shows that a density gradient tends to shift the location of the Stoneley wave peak. The abovementioned procedure of using only interface densities to treat a density gradient was able to account for the shift in peak location. It is expected that further work relating this shift to density gradients and other sediment parameters will be done.

The bottom loss curve for silt shown in Fig. II-28 has a feature which resembles a Stoneley wave peak at about 14°. This feature is not, however, due to excitation of a Stoneley wave since the feature remains intact when the substrate is treated as a liquid. This feature has an interesting behavior in that its prominence decreases with increasing ρ', whereas its location remains unchanged. The nature of this feature in silt is a topic for further consideration in future research.

4.   Conclusions

A survey of Figs. II-26, II-28, and II-29 indicates that, in general, the density gradient affects clay the most, silt to a lesser degree, and sand to the least degree. With the exception of the low angle ($\cong 14°$) anomalous behavior of silt and clay, the nonnegligible effects are in the higher grazing angle regions. Since the effects in this region are "boundary effects," it seems likely that the relative magnitude of the density gradient effect should be related to the fractional change of impedance at the substrate interface when density gradients are present relative to the impedance in the absence of a density gradient.

Table II-3 shows the values of the sediment characteristic impedances just above the rock substrate for 100 m clay, silt, and sand layers having sound velocity gradients of $1 \sec^{-1}$. The numbers in parentheses are the percent differences of the impedances for $\rho'=0.0001$ and 0.002 relative to $\rho'=0$. The trend of these ratios indicates a larger relative effect for clay, followed by silt, and then sand. This trend is borne out in the bottom loss model results. For $\rho'=0.002$ (g/cm)/m, the percent differences in bottom loss for the clay, silt, and sand layers in the angular range of 55° to 90° relative to $\rho'=0$ were 12.5%, 7.0%, and 3%,

-68-

TABLE II-3

SEDIMENT CHARACTERISTICS IMPEDANCES EVALUATED JUST
ABOVE THE SUBSTRATE

	Sand kg/(m²·sec)	Silt kg/(m²·sec)	Clay kg/(m²·sec)
$\rho' = 0 \ (g/cm^3)/m$	3.79×10^6	2.72×10^6	2.06×10^6
$\rho' = 0.001 \ (g/cm^3)/m$	$3.98 \times 10^6 \ (4.8\%)$	$3.88 \times 10^6 \ (5.9\%)$	$2.23 \times 10^6 \ (7.3\%)$
$\rho' = 0.002 \ (g/cm^3)/m$	$4.16 \times 10^6 \ (9.6\%)$	$3.04 \times 10^6 \ (11.9\%)$	$2.39 \times 10^6 \ (15.7\%)$

sediment sound speed gradient = $1 \ sec^{-1}$

sediment layer thickness = 100 m

respectively. While the absolute validity of this procedure might be suspect, especially in the light of a possible coupling between ρ' and other subbottom parameters, it does seem to provide a simple method of gauging the density gradient effects.

In the low angle region, which is actually of more interest in long range propagation studies, there is little that can be said about density gradient effects on a sediment-by-sediment basis. In this region the effects are usually buried in the wave equation and are not easily determined except near $\theta=0°$.

It is worth emphasizing at this point that the density gradient effects, whether in the high or low angle regions, are small effects. In fact, one goal of this and future research is to determine whether it is ever necessary to account for the density gradient, i.e., is the effect of a density gradient ever more than negligible? Since only three sediment types and one layering configuration were studied here, it is too soon to draw firm conclusions. However, based on the results quoted here, it is possible to make a few observations.

In the high angle region, the variations due to introduction of a density gradient, in general, occur over a wider angular range, as opposed to variations in narrow peaked regions in the low angle range. Hence, the potential for causing noticeable effects on propagation in the water column are the greatest. It seems likely, however, that there might be other effects which tend to counter this potential; one such effect is sediment thickness. As the sediment layer becomes thicker, it is conceivable that the added attenuation loss might tend to reduce the relative density gradient effect.

Another factor which tends to lessen the effect of density gradients in the high angle region is the diminishing importance of the high grazing angles in long range propagation studies.

In the low angle region (less than 20°) the examples considered in this study tend to show that the only time a density gradient might be

significant is when it is associated with some sort of anomalous behavior such as interface waves, intromission angles, etc. Since these anomalies tend to be fairly narrow in width, it is uncertain as to whether the effects due to density gradients would ever be noticeable at these angles.

D.   Additional Bottom Loss Studies

In addition to the studies reported in the first three sections of this chapter, various associated studies were carried out during this contract year. This section summarizes briefly some of the principal results found in the studies of hidden depth and the sensitivity of bottom loss variations in sediment type. Both of these subjects have been reported in detail by Hawker, Focke, and Anderson.[2]

1.   Hidden Depth Studies

Although the concept of a hidden depth intuitively appears to be clear, a more precise and quantitative definition will be required if specific results are to be obtained.

One approach to the problem is via mode theory, with the hidden depth defined as the depth below which the fractional change in the eigenvalues, caused by the introduction of a perfect reflector, is less than a specified tolerance. This approach necessitates specifying which modes are to be considered and therefore is not independent of the propagation geometry. This approach is the one taken by Williams[12] in his investigation of hidden depths.

An alternative approach, and the one adopted in this study, is to define the hidden depth in terms of the fractional change in the bottom loss caused by the introduction of a perfect reflector at some depth. When this change is less than a certain tolerance, the hidden depth has been reached. Here again some elements of the propagation geometry are hidden since the grazing angle, or angular interval, must be specified.

-71-

Also, in addition to the freedom to choose the tolerance, there is the possibility of modifying the definition to examine the difference between a normal sediment column and one with an absorber underneath, or perhaps the difference between the reflector and absorber cases. The most extreme contrast is obtained by comparing situations in which a column of sediment overlays alternately a perfect reflector and a perfect absorber. This definition will be adopted in this report. That is, the hidden depth, Z_H, is defined as the depth at which a reflector and then an absorber can be inserted in the sediment such that $\Delta(Z_H) = |20 \log (|R|_{Reflection}/|R|_{Absorber})| \le \epsilon$ where $|R|$ is the modulus of the plane wave reflection coefficient and ϵ is the tolerance. Investigation has shown that the precise nature of the comparison cases is not of great importance and the results would be little changed if the definition were somewhat altered.

In the remainder of this subsection we shall examine the hidden depth problem for two sediment types, a fine clay and a coarse silt. The clay sediment has a density ratio (relative to sea water) of 1.206, a sound speed ratio of 0.991, and a porosity of 87%. The silt sediment has a density ratio of 1.595, a sound speed ratio of 0.986, and a porosity of 63%. The frequency was chosen to be 50 Hz; at this frequency the attenuations were 0.00285 dB/m for clay and 0.012 dB/m for silt. The sediment properties and their relationship to porosity follows the work of Hamilton.[7]

Figures II-31 through II-33 show the bottom loss versus grazing angle versus layer thickness for a clay layer overlying a perfectly reflecting surface. These bottom loss curves, as well as all others appearing in this report, were computed using the bottom loss model developed at ARL:UT by Hawker and Foreman.[3] The sound speed profile was assumed to be linear $C(z)=C(0)+gz$, and the gradients g are 0.5 sec^{-1}, 1.0 sec^{-1}, and 1.5 sec^{-1} in the three figures. This range of sound speed gradients includes those most commonly found in deep ocean sediments.
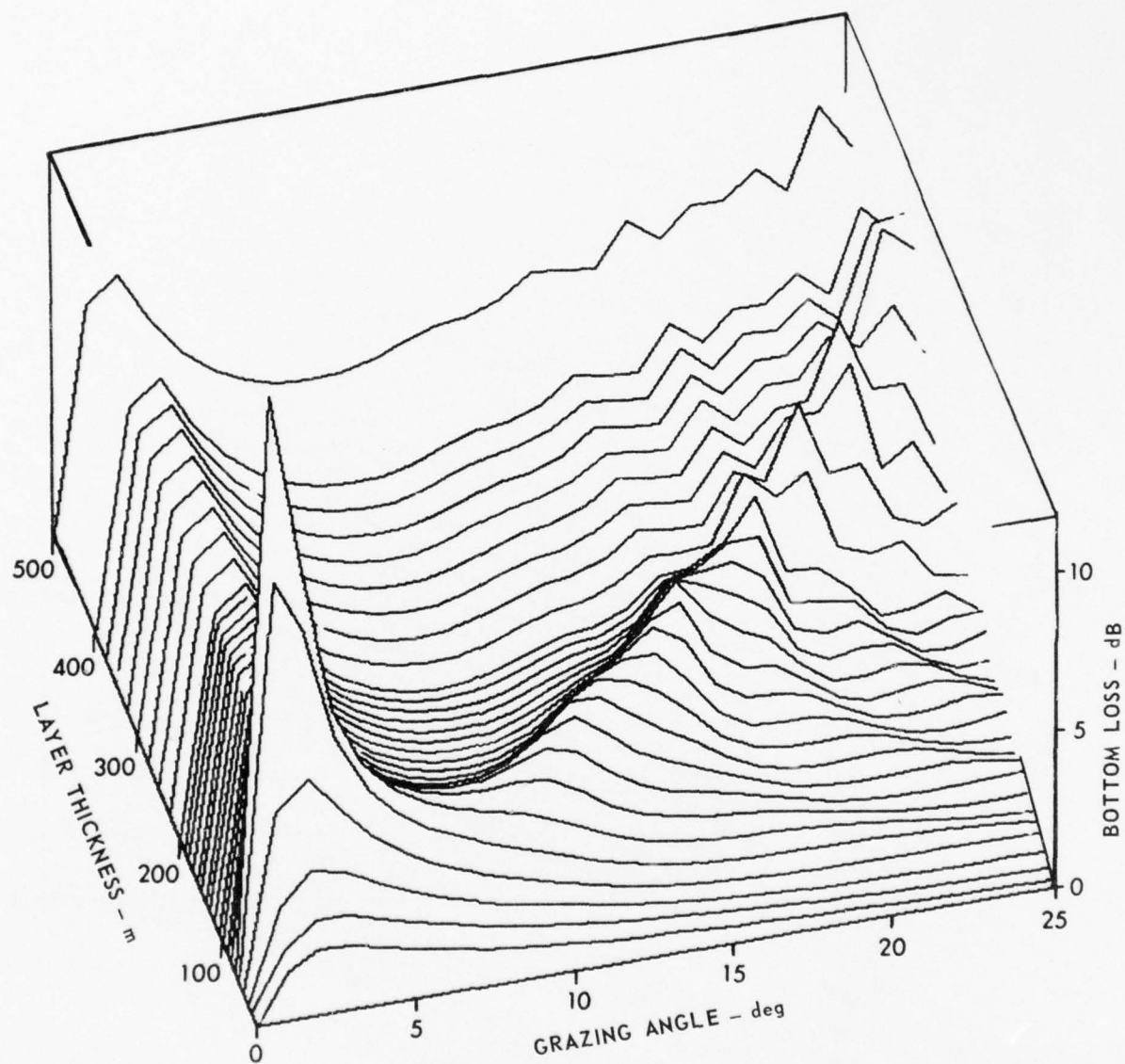
FREQUENCY: 50 Hz
MATERIAL: CLAY
GRADIENT: 0.5 sec^{-1}

FIGURE II-31
BOTTOM LOSS versus GRAZING ANGLE versus LAYER THICKNESS
WITH A SOUND SPEED GRADIENT OF 0.5 sec^{-1}

FREQUENCY: 50 Hz
MATERIAL: CLAY
GRADIENT: 1.0 sec^{-1}
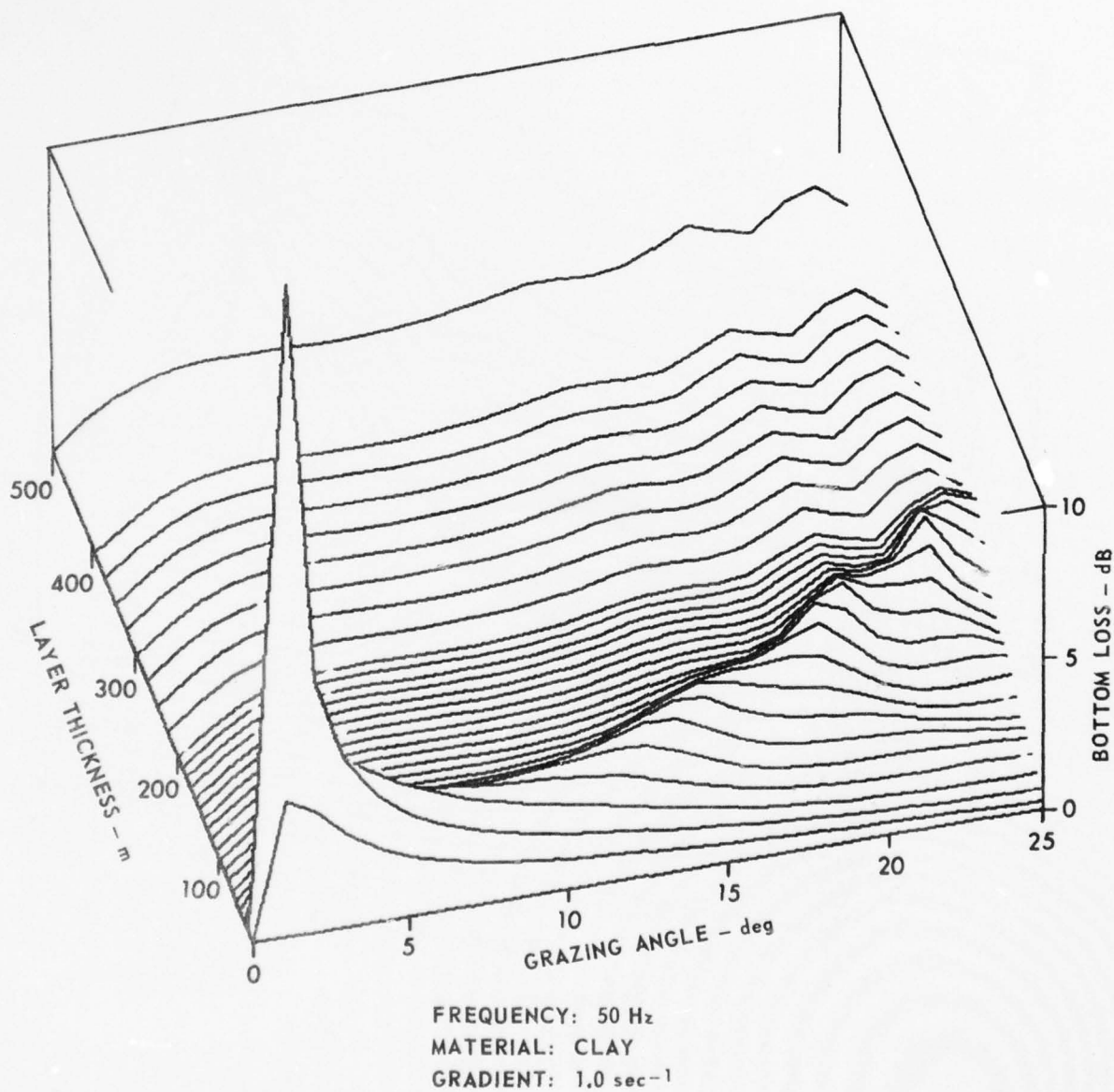
FIGURE II-32
BOTTOM LOSS versus GRAZING ANGLE versus LAYER THICKNESS
WITH A SOUND SPEED GRADIENT OF 1.0 sec^{-1}
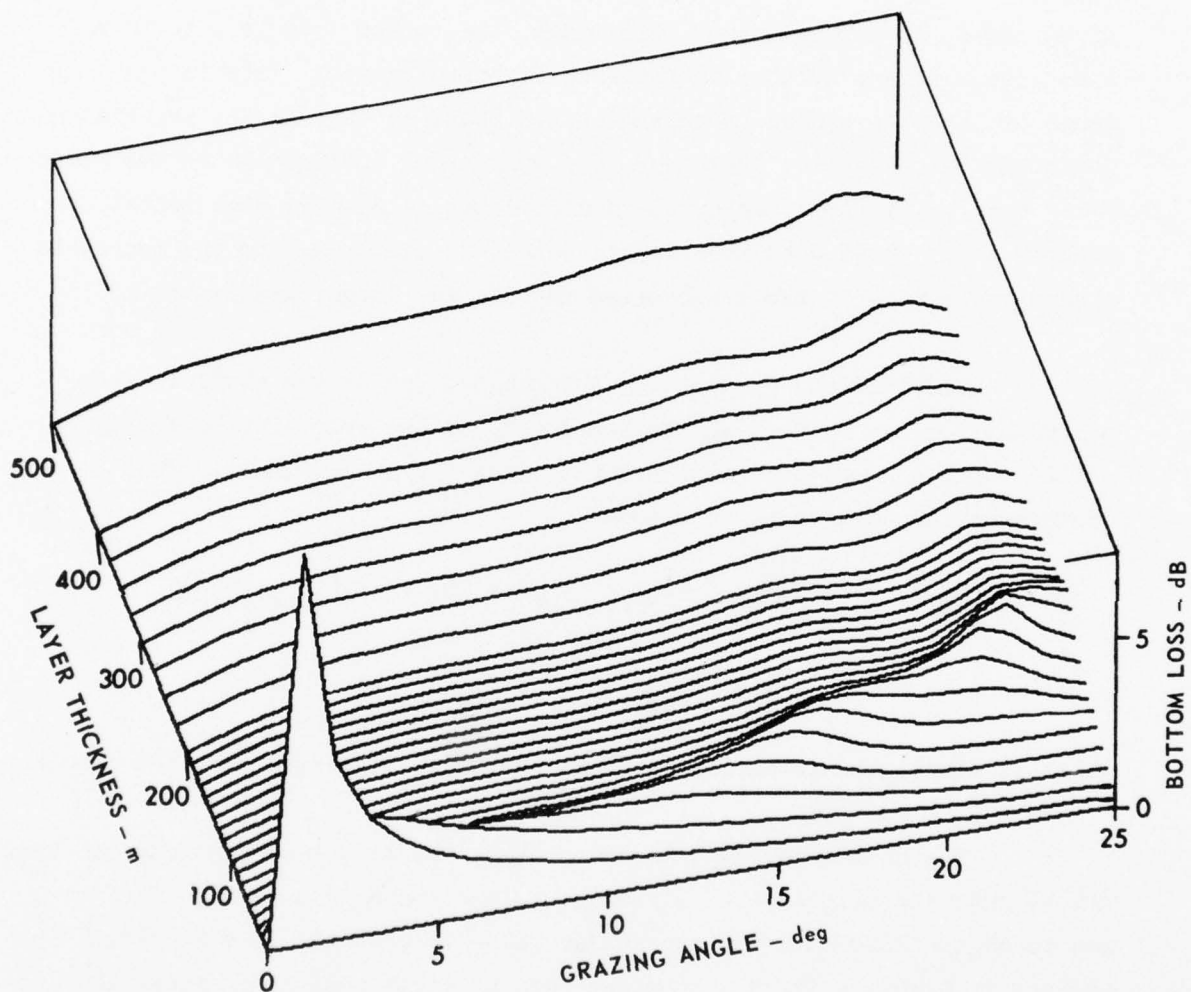
FREQUENCY: 50 Hz
MATERIAL: CLAY
GRADIENT: 1.5 sec^{-1}

FIGURE II-33
BOTTOM LOSS versus GRAZING ANGLE versus LAYER THICKNESS
WITH A SOUND SPEED GRADIENT OF 1.5 sec^{-1}

These three figures all display a prominent diagonal ridge with respect to the angle axis' decreasing with increasing gradient. For any given angle, at depths beyond this ridge, the bottom loss is seen to be independent of any further increase in layer thickness. This independence of layer thickness is an indication that, at this angle, the hidden depth has been reached. Moreover, the decreasing inclination of the ridge shows that, at a fixed angle, the hidden depth is reached more quickly for greater sound speed gradients. This effect is simply due to the increased upward refraction of the sound speed profile for larger gradients.

Consider now a quantity, $\Delta(\theta,z)$, defined as the absolute value of the difference between the bottom losses in the case of a perfectly reflecting plane and a perfect absorber inserted at a depth z. This difference can be seen to be simply

$$\Delta(\theta,z) = \left| -20 \log \left(|R|_{Reflector} \right) + 20 \log \left(|R|_{Absorber} \right) \right|$$

$$= 20 \left| \log \left(|R|_{Reflector} / |R|_{Absorber} \right) \right|$$

which is simply the intensity ratio in the two cases expressed in decibels.

The hidden depth, defined by $\Delta(\theta,z) \leqq \epsilon$, is directly obtainable from $\Delta(\theta,z)$ once the tolerance ϵ is chosen. Since there is no particular reason to choose ϵ to have any particular value in general (in a specific problem it might be fixed), it might seem at first that a considerable element of arbitrariness remains in the problem. However, it has been shown that the surface $\Delta(\theta,z)$ is displayed as a sharp transition in the vicinity of the hidden depth. As a result of this steep transition, a change of ϵ from, say, 0.1 dB to 0.01 dB, will cause very little change in the derived value of the hidden depth. In other words, the concept of a hidden depth will be a useful one and the tolerance ϵ need not be specified very precisely.

Figure II-34 shows the hidden depth, defined with $\epsilon = 0.1$ dB,
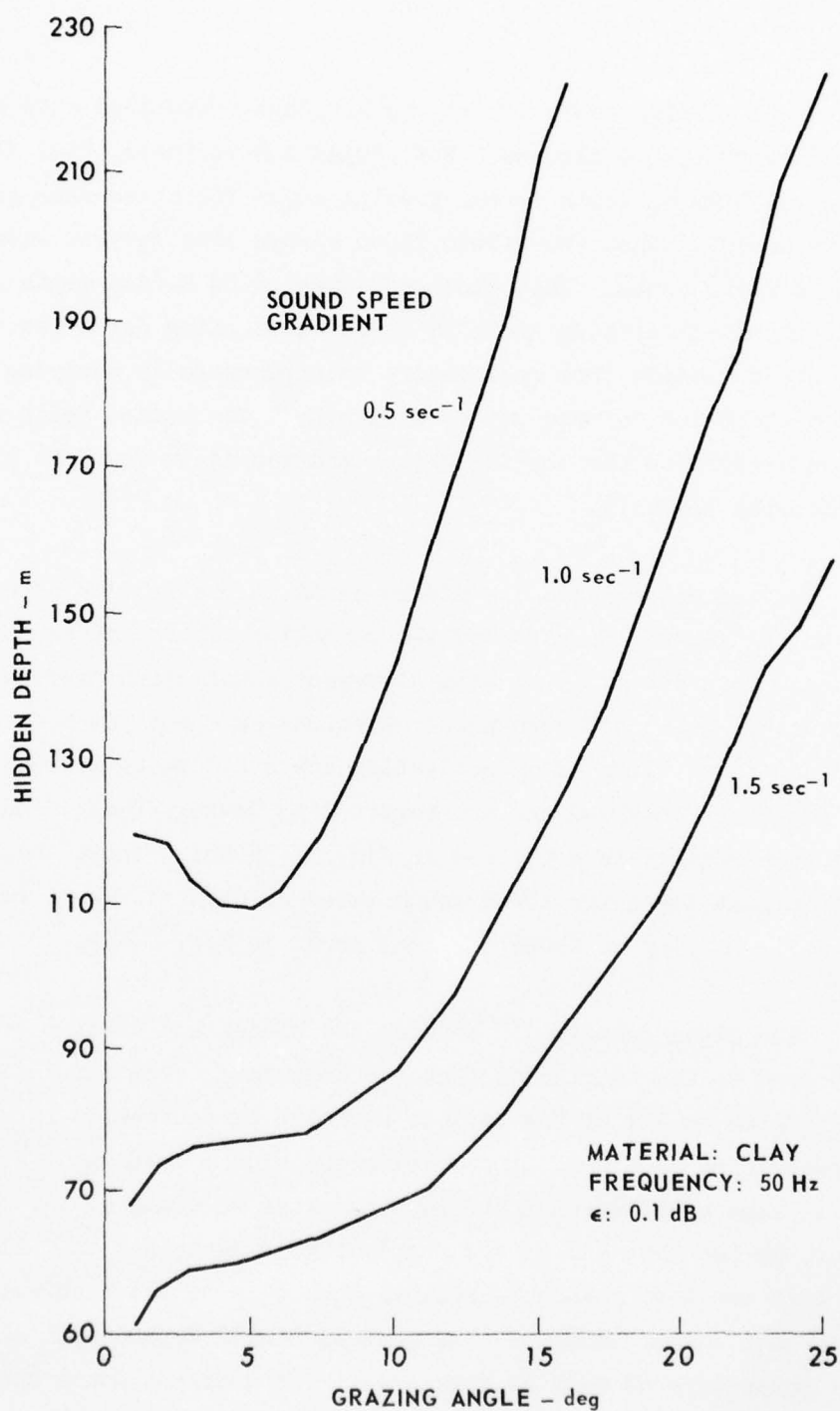
FIGURE II-34

HIDDEN DEPTH versus GRAZING ANGLE FOR A CLAY
LAYER WITH VARIOUS SOUND SPEED GRADIENTS

77

plotted versus grazing angle for the three sound speed gradients shown in the preceding groups of figures. For comparison purposes, Fig. II-35 shows the ray turning depth versus grazing angle for these same gradients. It will be observed that the hidden depth always lies several wavelengths below the turning depth. This close association of hidden depth and turning depth is not surprising since it is at the turning depth that the pressure field changes from oscillatory to exponentially decaying behavior. In the investigation carried out by Williams,[12] the hidden depth was in fact referenced to the turning depth, and was again found to lie a few wavelengths below it.

Having established the hidden depth in one particular case, we come to the general question of the variation of the hidden depth with changes in sediment type, with different sound speed profiles, with frequency, etc. Although these questions have not yet been completely resolved and these lines of investigation are still being pursued, some results have been obtained and are reported by Hawker, Focke, and Anderson.[2] A single such example is contained in Fig. II-36 which shows the hidden depth for a silt layer for three sound speed gradients. These results are generally similar to those for clay shown in Fig. II-34.

The close association between the hidden and turning depths leads at once to the conclusion that the apparently very complex dependence of hidden depth on all of the various sediment parameters is in actuality not an overriding problem. Upon writing the hidden depth as $Z_H = Z_T + \delta\lambda$, where λ is some sound wavelength (say the water wavelength) and δ is a parameter, we see that all of the complexity is contained in δ alone. Moreover, we now have reason to believe that δ is of order unity, that is, it is not much larger than one. In general δ will depend upon all the sediment parameters as well as frequency. The dominant sound speed profile dependence should be contained in the term Z_T.

Thus far we have restricted our investigation to the case of a linear sound speed profile. Although it is true that, in the uppermost
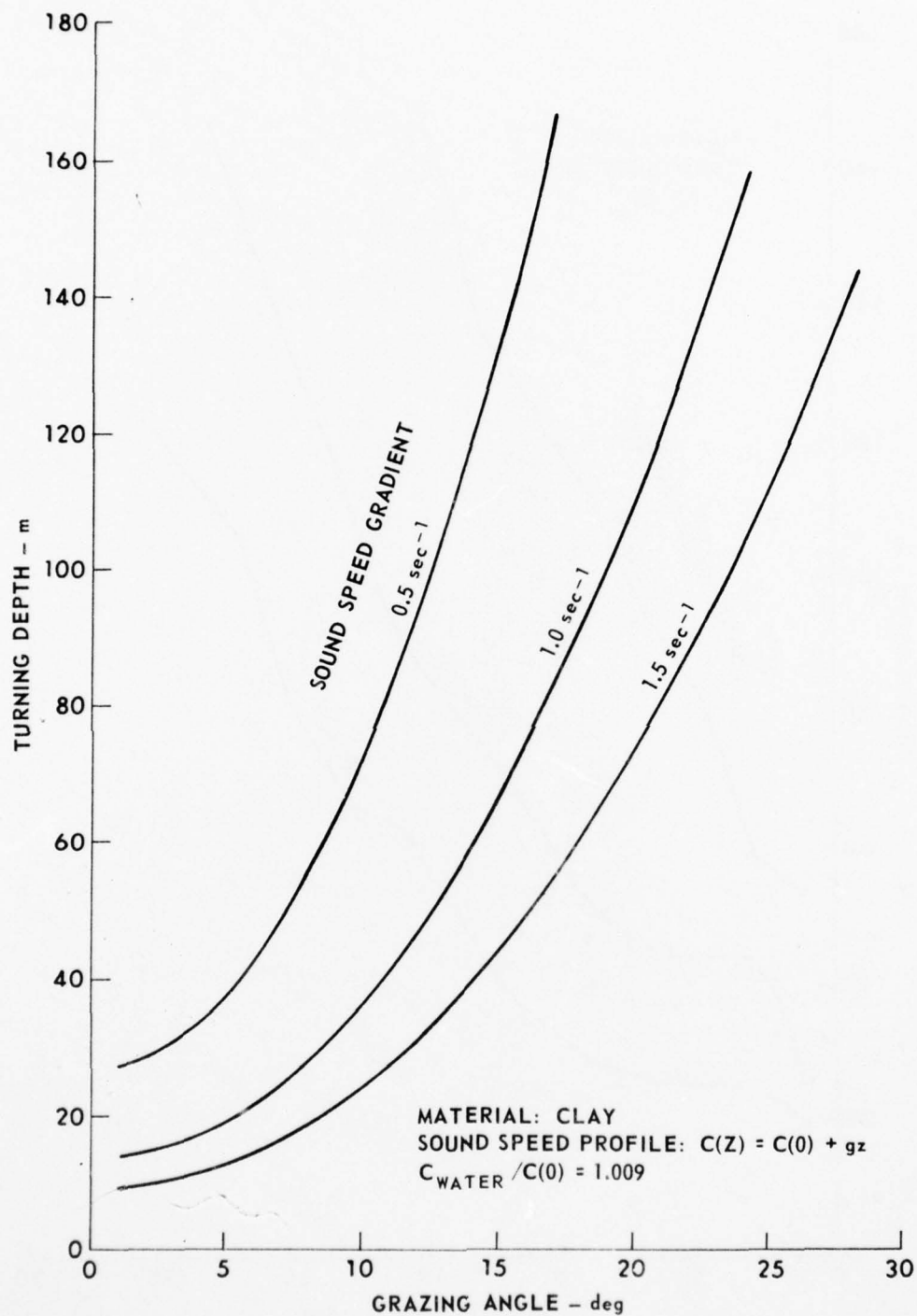
FIGURE II-35
TURNING DEPTH versus GRAZING ANGLE FOR A CLAY
LAYER HAVING VARIOUS SOUND SPEED GRADIENTS

79
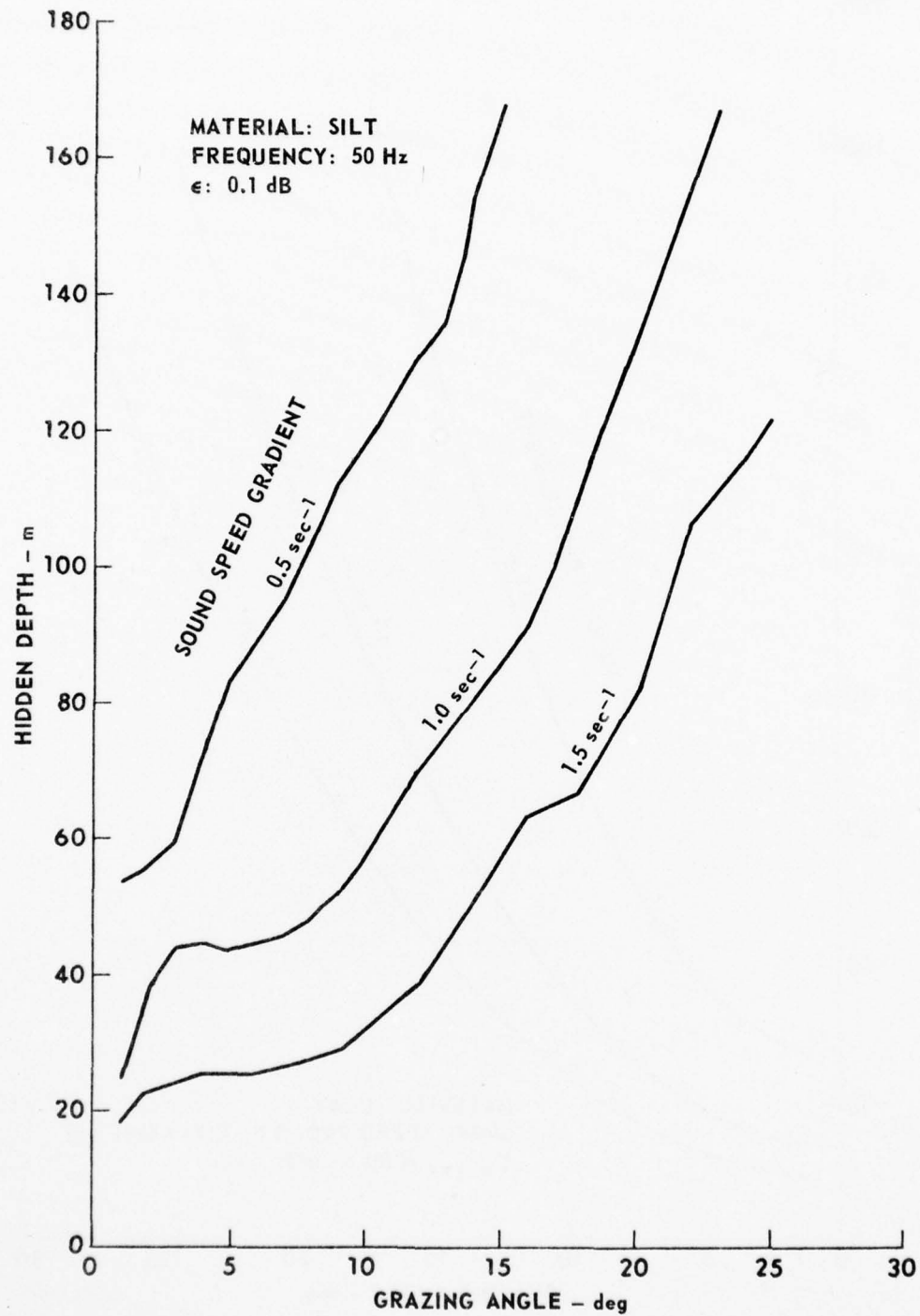
FIGURE II-36
HIDDEN DEPTH versus GRAZING ANGLE FOR A SILT
LAYER WITH VARIOUS SOUND SPEED GRADIENTS

80

sediment layers, the sound speed gradient is generally constant, seismic profiling measurements clearly show that the gradient decreases with depth. To gain some insight into how such behavior might affect the hidden depth picture, we shall examine the exponential sound speed profile proposed by Williams, given by $C(Z)=C(0)[1+A^2(e^{-\beta Z}-1)]^{-1/2}$. This profile is a 3-parameter one with $C(\infty)=C(0)[1-A^2]^{-1/2}$, $C'(Z)=C'(0) e^{-\beta Z}[1+A^2(e^{-\beta Z}-1)]^{-3/2}$, and $C'(0)=1/2\beta A^2 C(0)$. Figure II-37 shows $C'(Z)$ plotted versus depth for various values of $C(0)/C(\infty)$, with $C'(0)$ chosen to be unity. It will be observed that for $A^2 < 2/3'$, $C'(Z) < 1$ for all depths. Figure II-38 shows the ray turning depth for the case of water overlying sediment containing such an exponential sound speed profile. As would be expected from Fig. II-38 for $C(0)/C(\infty) > 1/\sqrt{3}$, the ray turning depth will always be larger than it is in the case of a linear profile (dotted line). For a given value of $C(0)/C(\infty)$, the turning depth approaches infinity at a certain angle. These critical angles are denoted by the asymptotes.

The most important result contained in these figures concerns the deviation of Z_T from linear behavior at low angles. It will be noted that, for $\theta \leq 25°$ and $0.8 \geq C(0)/C(\infty) \geq 1/\sqrt{3}$, the maximum deviation from linear behavior is 45 m. For this range of $C(0)/C(\infty)$, the sound speed gradient at 200 m can range from 0.66 to 0.975. Thus, although a considerable variation of $C'(Z)$ can occur the turning depth will range only over a comparatively narrow interval. Consequently, the hidden depth values which are previously determined in several cases using the linear profile will not be greatly altered by the introduction of such an exponential profile.

2.   Sensitivity of Bottom Loss to Variations in Sediment Type

Even with all other problem parameters fixed (layering, sound speed profile function and gradient, substrate, etc.) the problem of the influence of sediment type variations on bottom loss involves, at a minimum, variations in sound speed, density, and attenuation. One possibility for circumventing this difficulty is to relate these three parameters to a single parameter such as porosity or mean grain size. The work of
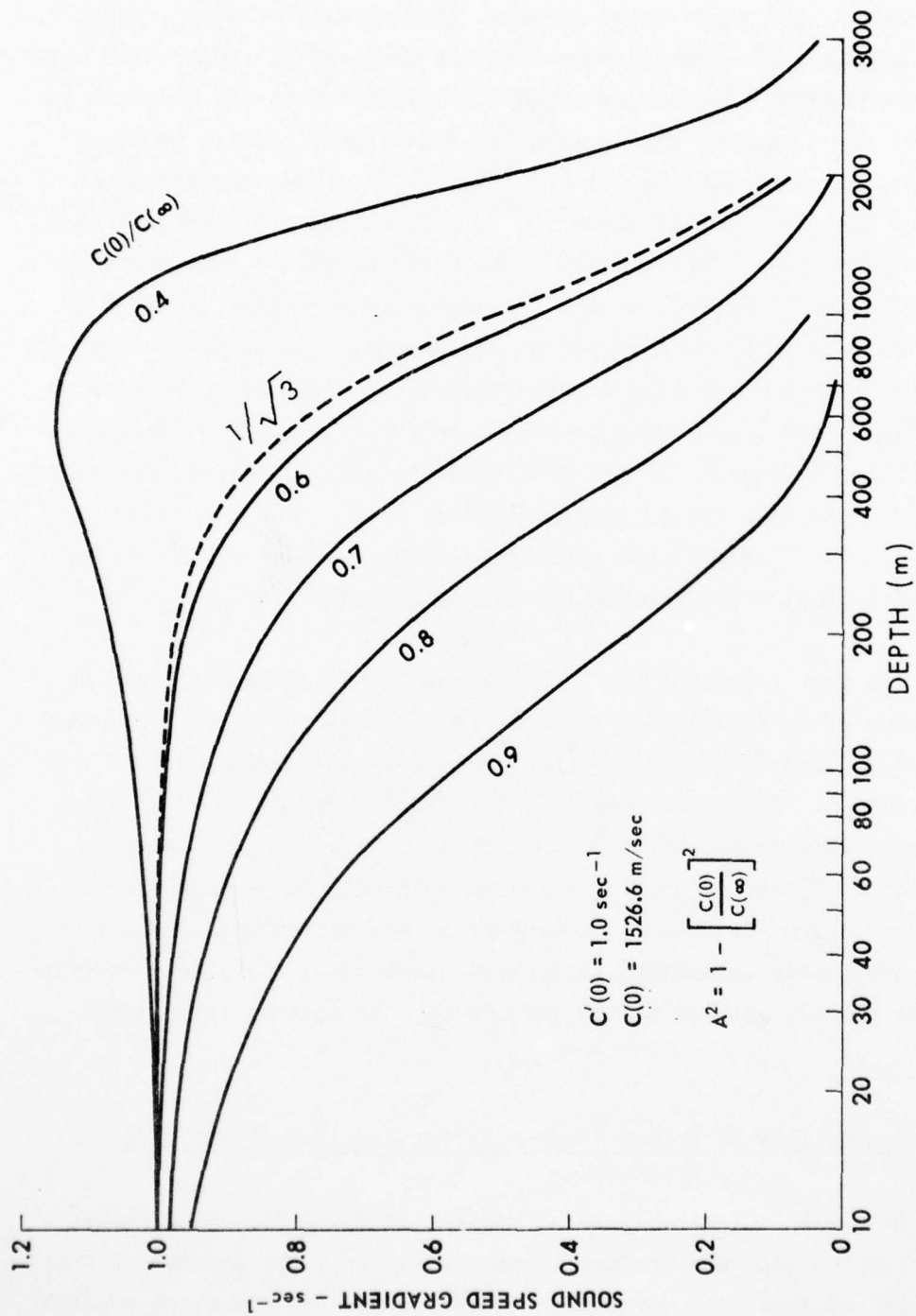
FIGURE II-37

SOUND SPEED GRADIENT versus DEPTH FOR AN
EXPONENTIAL PROFILE WITH VARIOUS VALUES OF $C(0)/C(\infty)$

$C'(0) = 1.0 \text{ sec}^{-1}$
$C(0) = 1526.6 \text{ m/sec}$

$A^2 = 1 - \left[\dfrac{C(0)}{C(\infty)} \right]^2$

FIGURE II-38
TURNING DEPTH versus GRAZING ANGLE FOR AN
EXPONENTIAL PROFILE WITH VARIOUS VALUES OF $C(0)/C(\infty)$

ARL - UT
AS-76-741
KEH - DR
7 - 5 - 76

83

Hamilton[7] and Akal[10] has shown that, for a considerable variety of sediments, these three parameters can be usefully related to porosity and the appropriate equations have been developed by these authors.

Upon fixing all other parameters in the problem then, it is possible to study sediment type variations be examining the behavior of bottom loss versus angle versus porosity. An empirical approach to this type of study was taken by Hall and Watson[11] who used empirical fits to AMOS data and developed curves giving bottom loss versus grazing angle parameterized by porosity.

It is quite straightforward to employ the aforementioned results of Hamilton and Akal to generate appropriate parameter sets for use in our bottom loss model. This has been done and Figs. II-39 and II-40 show two resulting 3-dimensional surfaces in the case of a linear sound speed profile with a gradient of 1.2 $\sec^{-1}$ in a 100 and 200 m layer, respectively. The substrate is a homogeneous solid.

There are two striking features of these surfaces, the bladed structures at low angles and the curving ridge at higher angles. The prominent curving ridge is associated with Stoneley waves at the sediment-substrate interface whereas the bladed structures seem to be a residue of an intromission angle effect. It is noteworthy that, since the bladed structures lie at angles such that the substrate is below the hidden depth, no change is seen in these structures between the 100 m and 200 m cases.

These curves show directly how the bottom loss can be expected to change with sediment type variations. Future work will include producing additional such curves with different sound speed gradients and at different frequencies.
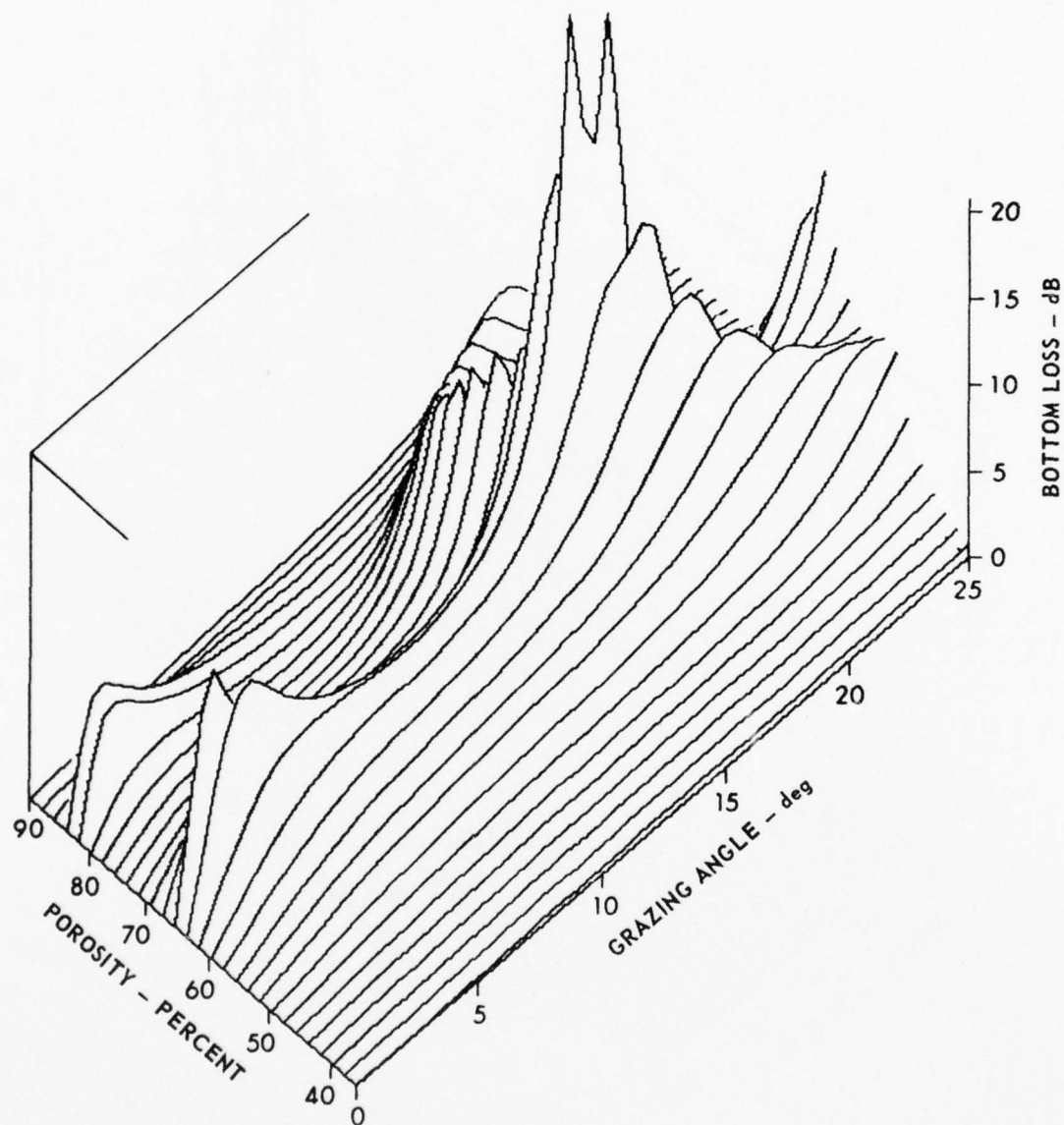
FREQUENCY: 50 Hz
LAYER THICKNESS: 100 m
SOUND SPEED GRADIENT: 1.2 sec^{-1}

FIGURE II -39

BOTTOM LOSS versus GRAZING ANGLE
versus POROSITY FOR A 100 m LAYER
OVERLYING A SOLID SUBSTRATE
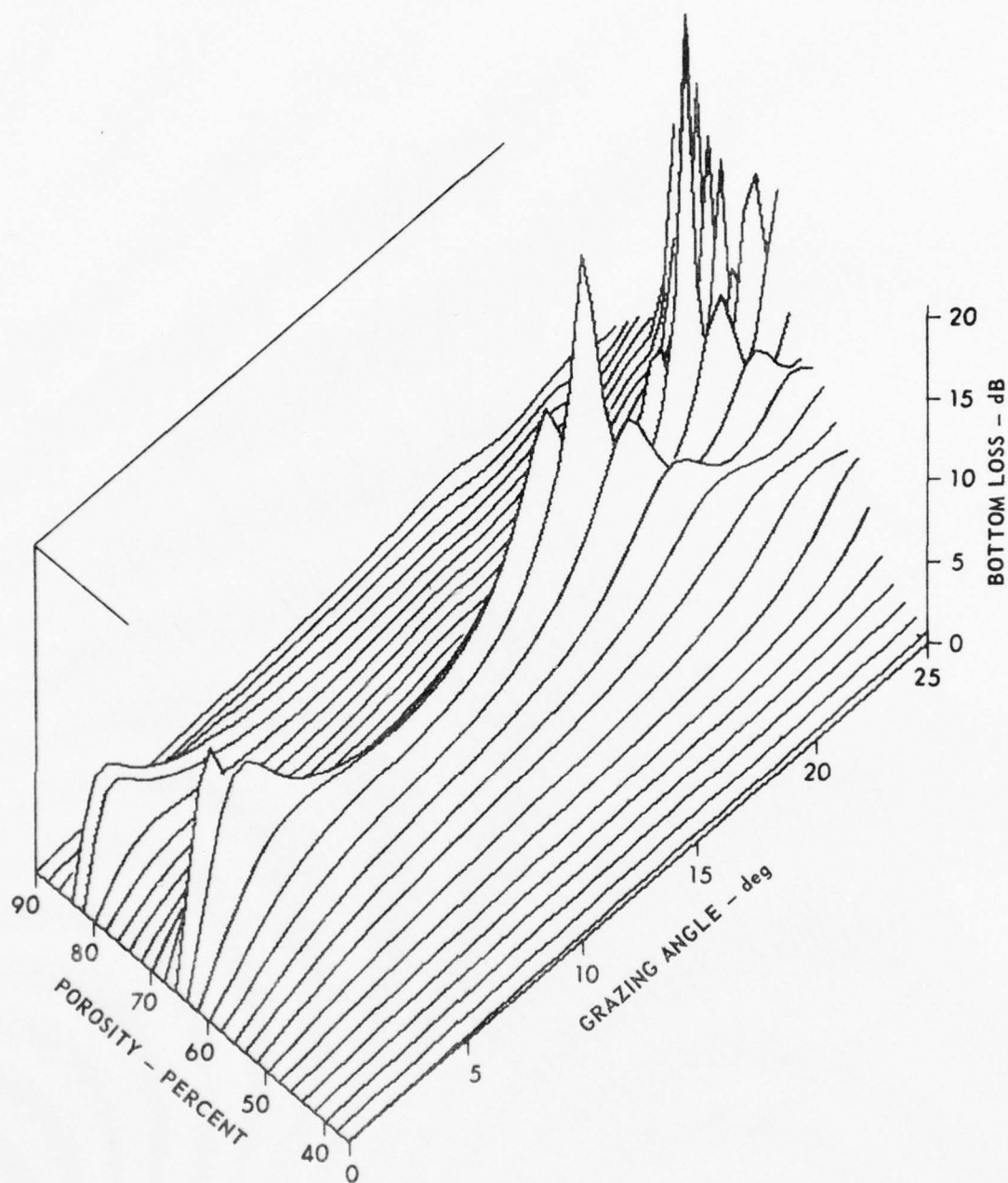
FREQUENCY: 50 Hz
LAYER THICKNESS: 200 m
SOUND SPEED GRADIENT: 1.2 sec^{-1}

FIGURE II-40
BOTTOM LOSS versus GRAZING ANGLE
versus POROSITY FOR A 200 m LAYER
OVERLYING A SOLID SUBSTRATE

References - Chapter II

1. K. E. Hawker, A. L. Anderson, K. C. Focke, and T. L. Foreman,
    "Initial Phase of a Study of Bottom Interaction of Low Frequency
    Underwater Sound", Applied Research Laboratories Technical Report
    No. 76-14 (ARL-TR-76-14), Applied Research Laboratories, The University
    of Texas at Austin, 6 April 1976.

2. K. E. Hawker, K. C. Focke, and A. L. Anderson, "A Sensitivity Study
    of Underwater Sound Propagation Loss and Bottom Loss", Applied
    Research Laboratories Technical Report No. 77-17 (ARL-TR-77-17),
    Applied Research Laboratories, The University of Texas at Austin,
    28 February 1977.

3. K. E. Hawker and T. L. Foreman, "A Plane Wave Reflection Coefficient
    Model Based on Numerical Integration: Formulation, Implementation and
    Application", Applied Research Laboratories Technical Report No. 76-23
    (ARL-TR-76-23), Applied Research Laboratories, The University of Texas
    at Austin, 21 June 1976.

4. I. Tolstoy and C. S. Clay, Ocean Acoustics, (McGraw-Hill Book Co., Inc,
    New York, 1966).

5. E. L. Hamilton, "Sound Attenuation as a Function of Depth in the Sea
    Floor", J. Acoust. Soc. Am. 59, 528 (1976).

6. D. J. Shirley, private communications.

7. E. L. Hamilton, "Prediction of Deep-Sea Sediment Properties: State
    of the Art", Deep-Sea Sediments, A. C. Inderbitzen, ed. (Plenum Press,
    New York, 1974).

8. E. L. Hamilton, "Variations of Density and Porosity with Depth in the
    Deep-Sea Sediments", J. Sedim. Petro. 46, 280 (1976).

9. K. E. Hawker, "The Dependence of Surface Waves on Plane Wave Bottom
    Reflection Loss for Realistic Ocean Sediments", Paper presented at
    the 92nd Meeting of the Acoustical Society of America, San Diego,
    California, November, 1976.

10. T. Akal, "The Relationship Between the Physical Properties of Under-
    water Sediments that Affect Bottom Reflections", Marine Geology 13,
    251 (1972).

11. H. R. Hall and W. H. Watson, "An Empirical Bottom Reflection Loss
    Expression for Use in Sonar Range Prediction", Naval Underwater
    Warfare Center Report NUWC-TN-10, July 1967.

12. A. O. Williams, "Hidden Depths: Acceptable Ignorance about Ocean
    Bottoms", J. Acoust. Soc. Am. 59, 1175 (1976).

III.   SENSITIVITY OF SOUND PROPAGATION TO VARIATION
IN BOTTOM LOSS

The objectives of this study allow the bottom interaction problem
to be defined by the questions "what influence does the bottom have on
long range acoustic propagation?" and "how much information about the
(sub)bottom is required in order to adequately predict these effects?"
This restricted form of the problem is still quite complex and requires
the problem to be separated into simpler components.

A systematic sensitivity study, summarized in this chapter, was
conducted to isolate regions in the water column exhibiting strong bottom
influence from regions which are relatively insensitive to bottom effects.
For this purpose simple bottom loss descriptions were used to control the
bottom interactions. Throughout most of this study variations in the
bottom loss were restricted to changes in critical angle: bottom loss
was 0 dB below the critical angle and essentially infinite above. Many
of the results here have been given by Hawker, Focke, and Anderson.[1]

A.   Methodology

Two propagation models were used in this investigation, FACT, a ray
trace model reported by Spofford[2] and Baker and Spofford,[3] and a parabolic
equation model reported by Brock.[4] The nature of the ARL:UT implemen-
tation of these models is described by Hawker, Foreman, and Focke.[5] FACT
defines the bottom in terms of a plane wave reflection coefficient applied
at the water-sediment interface. The parabolic equation model simulates
a critical angle effect by introducing below the water column a thin layer
with a sound speed gradient and zero attenuation, which in turn overlies
a homogeneous attenuating layer.

Various terms used throughout this chapter are defined here. The
depth at which the sound speed is the same as that at the source depth is
referred to as the source conjugate depth. The depth at which the sound

speed is the same as that at the surface is called the critical depth. The distance between the critical depth and the bottom (if the bottom lies below critical depth) is called the depth excess.

A sensitivity study is designed to measure the influence of a given input parameter on a specified output parameter. For the study discussed in this chapter, systematic variations are introduced in the bottom loss to determine their effects upon the total calculated acoustic propagation. The major intensity contribution from bottom interacting energy will be within the shadow zones, away from the convergence zones where waterborne paths dominate the intensity calculations. Figure III-1 demonstrates this bottom influence on the energy contributions within the shadow zones. This range dependence of the influence of the bottom (dominant only in the shadow zones) is a function of the environment and the source/receiver geometry. To remove problems associated with this range dependence in a manner independent of the environment, average propagation losses were computed as the output of primary importance. Major conclusions from the sensitivity study are based on the resultant variations in these averages.

The form of averaging used in this study computes the propagation loss for the average intensity at a given receiver depth within the 100 to 200 nmi range interval. This range interval will not include the nearfield effects (the direct ray paths). It will cover several convergence zones and will have only a nominal 3 dB increase in loss due to increases in range. Run times for the P.E. model will not be excessive out to 200 nmi.

Variations in the bottom loss were limited to changes in the critical angle, using values of 0°, 1°, 5°, 10°, 15°, and 20°. Figure III-1 presents the propagation loss versus range using these various bottom descriptions for a given source/receiver depth combination. The profile used is from the mid-Pacific Ocean. It has a critical depth of 3952 m, an axis depth of 600 m, and a 44 m/sec difference in sound speed between the surface and the axis. As expected, the bottom descriptions with the higher critical

CRITICAL ANGLE

1 20°
2 15°
3 10°
4 5°
5 1°
6 0°

RANGE – nm

PROPAGATION LOSS – dB

FIGURE III-1

PROPAGATION LOSS FOR VARIOUS BOTTOM LOSS CRITICAL ANGLES

SOURCE DEPTH: 152 m, RECEIVER DEPTH: 3350 m, BOTTOM DEPTH: 3952 m, MODEL: FACT
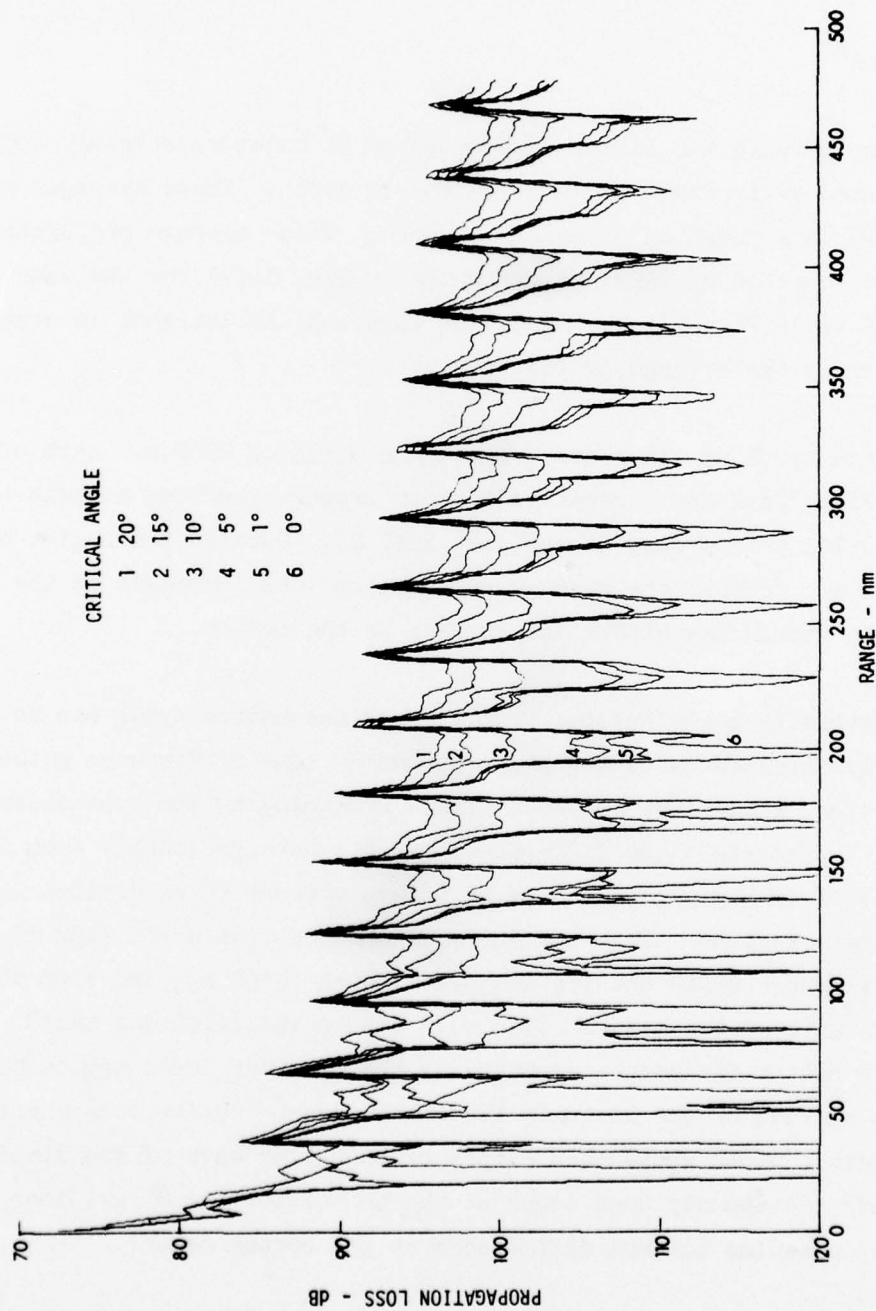
ARL - UT
AS-76-560
KCF - DR
4 - 21 - 76

angles contribute more energy within the shadow zones. The maximum acoustic intensities within the convergence zones, however, remain virtually unchanged for the bottom variations.

B.   Results

Average propagation losses were computed at numerous receiver depths for a selected environment and a given source depth. These averages were then plotted as a function of receiver depth. These average propagation loss curves computed by FACT are presented in Fig. III-2 for the same environment as in Fig. III-1. Again, as expected, an increase in critical angle decreases the average propagation loss.

A source depth of 152 m has a conjugate depth of 2500 m. Each of the curves in Fig. III-2 has a relative minimum propagation loss at both these depths (resulting from cusped caustics, Ref. 2). Outside the region between these two depths, the average propagation loss increases as the receiver depth approaches either the surface or the bottom.

The intensity contributions from the various bottom types can be more readily observed by taking the propagation loss differences between the 0° critical angle case and each of the remaining bottom type cases. Figure III-3 presents these differences for the data previously seen in Fig. III-2. From Fig. III-3 the water column appears to be divided into three separate regions: from the surface to the source depth (152 m), between the source depth and its conjugate depth (2500 m), and from the source conjugate to the bottom (3952 m). Within the first and third regions the bottom influence increases as the receiver depth approaches either the surface or the bottom. The bottom loss contributions increase as the receiver depth approaches either boundary for each of the specified bottom types (an anomaly does occur at the bottom for the 0° critical angle case, creating maximum differences at the bottom depth).

Within the second region of the water column, the bottom influence
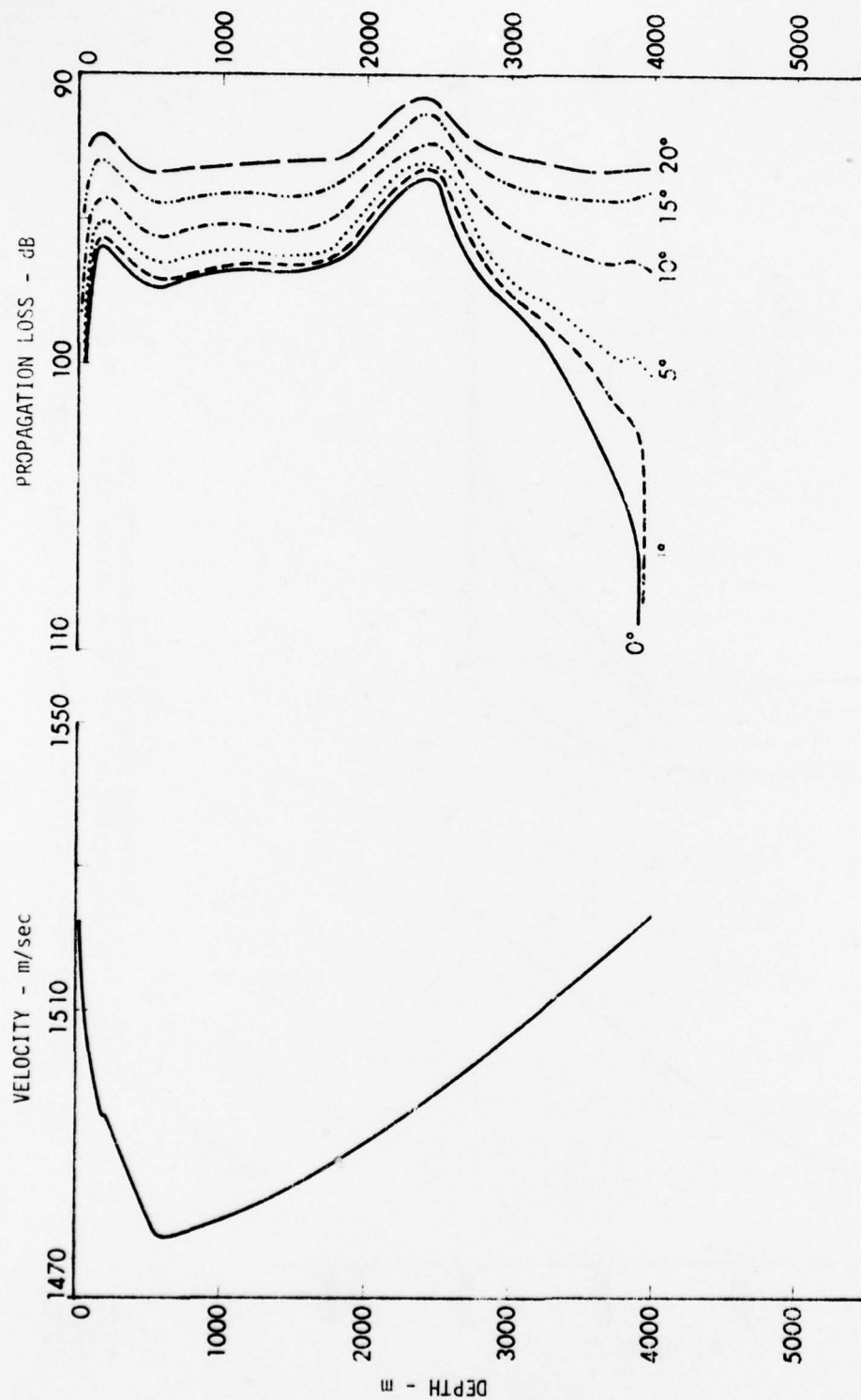
FIGURE III-2
AVERAGE PROPAGATION LOSS
Range Interval: 100-200 nm

MID-PACIFIC PROFILE
SOURCE DEPTH: 152 m, BOTTOM DEPTH: 3952 m, MODEL: FACT

FIGURE III-3

Δ - DIFFERENCE BETWEEN ABSORBING BOTTOM CASE
AND THE PARTIALLY REFLECTING BOTTOM CASES

SOURCE DEPTH: 152 m (500 ft), BOTTOM DEPTH: 3952 m, MODEL: FACT

is almost independent of the receiver depth. The propagation loss has a regular dependence on the bottom loss within this region. Table III-1 presents a comparison between the propagation differences in this second region and the bottom bounce energy. This bottom bounce energy is the additional energy introduced into the problem by the bottom bounce rays in the form of total energy divided by water refracted energy. These numbers are based on Snell's law using the sound speed at the source depth and at the bottom. Within this second region of the water column, there is at most a 0.2 dB difference between the intensity contribution and the energy contributions for the bottom bounce rays in this one case.

Similar calculations were performed for various source depths. Figure III-4 presents the propagation loss differences between the 0° and 20° critical angle cases for five source depths. The conjugate depths for these five source depths are 3874 m (33.5 m), 3410 m (50 m), 2963 m (90 m), 2500 m (152 m), and 600 m (600 m). For each source depth the water column is divided into the regions defined by the source depth and its conjugate depth. The characteristics described earlier are seen to be consistent for each of these source depths.

Table III-2 presents comparisons of the bottom bounce energy and the bottom bounce contributions to the average propagation loss. The two calculations differ by less than 1.0 dB, except at the axis depth of 600 m. (The 600 m source is a special case where the source depth is its own conjugate depth.) The bottom bounce contributions to the average propagation loss can be estimated by a calculation of the bottom bounce energy for receiver depths between the source and source conjugate depths.

Additional studies have been conducted using this same mid-Pacific profile in a parabolic equation model (P.E.). Those calculations presented in Fig. III-2 have also been computed with the P.E. model. These results are presented in Fig. III-5. Comparisons between these two figures show 1 to 2 dB differences between these results from the two models. However, the results from both models do have similar characteristics.

TABLE III-1

COMPARISON BETWEEN BOTTOM BOUNCE ENERGY AND BOTTOM BOUNCE
CONTRIBUTIONS TO THE AVERAGE PROPAGATION LOSS

Bottom Loss Critical Angle (deg)	Bottom Bounce Energy (total energy/water refracted energy)	Bottom Bounce Contributions to Prop. Loss
0	0	0
1	0.02	0.23
5	0.47	0.63
10	1.46	1.50
15	2.50	2.61
20	3.43	3.47
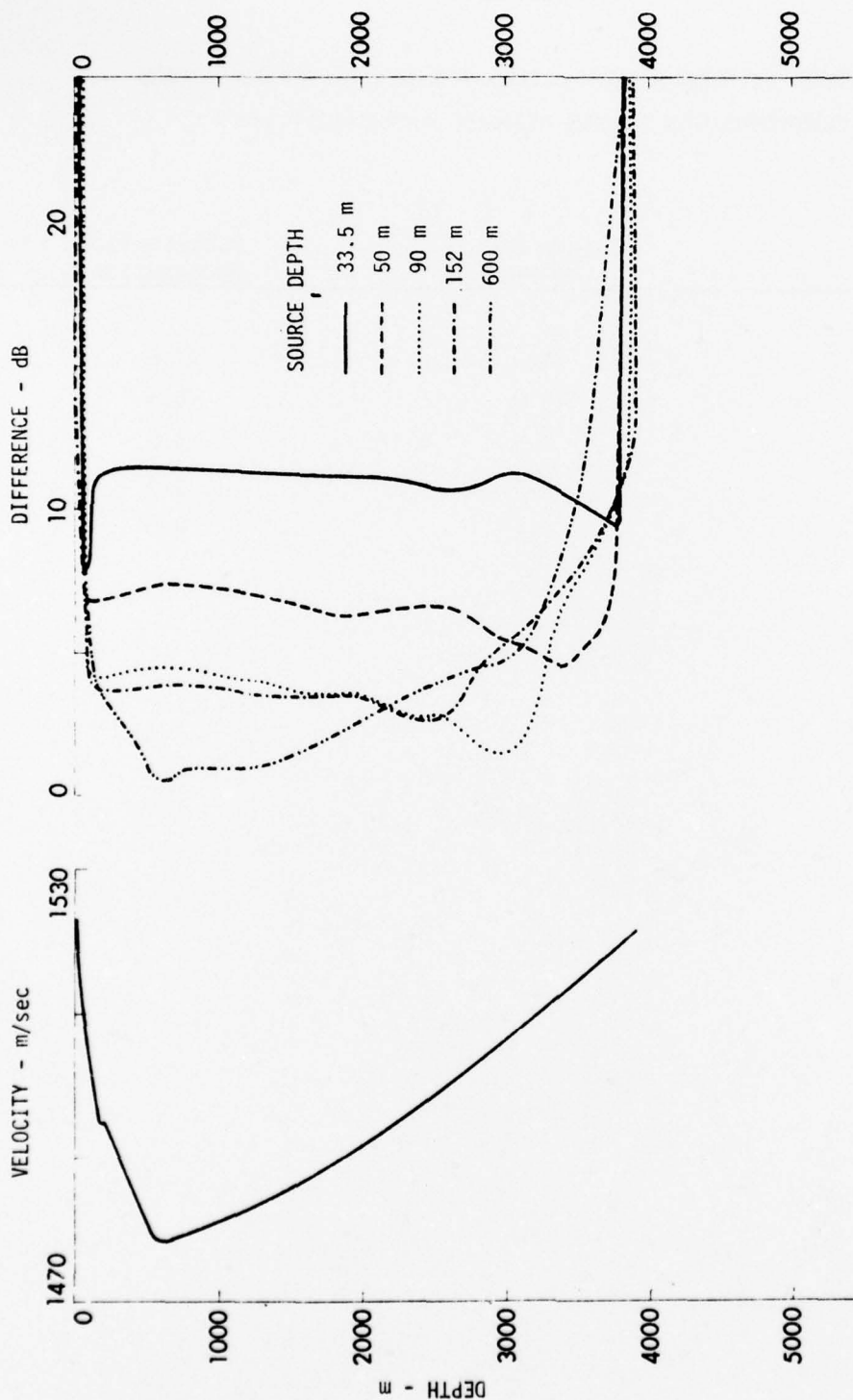
FIGURE III-4
DIFFERENCES BETWEEN THE 0° AND 20° BOTTOMS
FOR VARIOUS SOURCE DEPTHS
MID-PACIFIC PROFILE

BOTTOM DEPTH: 3952 m, MODEL: FACT

TABLE III-2

COMPARISON BETWEEN BOTTOM BOUNCE ENERGY AND BOTTOM BOUNCE
CONTRIBUTIONS TO THE AVERAGE PROPAGATION LOSS

| Source Depth (m)	Bottom Bounce Energy	Contributions to Propagation Loss
33.5	11.9	12.2
50.0	5.4	6.3
90.0	4.1	3.6
152.0	3.4	3.5
600.0	2.4	0.5
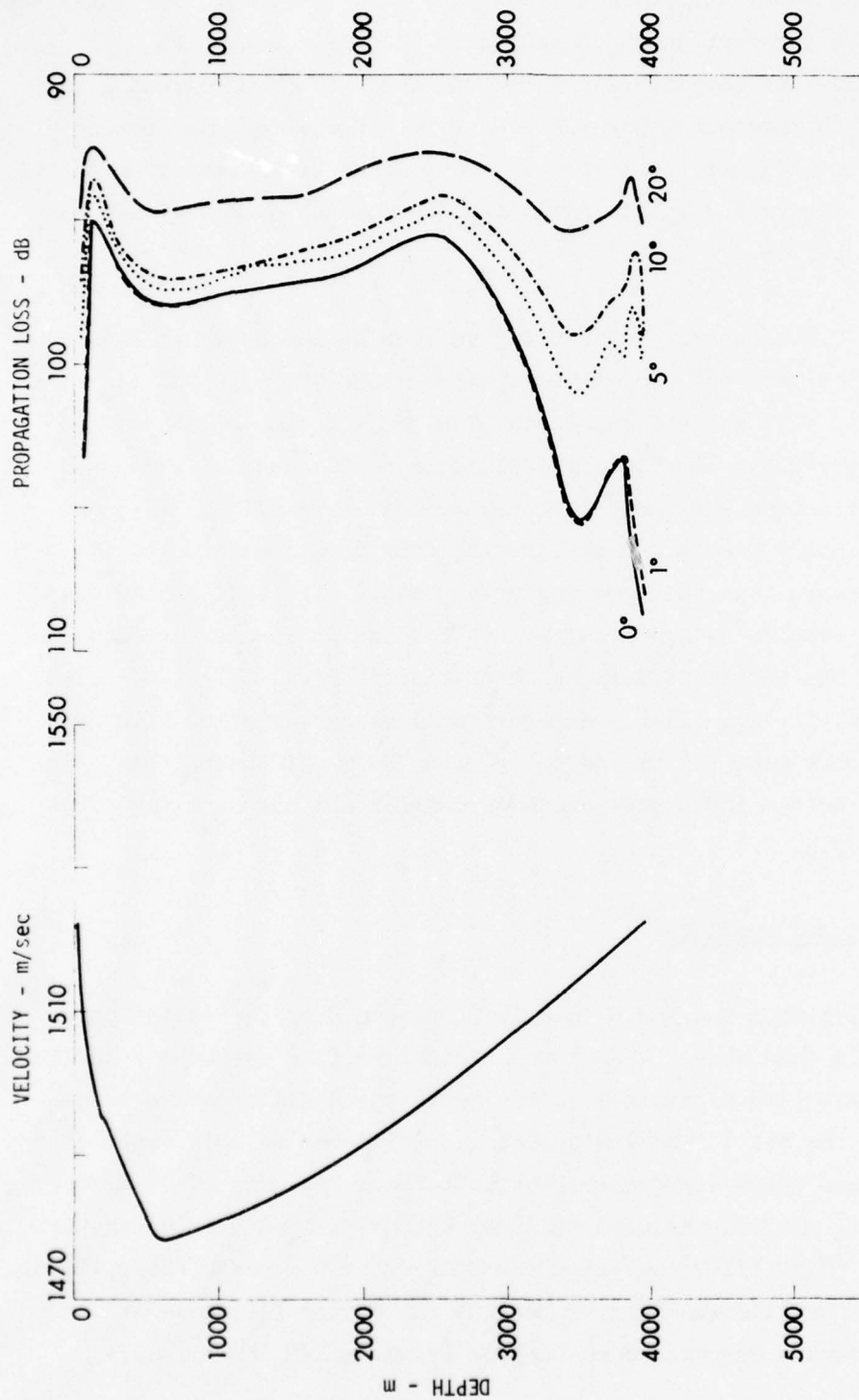
FIGURE III-5

AVERAGE PROPAGATION LOSS

Range Interval: 100-200 nm

MID-PACIFIC PROFILE

SOURCE DEPTH: 152.4 m,   BOTTOM DEPTH: 3952 m,   MODEL: P.E.

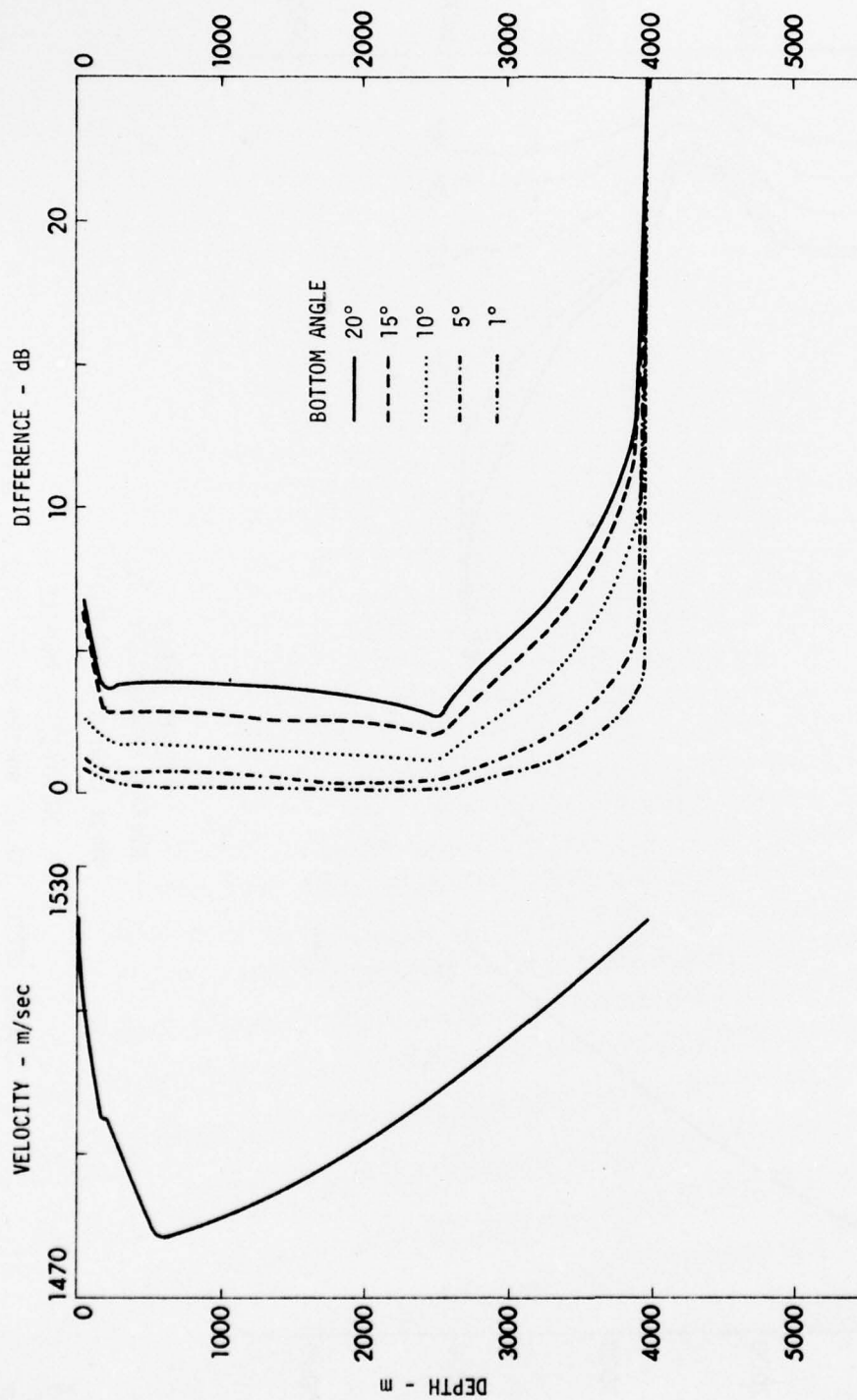ARL - UT
AS-76-526
KCF - DR
4 - 19 - 76

In both cases the water column is divided into three regions. The influences of the bottom are receiver depth dependent in the first and third regions; generally the sensitivity to bottom loss variation increases as the receiver depth approaches the surface or bottom. Within the second region the bottom influence is regular: independent of the receiver depth. The P.E. model, however, predicts additional bottom influences within 400 to 700 m of the bottom.

Additional P.E. runs were made using various bottom depths. The bottom depths used were 3647 m (critical depth minus 305 m), 3952 m (critical depth), 4257 m (critical depth plus 305 m), and 5543 m (actual depth for this profile). Bottom critical angles of 1° and 10° were used to determine the bottom influence in a manner similar to Figs. III-3 and III-4. (The 10° angle was chosen on run time considerations and the 1° was chosen to ensure that the same logic was used.) The differences obtained from the results using these two bottom descriptions are presented in Fig. III-6. The bottom influences observed from Figs. III-3 and III-4 are again present in Fig. III-6. An additional characteristic, however, appears in the very near bottom region (400 to 700 m off the bottom). In this region the bottom influences are more complex and are also dependent on the bottom depth.

1. Additional Profiles

Profiles from the North Pacific Ocean and from the Indian Ocean were also used in this study. The North Pacific profile presents a shallow sound channel axis (120 m) and a 26 m/sec sound speed difference between the surface and the axis. The Indian Ocean profile has an axis depth of 1800 m and a sound speed difference between surface and axis of 44 m/sec. The North Pacific profile was used to study bottom influence as a function of source depth (Fig. III-7) and as a function of bottom depth (Fig. III-8). The Indian Ocean profile was used to present the bottom influence at various bottom depths for two source depths (Figs. III-9 and III-10).

-100-
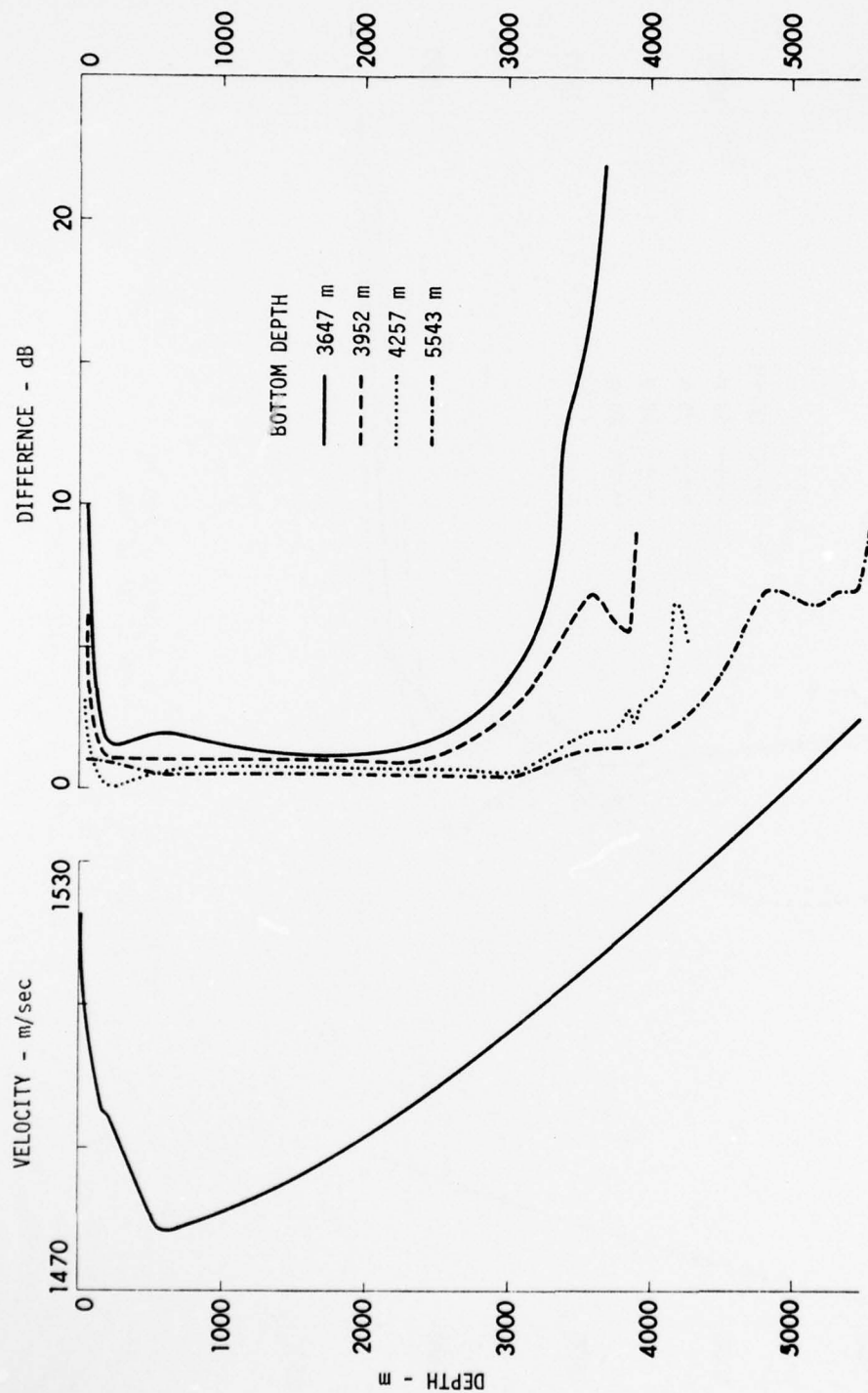
FIGURE III-6
DIFFERENCES IN 1° AND 10° BOTTOMS FOR VARYING BOTTOM DEPTHS
MID-PACIFIC PROFILE

SOURCE DEPTH: 152 m, MODEL: P.E.
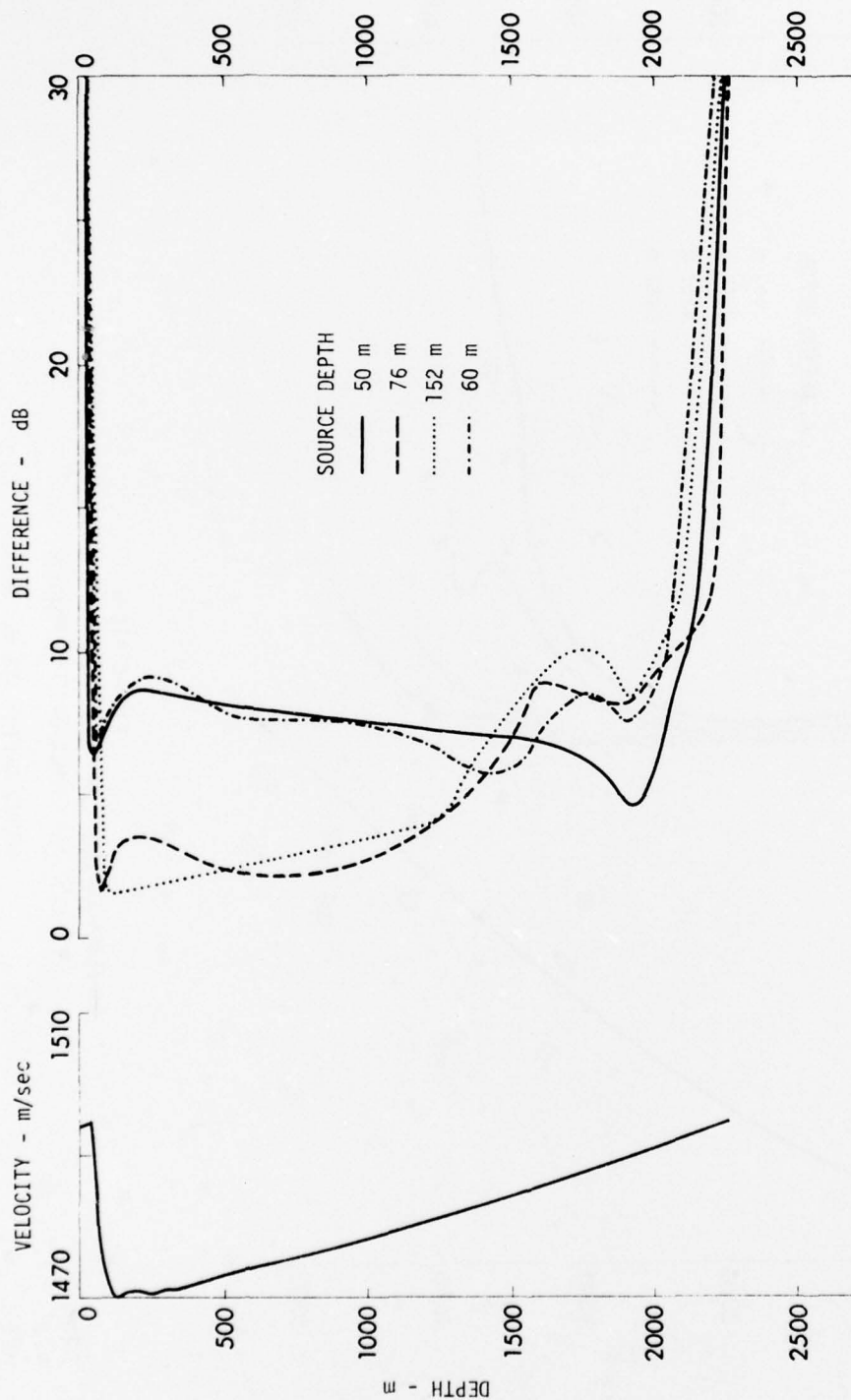
FIGURE III-7
PROPAGATION LOSS DIFFERENCES BETWEEN 0° AND 20°
BOTTOM CASES WITH VARYING SOURCE DEPTHS

NORTH PACIFIC PROFILE

BOTTOM DEPTH: 2260 m, MODEL: FACT

ARL - UT
AS-76-567
KCF - DR
4 - 27 - 76

102
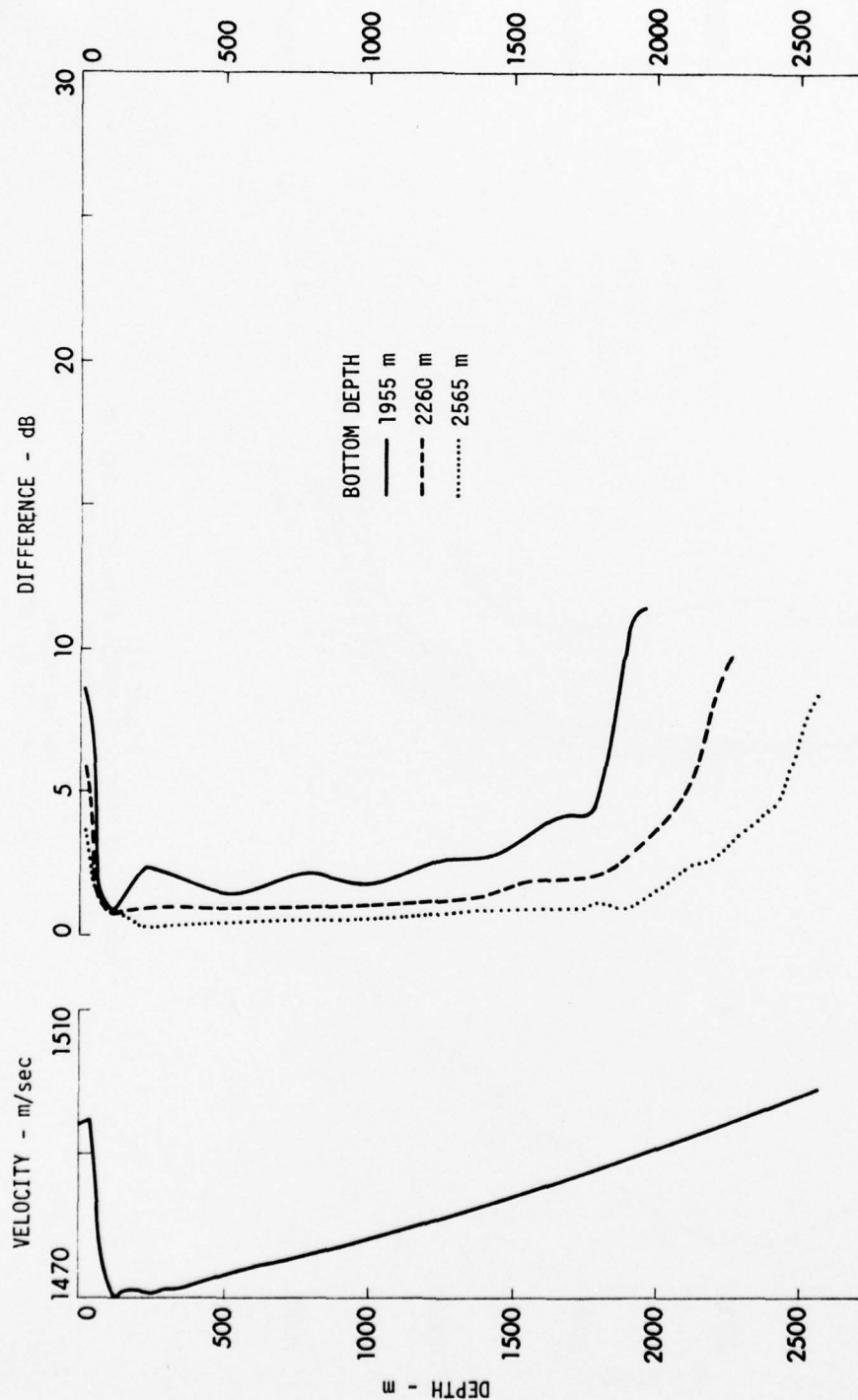
FIGURE III-8
PROPAGATION LOSS DIFFERENCES BETWEEN 1° AND 10°
BOTTOM CASES WITH VARYING BOTTOM DEPTHS

NORTH PACIFIC PROFILE
SOURCE DEPTH: 76 m, MODEL: P.E.

ARL - UT
AS-76-564
KCF - DR
4 - 27 - 76

103
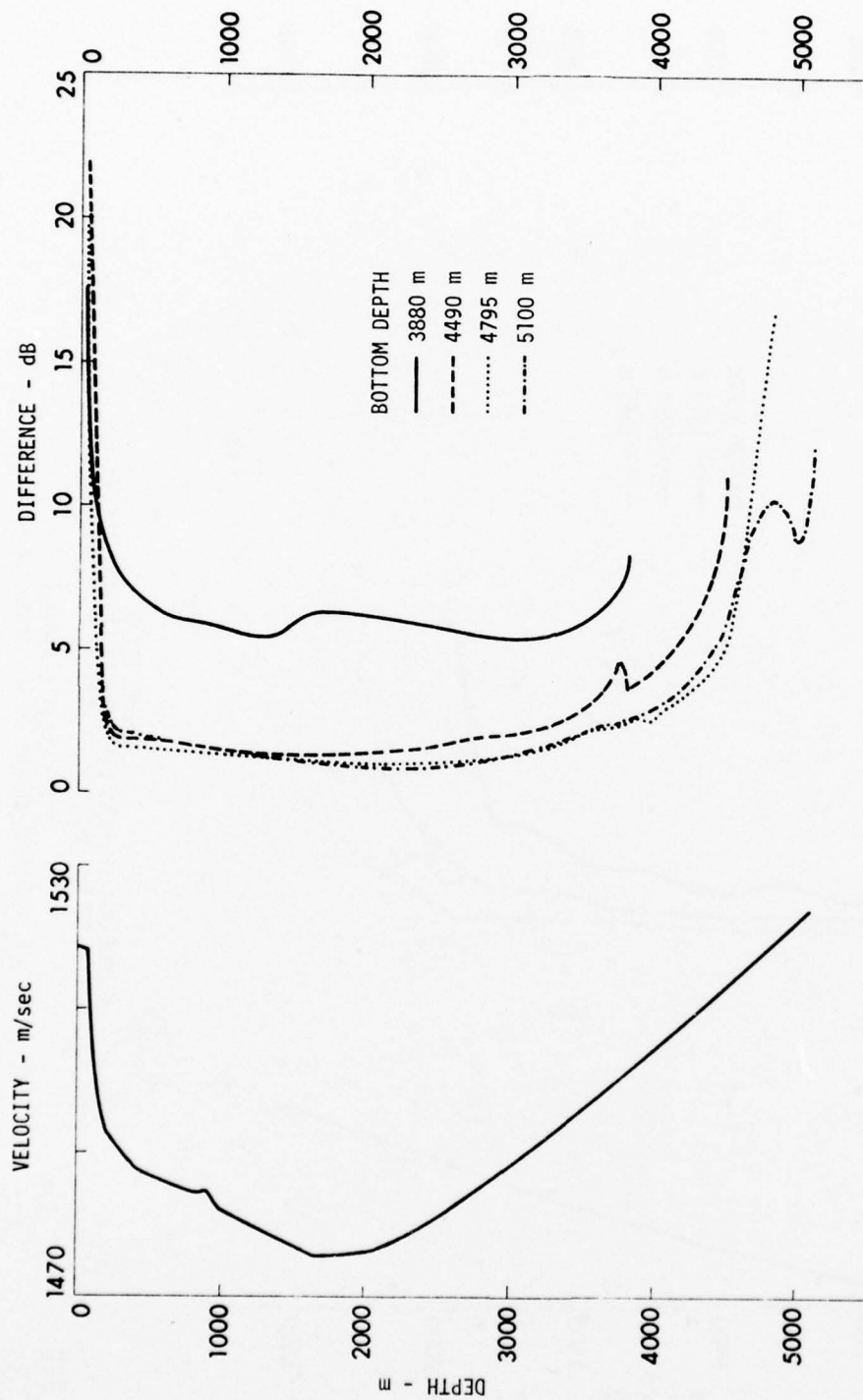
FIGURE III-9
PROPAGATION LOSS DIFFERENCES BETWEEN 1° AND 10°
BOTTOM CASES WITH VARYING BOTTOM DEPTHS

INDIAN OCEAN
SOURCE DEPTH: 152 m, MODEL: P.E.

ARL - UT
AS-76-565
KCF - DR
4 - 27 - 76

104
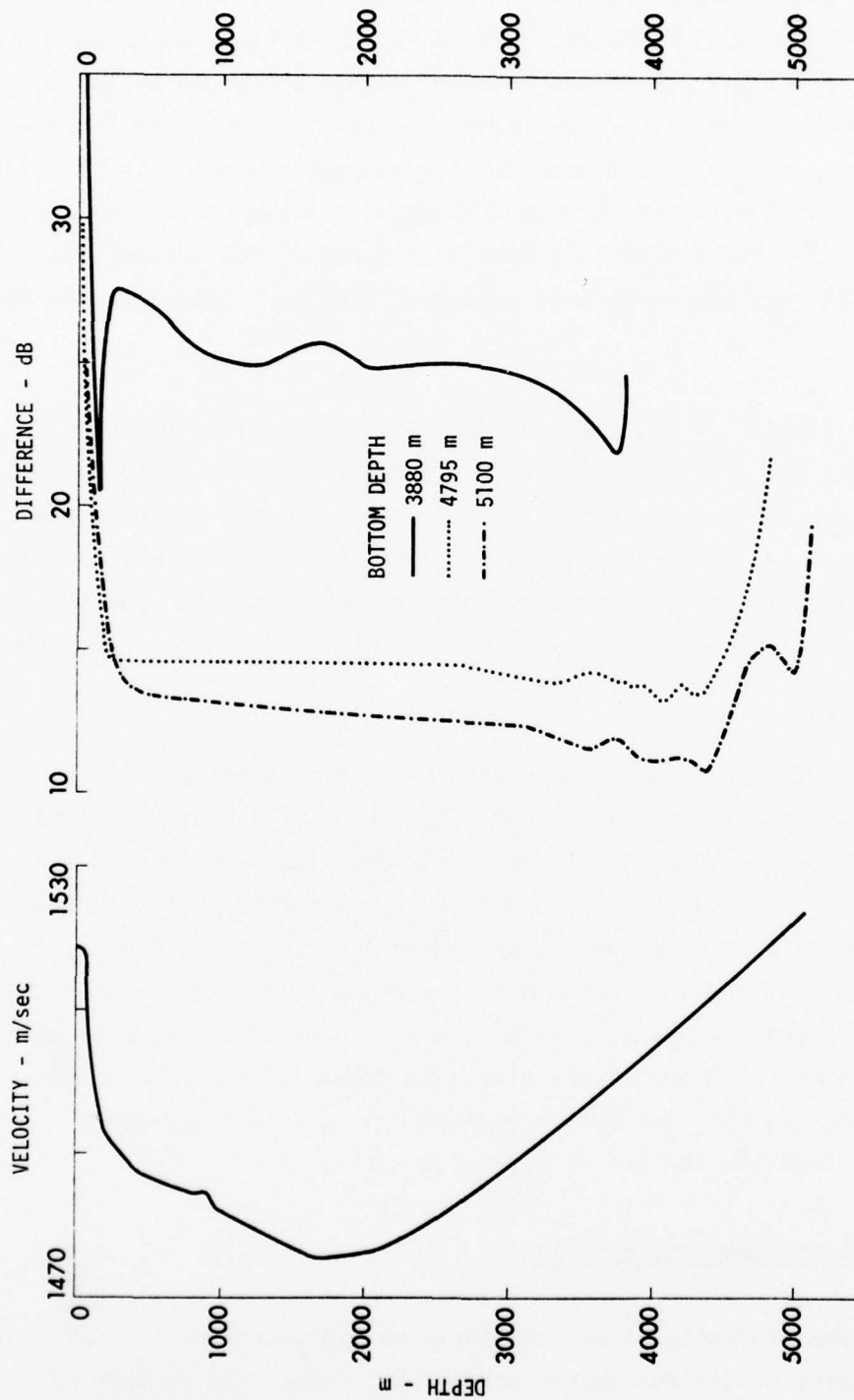
FIGURE III-10
PROPAGATION LOSS DIFFERENCES BETWEEN 1° AND 10°
BOTTOM CASES WITH VARYING BOTTOM DEPTHS

INDIAN OCEAN
SOURCE DEPTH: 18 m, MODEL: P.E.

The source depths used with the North Pacific profile had conjugate depths of 1945 m (50 m), 1514 m (60 m), 830 m (76 m), and 107 m (152 m). In Fig. III-7 the bottom influence again increases as the receiver depth approaches either the surface or the bottom in the first and third regions defined by the source and its conjugate depth. In the region between these two depths, the bottom influence no longer is as well defined as it is for the mid-Pacific profile. However, the propagation loss within this region attempts to present a regular dependence upon the bottom loss.

The studies on the effects of bottom depth variations were conducted using the P.E. model for both profiles. For the North Pacific profile the effects on propagation loss of varying bottom depths appears to increase the region of a regular dependence upon the bottom loss down into the third region defined by the source conjugate depth. The bottom influences again increase as a receiver above the source depth approaches the surface.

The two source depths used with the Indian Ocean profile had conjugate depths of 3585 m (152 m) and 4795 (18 m). The bottom depths used were critical depth (4795 m), critical depth plus and minus 305 m (5100 m and 4490 m), and the measured depth (3800 m). With the Indian Ocean profile the bottom influences are again seen to be divided into three regions. The major effects of bottom depth variations occur within the first and third regions along with the very near bottom effects seen earlier. However, when the source conjugate depth is within this very near bottom region, the near bottom effects extend into the region between the source and the source conjugate depth.

2. Bottom Bounce Energy Only

Further investigations have included modifications to FACT to provide propagation loss for bottom bounce rays only. The purpose of these modifications was to determine the distribution of bottom bounce intensity throughout the water column. The average propagation losses

were calculated and plotted in the same manner as before. Only the mid-Pacific profile has been used.

Figure III-11 is a representative set of these average propagation loss curves for the bottom bounce rays. The bottom loss descriptions for this figure are again a 0 dB loss below the critical angle and a 50 dB loss above. The distribution of bottom bounce intensities (the shape of these curves) is seen to be virtually independent of these bottom descriptions. (The propagation loss for the 1° critical angle case may have been undersampled in range, resulting in the modified shape of the curve). The distribution of these intensities, although not presented here, were also seen to be independent of variations in source depth. Figure III-11 could have represented variations in source depth. Variations in bottom depth simply displaced the near-bottom propagation loss decay in depth, leaving the shape of the upper portion unchanged. For these bottom loss descriptions the distribution of bottom bounce energy appears to be a function of the profile only. The bottom bounce energy is within 3 dB of being uniformly distributed throughout the water column.

Additional bottom loss descriptions were also investigated. When the bottom loss was monotonically increasing with grazing angle (Fig. III-12), the propagation loss curves again were characterized by the shape of the curves in Fig. III-11. Again, variations in source depth and bottom depth did not greatly modify the shape.

The bottom loss curve (solid line) in Fig. III-13 was also used in part of this study. Figure III-14 presents the propagation loss curves for four source depths. Although these curves are still similar in shape, there are definite differences. As the source depth increases, the near-axis propagation loss increases.

Two modifications to this bottom loss curve were used (dashed and dotted curves in Fig. III-13) to isolate the cause of the differences mentioned above. The propagation loss curves for the 600 m source appear in Fig. III-15. The modified bottom loss curve represented by the dotted
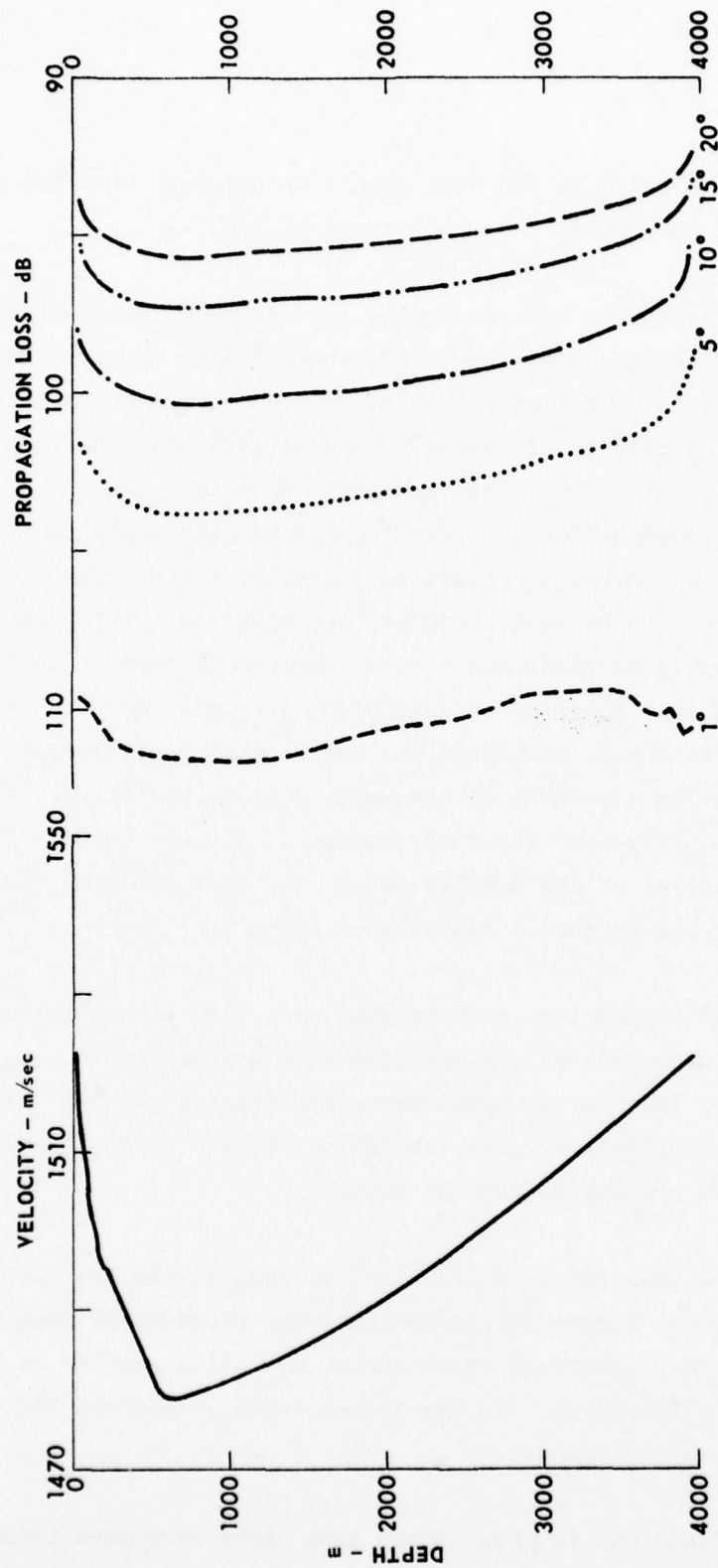
FIGURE III-11
AVERAGE PROPAGATION LOSS FOR BOTTOM BOUNCE RAYS ONLY
RANGE INTERVAL: 100 - 200 nm
MID-PACIFIC PROFILE
SOURCE DEPTH: 91 m, BOTTOM DEPTH: 3952 m, MODEL: FACT

ARL - UT
AS-77-198
KCF - DR
3 - 8 - 77

108
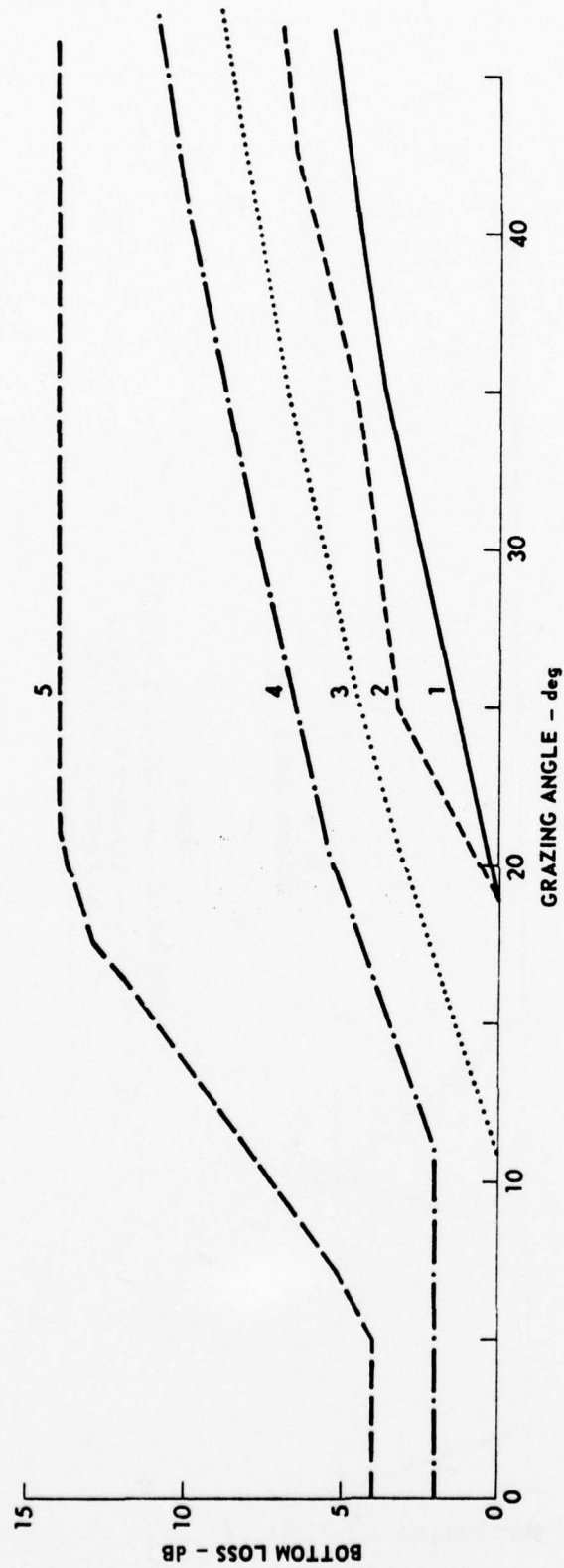
FIGURE III-12
STANDARD FACT BOTTOM LOSS CURVES FOR LOW FREQUENCIES
CURVE NUMBER CORRESPONDS TO BOTTOM CLASS

ARL - UT
AS - 77 - 199
KCF - DR
3 - 8 - 77

109
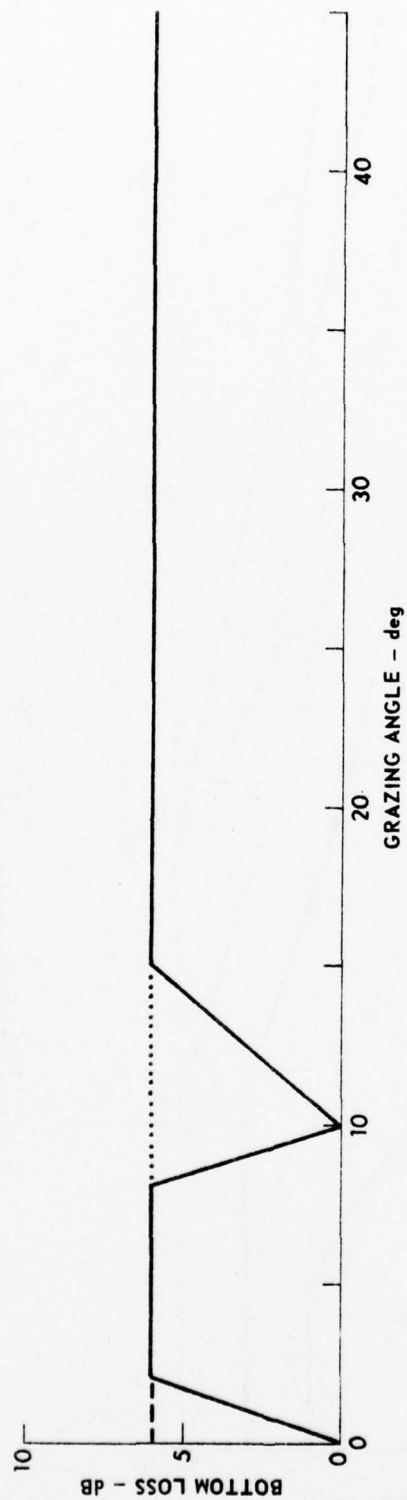
FIGURE III-13
BOTTOM LOSS versus GRAZING ANGLE

——— STYLIZED FIT TO DATA
··········· REMOVING 10° NOTCH
— — — REMOVING 0° FALLOFF

ARL - UT
AS - 77 - 200
KCF - DR
3 - 8 - 77

110
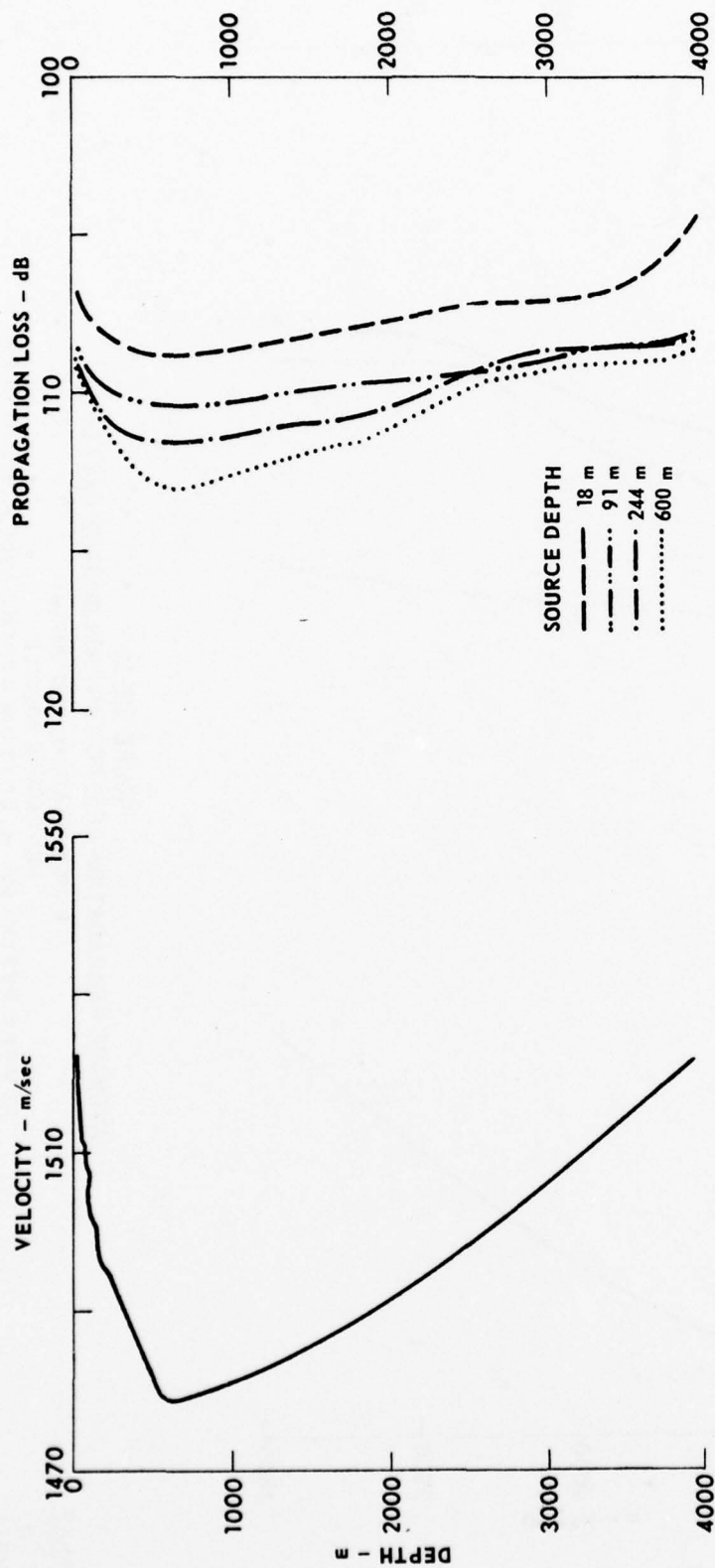
FIGURE III-14

AVERAGE PROPAGATION LOSS FOR BOTTOM BOUNCE RAYS ONLY
USING THE BOTTOM LOSS CURVE (SOLID LINE) FROM Fig. III-13

RANGE INTERVAL: 100 - 200 nm
BOTTOM DEPTH: 3952 m, MODEL: FACT
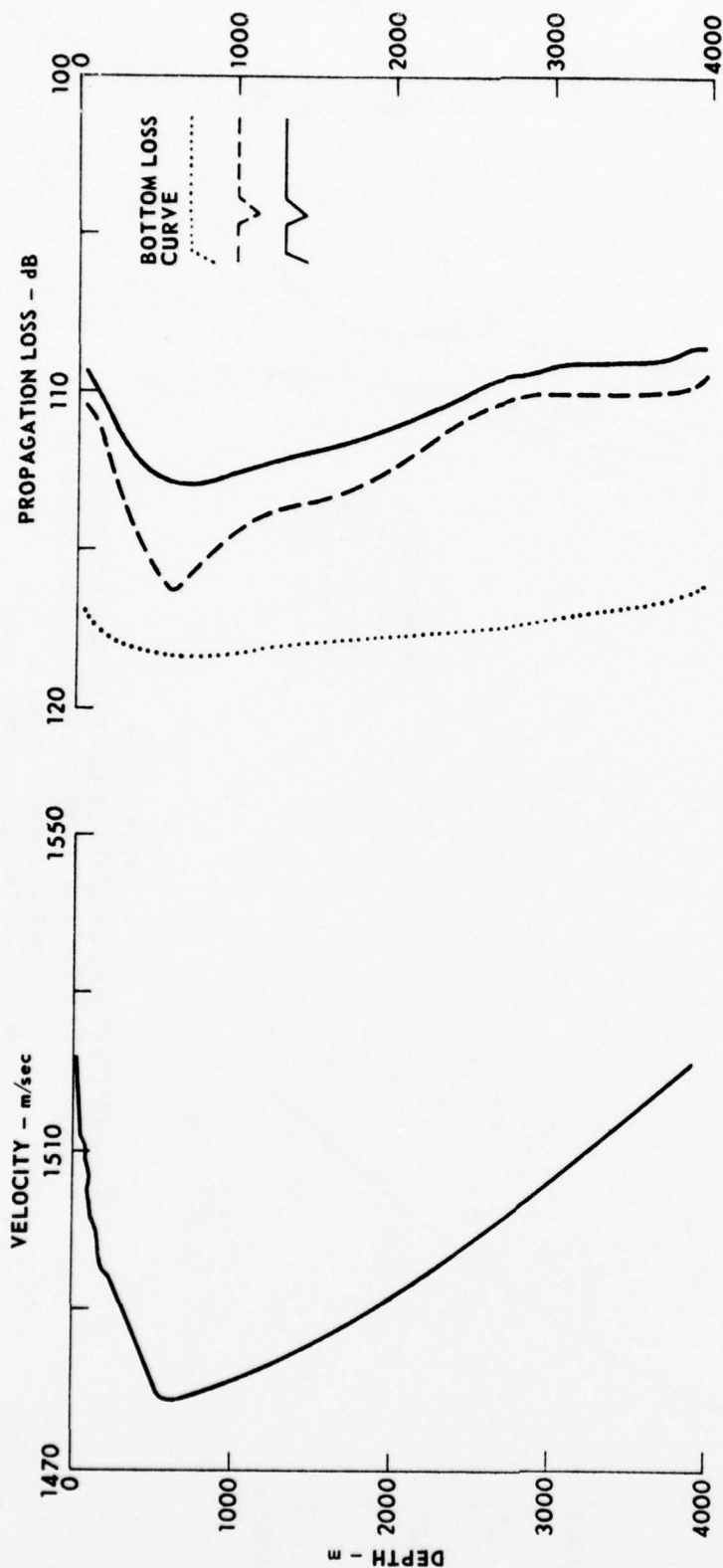
FIGURE III-15

AVERAGE PROPAGATION LOSS FOR BOTTOM BOUNCE RAYS ONLY

RANGE INTERVAL: 100 - 200 nm

MID-PACIFIC PROFILE

SOURCE DEPTH: 600 m, BOTTOM DEPTH: 3952 m, MODEL: FACT

curve generated a curve with the familiar shape presented in Fig. III-11. The modified bottom loss curve represented by the dashed line magnifies the variation in the shape of the propagation loss curves seen in Fig. III-14.

The propagation loss versus range curves for a monotonically increasing bottom loss curve and for the bottom loss curve in Fig. III-13 are presented in Fig. III-16 for the 600 m to 600 m source-receiver depth combination. This comparison was made to help isolate the cause of the differences seen in Figs. III-14 and III-15. The monotonically increasing bottom loss results in a smooth propagation loss curve. The notched bottom loss curve, however, results in a sawtooth curve; this indicates there is a bundling of bottom bounce energy. As the receiver moves off axis, the sawtooth structure decreases in amplitude approaching the smooth structure of the monotonically increasing bottom loss.

C. Conclusions

Bottom influences on propagation loss divide the water column into three regions based on the source and source conjugate depths. The total propagation loss within the region between the source and its conjugate depth has a regular dependence on the bottom loss. In the remaining two regions the bottom influence is dependent on the receiver depth. As the receiver approaches the surface, as well as the bottom, the bottom influence generally increases. In the very near bottom region (400 to 700 m from the bottom), wave theory may be required to adequately predict the depth dependence of the bottom influence.

Most bottom loss curves used in ray theory models are described by a monotonically increasing reflection coefficient. Additional attention needs to be placed on anomalous dips seen at the lower grazing angles in bottom bounce data.
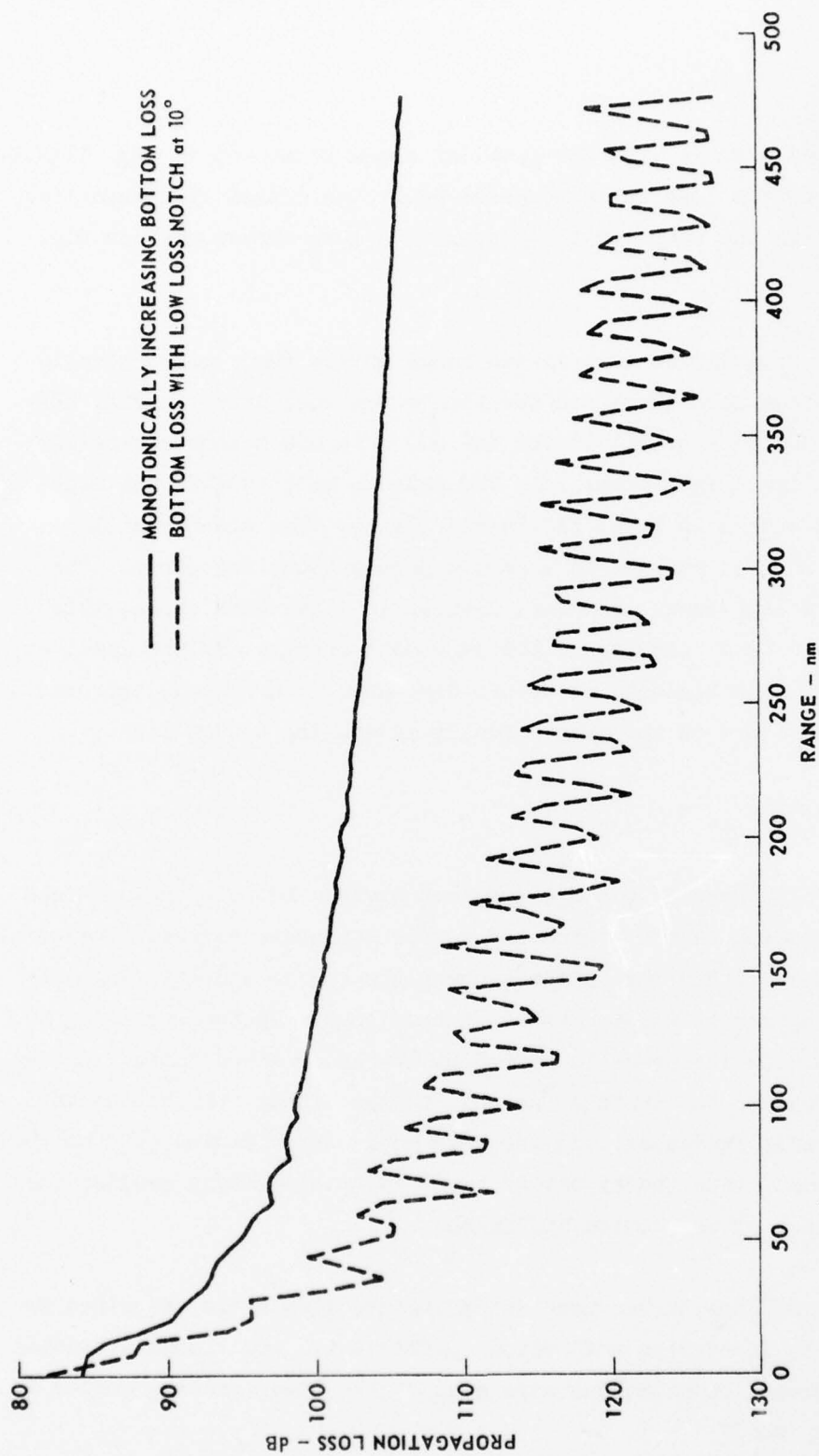
FIGURE III-16
PROPAGATION LOSS versus RANGE FOR BOTTOM BOUNCE ENERGY ONLY

— MONOTONICALLY INCREASING BOTTOM LOSS
– – BOTTOM LOSS WITH LOW LOSS NOTCH at 10°

RANGE – nm

PROPAGATION LOSS – dB

References - Chapter III

1. K. E. Hawker, K. C. Focke, and A. L. Anderson, "A Sensitivity Study of Underwater Sound Propagation Loss and Bottom Loss", Applied Research Laboratories Technical Report No. 77-17 (ARL-TR-77-17), Applied Research Laboratories, The University of Texas at Austin, 28 February 1977.

2. C. W. Spofford, "The FACT Model", Vol. I, AESD, Maury Center Technical Report No. 109, November 1974.

3. C. L. Baker and C. W. Spofford, "The FACT Model", Vol. II, AESD, Maury Center Technical Note TN-74-04, December 1974.

4. H. K. Brock, "The AESD Parabolic Equation Model", AESD, Maury Center Technical Note TN-75-07, December 1975.

5. K. E. Hawker, T. L. Foreman, and K. C. Focke, "A Status Report on Propagation and Bottom Loss Models in Use at ARL:UT", Applied Research Laboratories Technical Report No. 77-1 (ARL-TM-77-1), Applied Research Laboratories, The University of Texas at Austin, 28 February 1977.

IV. EFFECTS OF RANGE VARIABLE BATHYMETRY

This chapter contains a synopsis of work carried out during this contract year on the problems of sloping bottom and rough interface effects in propagation.

A. Sloping Bottom Effects

In the remainder of this section we will examine some data which show slope enhancement. The data will be compared to transmission loss curves generated using the parabolic equation model.

We shall define slope enhancement as the increase in sound level over the sloping area of a reflecting bottom above the sound level measured over the same sloping area of an absorbing bottom (critical angle$\equiv 0°$). This increase is illustrated in Figs. IV-1 and IV-2. The transmission loss curves presented in these figures were computed using the parabolic equation model described in a previous report (Hawker et al.[1]). The bathymetry and sound speed profile used in these model runs are shown in Fig. IV-3. Computations were done at a frequency of 93 Hz.

During a Naval exercise in the Atlantic Ocean, a continuous wave source was driven through deep water, over the continental slope, and over the continental shelf. Figure IV-4 sketches the bathymetry of the exercise area. Note that the steepest part of the continental slope lies between the ranges of 175 and 190 nmi.

Figure IV-5 shows a typical sound speed profile. All of the sound speed profiles in the area of interest were very similar to Fig. IV-5. The receiver depths having good data are indicated in the main section of the figure and the source depths in the inset. There is one receiver in each sound channel, one just below critical depth, and one on the upper border between the two sound channels. The shallow source lies in
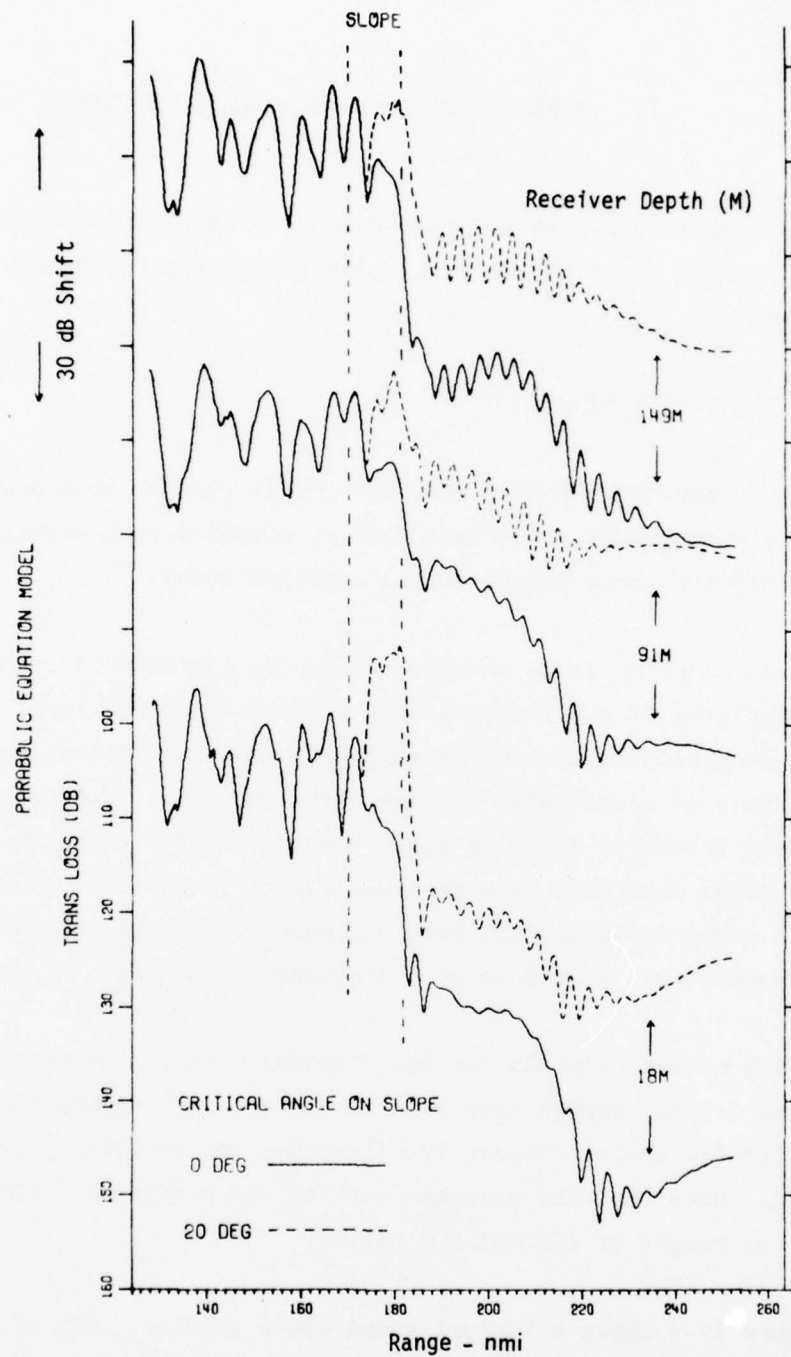
FIGURE IV-1
TRANSMISSION LOSS versus RANGE
FOR 3 RECEIVER DEPTHS WITH A
715 m SOURCE DEPTH

BS-76-162

118
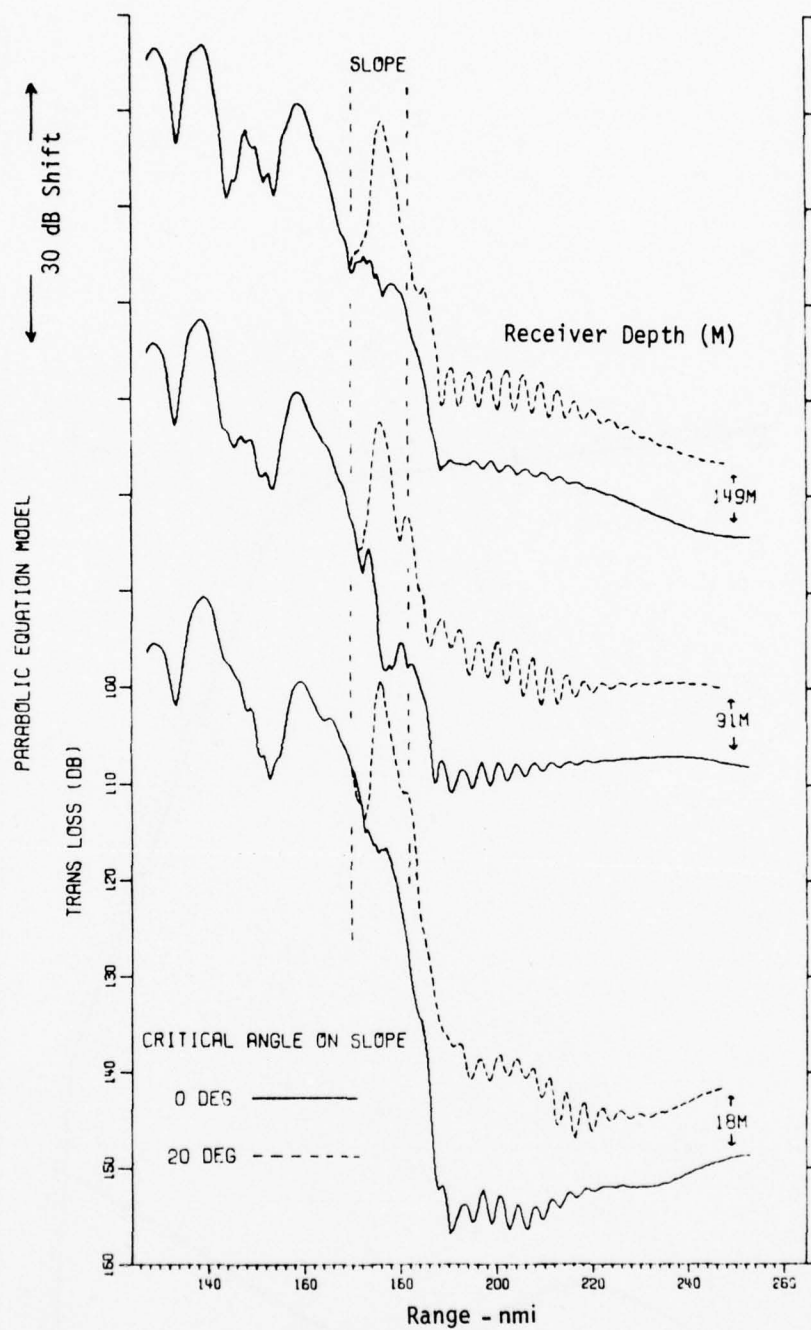
FIGURE IV - 2
TRANSMISSION LOSS versus RANGE
FOR 3 RECEIVER DEPTHS WITH A
2467 m SOURCE DEPTH

119
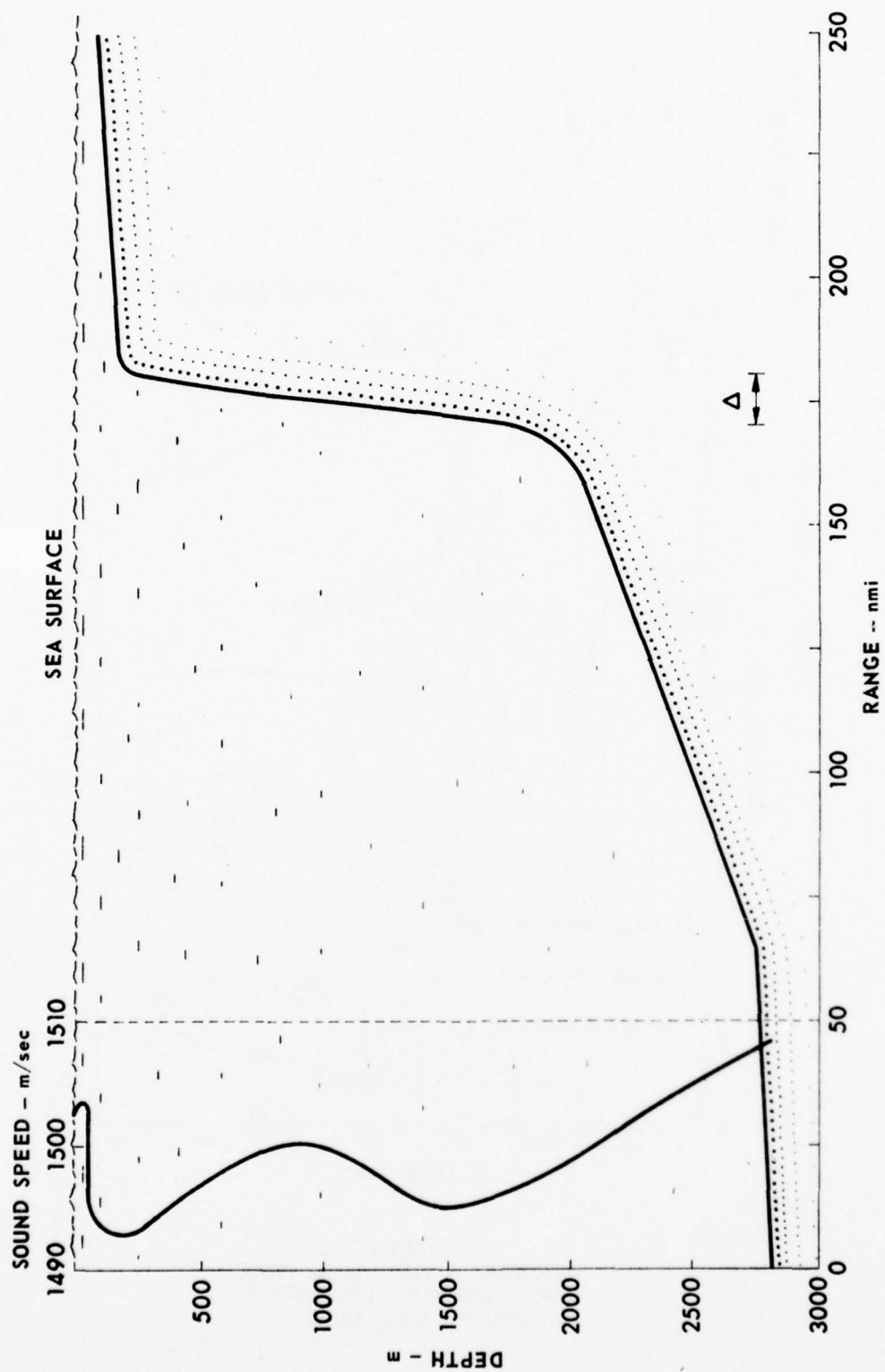
FIGURE IV-3
SOUND SPEED PROFILE AND BATHYMETRY
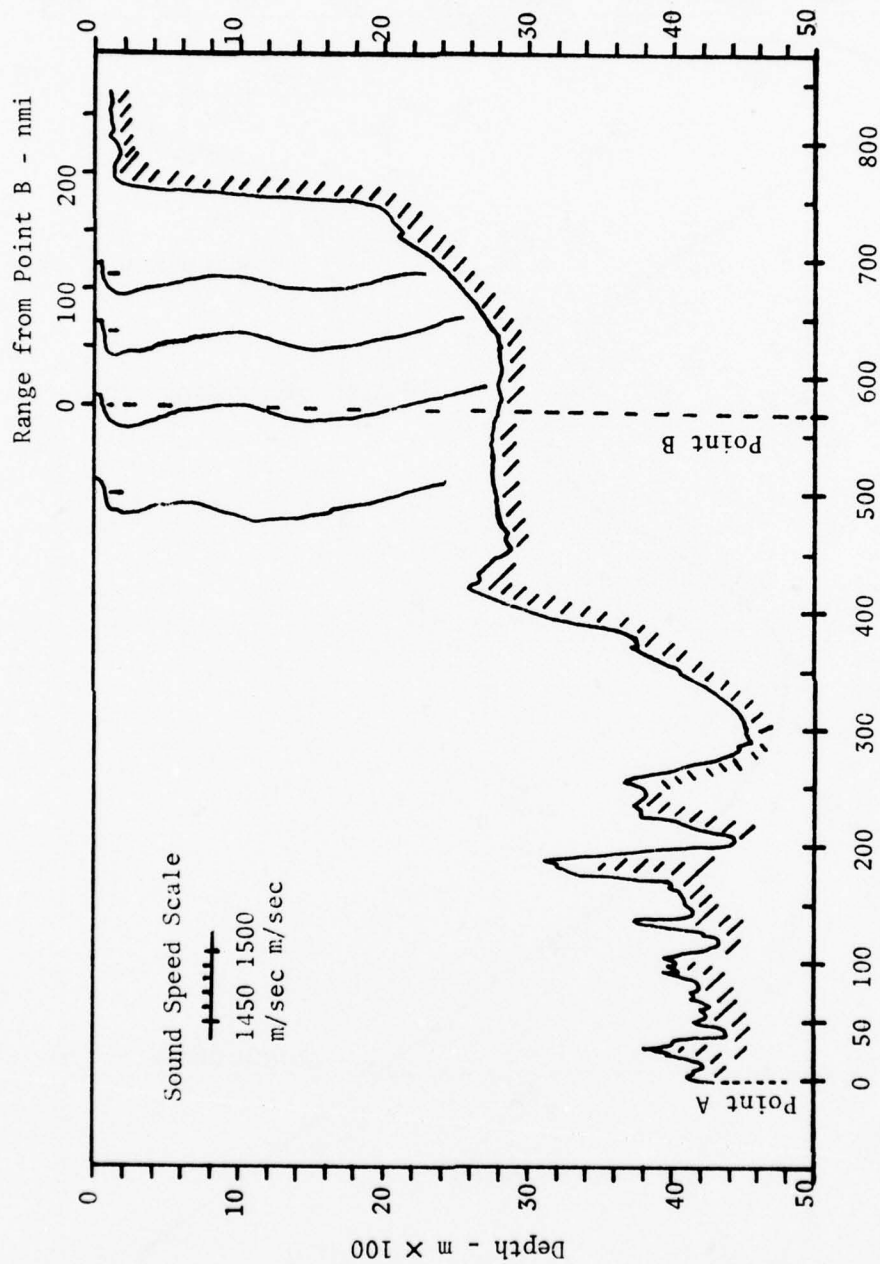
FIGURE IV-4

BATHYMETRY AND SOUND SPEED PROFILES

121

AS-76-164
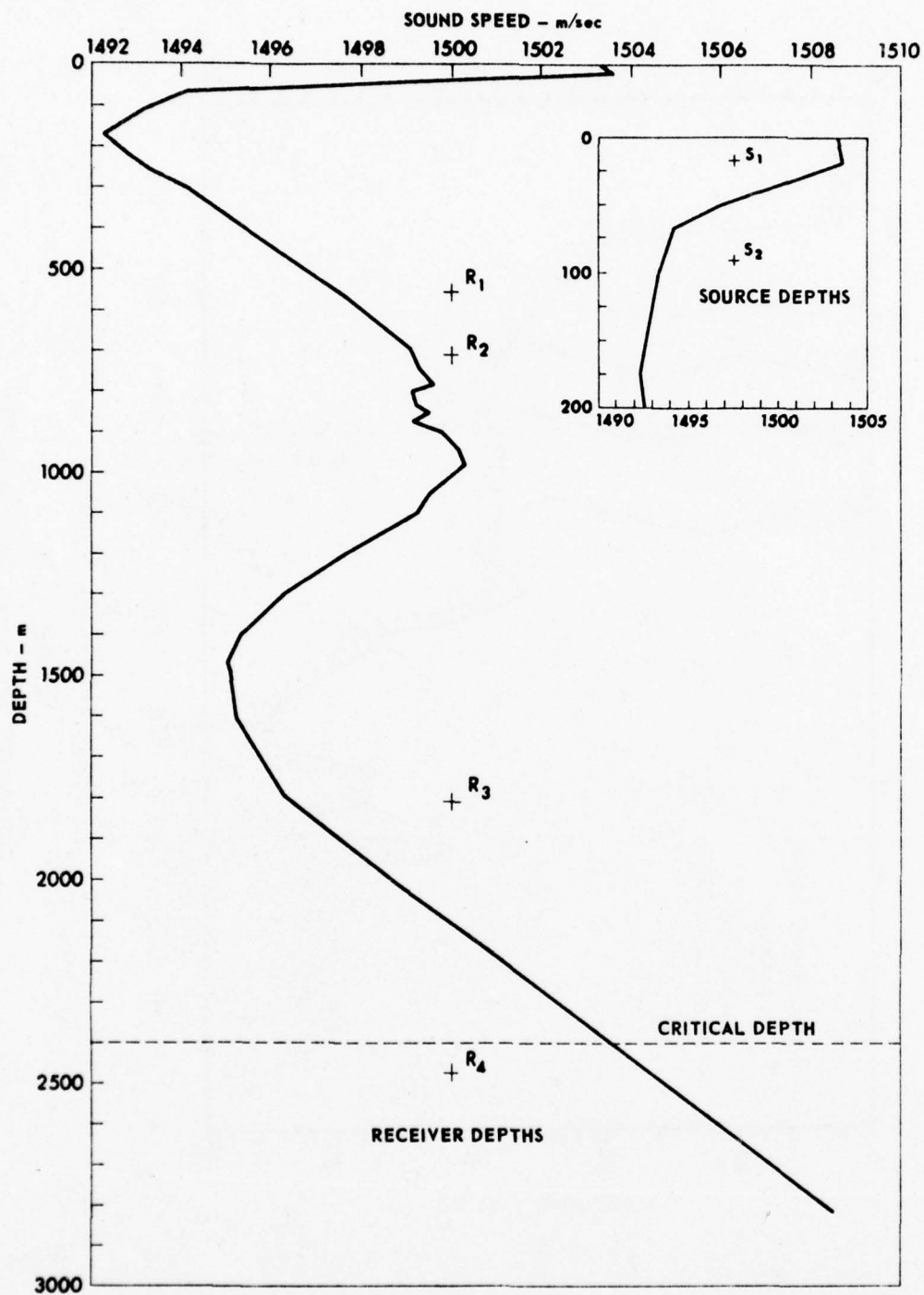
FIGURE IV-5
SOUND SPEED PROFILE FOR CONTINENTAL SLOPE DATA

the surface duct and the deeper source lies in the upper sound speed channel. Transmission loss was measured at 35 and 93 Hz for the shallow source and at 105 and 144 Hz for the deeper source.

The data have been smoothed by taking an equally weighted average of observations within 5 nmi of the desired range point. There is one bad data point at about 140 nmi for the receiver at 1810 m; this is suspected to be an unremoved shot. Such a point causes a spike in the smoothed data spread over 10 nmi; this area is shaded out of the data presented in Figs. IV-6, IV-7, and IV-8.

As a reference device, the dotted lines on Figs. IV-6, IV-7, and IV-8 indicate transmission loss given by simple cylindrical spreading. These reference lines were set by selecting a source level that would match the roughly averaged data around 100 nmi and computing cylindrical spreading from this selected pseudo-original source level. Note that, in Figs. IV-1 and IV-2, the transmission loss for the absorbing bottom drops sharply after the leading edge of the continental slope is encountered. Therefore, data levels remaining nearly at or above the cylindrical spreading line throughout the slope area will be interpreted as indicating slope enhancement.

Using the criterion discussed above, all of the data presented show some slope enhancement. The data at 93 Hz (Fig. IV-6) is clearest and has the most obvious slope enhancement of all the data examined. Transmission loss is enhanced by approximately 8 dB above the cylindrical spreading line for all but the deepest hydrophone. The deepest (2467 m) hydrophone is below critical depth and evidences reduced slope enhancement as well as a generally lower level for all frequencies and source depths examined here.

The data taken at 105 Hz (Fig. IV-7) shows a moderate slope enhancement of about 5 dB above the cylindrical spreading line for the 715
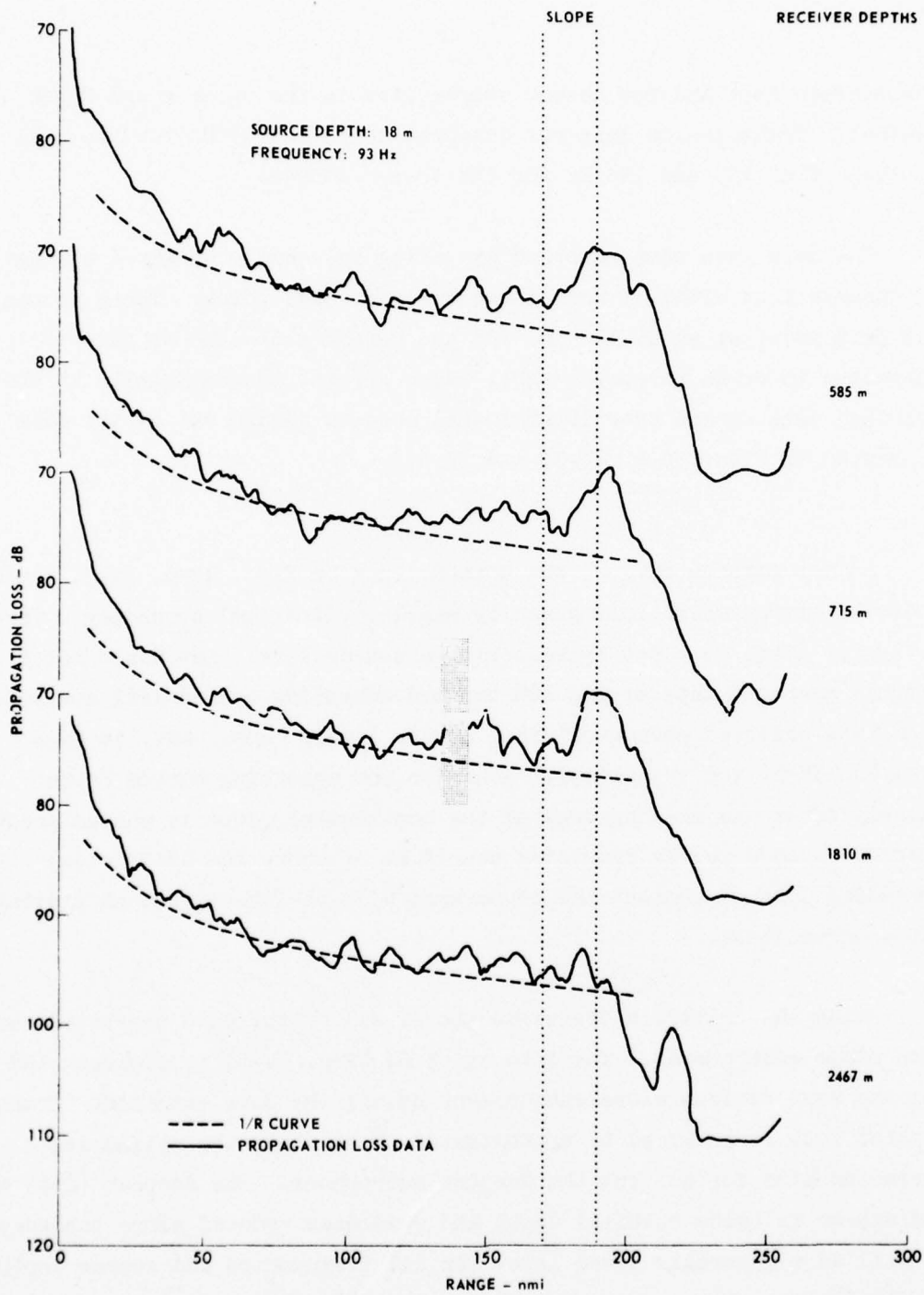
FIGURE IV-6
CONTINENTAL SLOPE DATA
f = 93 Hz
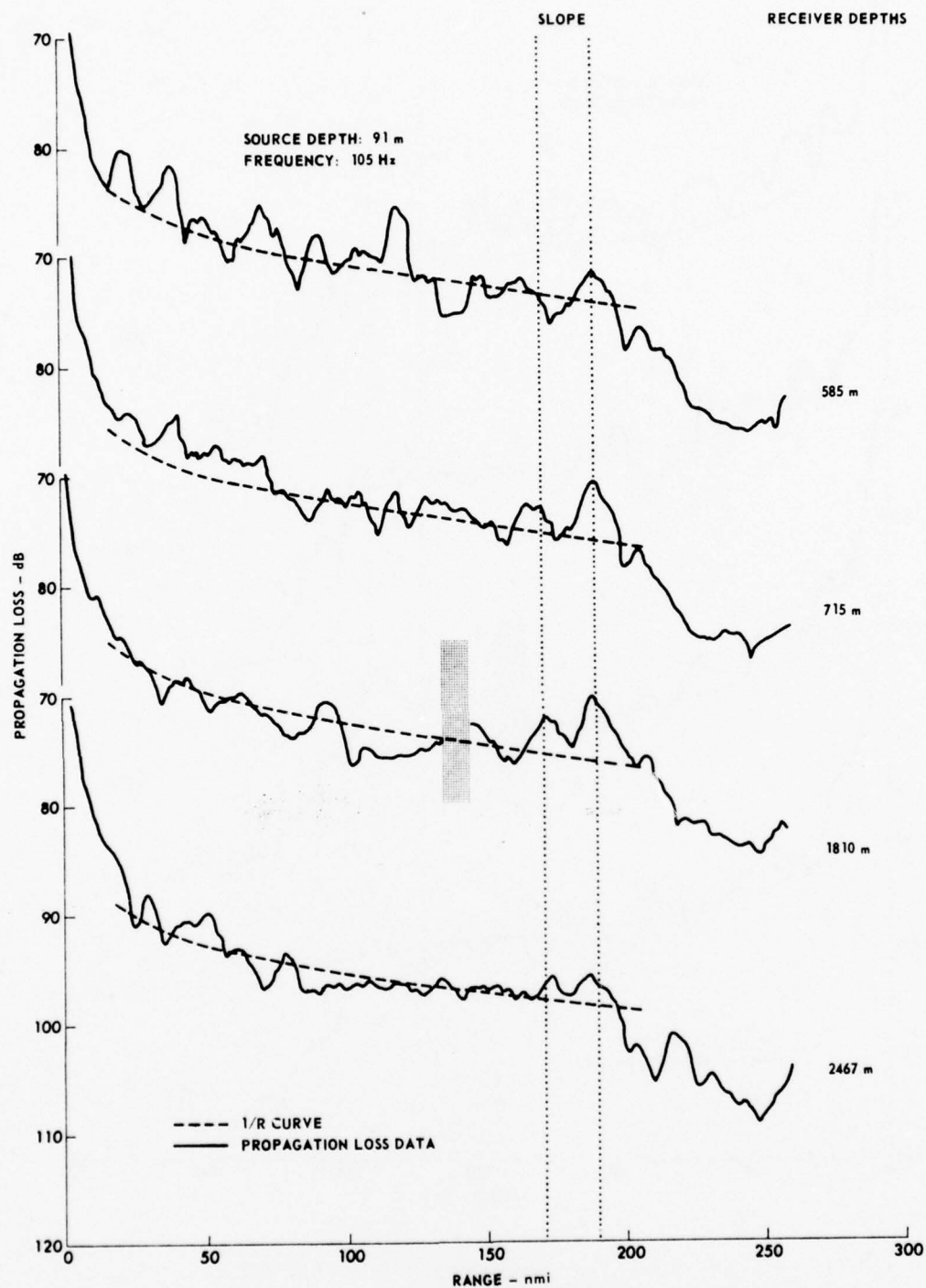
FIGURE IV-7
CONTINENTAL SLOPE DATA
f = 105 Hz

125
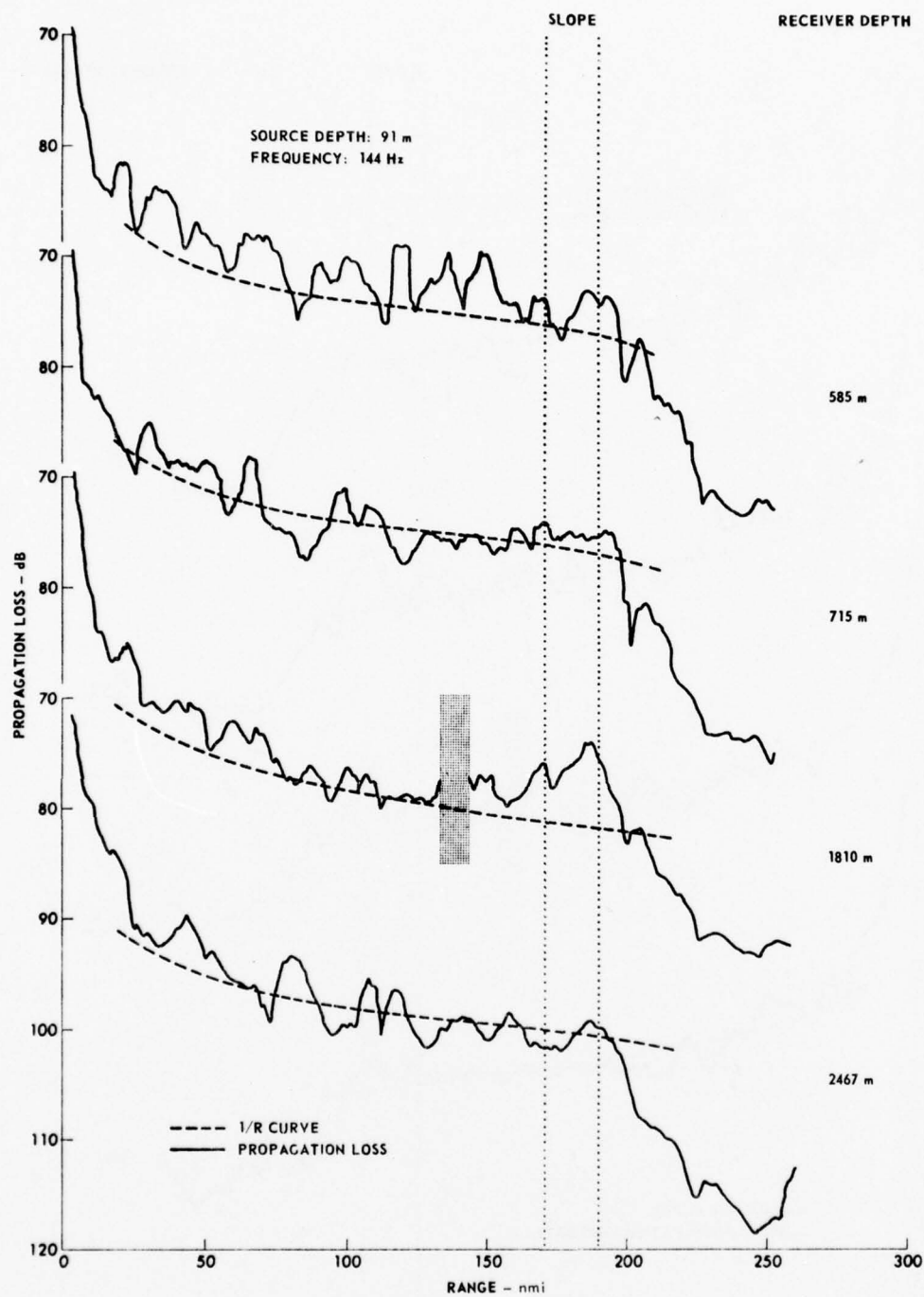
FIGURE IV-8
CONTINENTAL SLOPE DATA
f = 144 Hz

126

and 1810 m hydrophones. The hydrophone at 585 m shows less enhancement about 3 dB, than the middle hydrophones.

At 144 Hz (Fig. IV-8) the 585 m hydrophone shows moderate slope enhancement and 1810 m hydrophone strong enhancement. The 715 m hydrophone data evidence less enhancement than the data of other frequencies at this depth. The 2467 m hydrophone at 144 Hz shows less slope enhancement than any of the data. The data average to the cylindrical spreading level but, by the criterion stated earlier, slope enhancement is still present.

The 35 Hz data reflected cable strumming contamination and is not considered in this report.

In a previous report, Hawker et al.[1] drew three conclusions from the modeled transmission loss curves then available. We will compare the conclusions quoted from the report with the data presented here.

(1) Model conclusion -- All receiver depths show a slope enhancement with enhancement increasing with decreasing depth.

Data conclusion -- For the modeled transmission loss curves, "source depth" is receiver depth for the data and vice versa. Rectifying the switch in terms, shallower sources show more slope enhancement for the modeled curves. All data receiver depths show slope enhancement. The data from the 91 m source shows uniformly less enhancement than the data from the 18 m source. The change in frequency from 93 Hz to 105 Hz should not, by itself, cause any significant differences.

(2) Model conclusion -- The enhancement begins at a location corresponding to approximately 40% up the continental slope and peaks at the top of the slope.

Data conclusion -- The slope enhancement becomes apparent at about 40% up the continental slope, a range of about 180 nmi. The enhancement

peaks at or very near the top of the slope in all cases.

(3) Model conclusion -- Although the enhanced energy decays with distance beyond the top of the slope, the decay rate is nearly the same in all cases.

Data conclusion -- For all data at one frequency, the slope enhancement decays at nearly the same rate to nearly the same level for all receiver depths. The deepest hydrophone decays at the same rate as its shallower compatriots and to a level decreased by 4 to 8 dB.

The data conclusions generally agree with those drawn from the modeled transmission loss curves. The models show promise as an effective tool for studying slope enhancement aspects of the sloping bottom problem.

In addition to the work just described, additional studies have been carried out on the feasibility of employing normal mode coupling methods to the solution of sloping bottom problems. The chief advantage of such techniques would be the automatic incorporation of a detailed description of the bottom into the calculations. Assessments of existing techniques, such as ray trace methods and a parabolic equation approach already carried out under this program, indicate that it is necessary to consider the sub-bottom structure in detail, especially at very low frequencies.

The work carried out on a mode coupling approach is still in a formative stage and no quantitative results are yet available. It is expected that during the next contract year (FY 77) a definite decision will be made concerning the applicability and usefulness of this approach.

B. Rough Interface Studies

The general goal of the rough interface studies being conducted as part of the Naval Electronic Systems Command (NAVELEX), Code 320, sponsored bottom interaction program is to assess the usefulness of existing

techniques in accounting for the influence of bottom roughness on propagation. Also, the most viable of these techniques are to be used in a sensitivity study designed to define roughness regimes which are of practical importance to propagation problems.

During the present contract year (FY 76), research efforts in the area of rough interface effects have centered around the theoretical understanding of scattering theory and its applicability to propagation problems, as well as the nature and usefulness of a smoothed (or average) boundary condition approach. These efforts are still largely in a formative stage and will not yield significant quantitative results until the next contract year (FY 77).

The remainder of this section is devoted to a discussion of the nature of the rough surface problem and its relationship to the general problem of range changing bathymetry.

A plane wave incident on a statistically rough surface at a given angle gives rise to an outgoing scattered wave which is made up of an average or coherent field and a fluctuating or incoherent field. If the surface is only slightly rough (on the scale of a sound wavelength), the scattered energy will be primarily coherent and will be concentrated in the specular direction (reflection from a lossy mirror). As the roughness increases, the coherent component decreases and the incoherent component dominates, causing the scattered field to become more and more diffuse. In a propagation context these processes would be described in terms of mode conversion and energy flow from the coherent field into the incoherent field. Mathematically, the two problems, scattering and propagation, are quite different. In the scattering problem one seeks an asymptotic quantity, a scattering coefficient; in a propagation problem, however, the roughness affects the mode structure everywhere and nearfield effects, as well as coupling to refractive effects, cannot be ignored.

It is clear from research on scattering theory that both the amplitude

and phase of scattered fields can be appreciably altered by small roughnesses. This will cause a modification of arrival angle structure seen by an array as well as a redistribution of energy along the propagation path in such a way that the propagation loss is increased.

Various geophysical processes shaping the ocean basins have led to a wide spectrum of bottom roughness scales, ranging from the walls of the ocean basins (continental slopes) to minute ripples on otherwise smooth abyssal plains. Figure IV-9 shows a schematic representation of these scales as well as the ranges over which echo sounding and other methods can be used.

The bottom interaction program at ARL:UT has concentrated on examining the effects of bathymetry variations having wave numbers on the extremes of this spectrum. On the one hand there are the very large scale effects 10^3 m to 10^5 m which are being investigated under the heading of sloping bottom problems. Examples of effects in this range were given in the previous two sections of this chapter. At the other extreme there are the small scale irregularities, treated stochastically, which are part of the bottom roughness study. As ever, the intermediate ground is the most difficult and techniques applied to either extreme are not necessarily well adapted for use there. The topic of roughness scales as well as acoustic interaction is discussed at length by Clay and Leong.[2]

The points made about topographical scales in Fig. IV-9 can be given added force with a realistic example. The bathymetry of the baseline track for a Naval exercise in the Pacific Ocean was analyzed for its statistical properties. The distribution of heights around the mean plane for this section is given in Fig. IV-10. The rms height was found to be 119 m. The correlation coefficient of heights given in Fig. IV-11 is seen to decay rapidly toward zero at approximately 25 km, followed by quasi-periodic behavior. The rms slope computed for this track interval is 1.1°. The "average length" computed using an "average" slope of 1.1° and an "average" height of 120 m is 6.25 km, which agrees well with the range
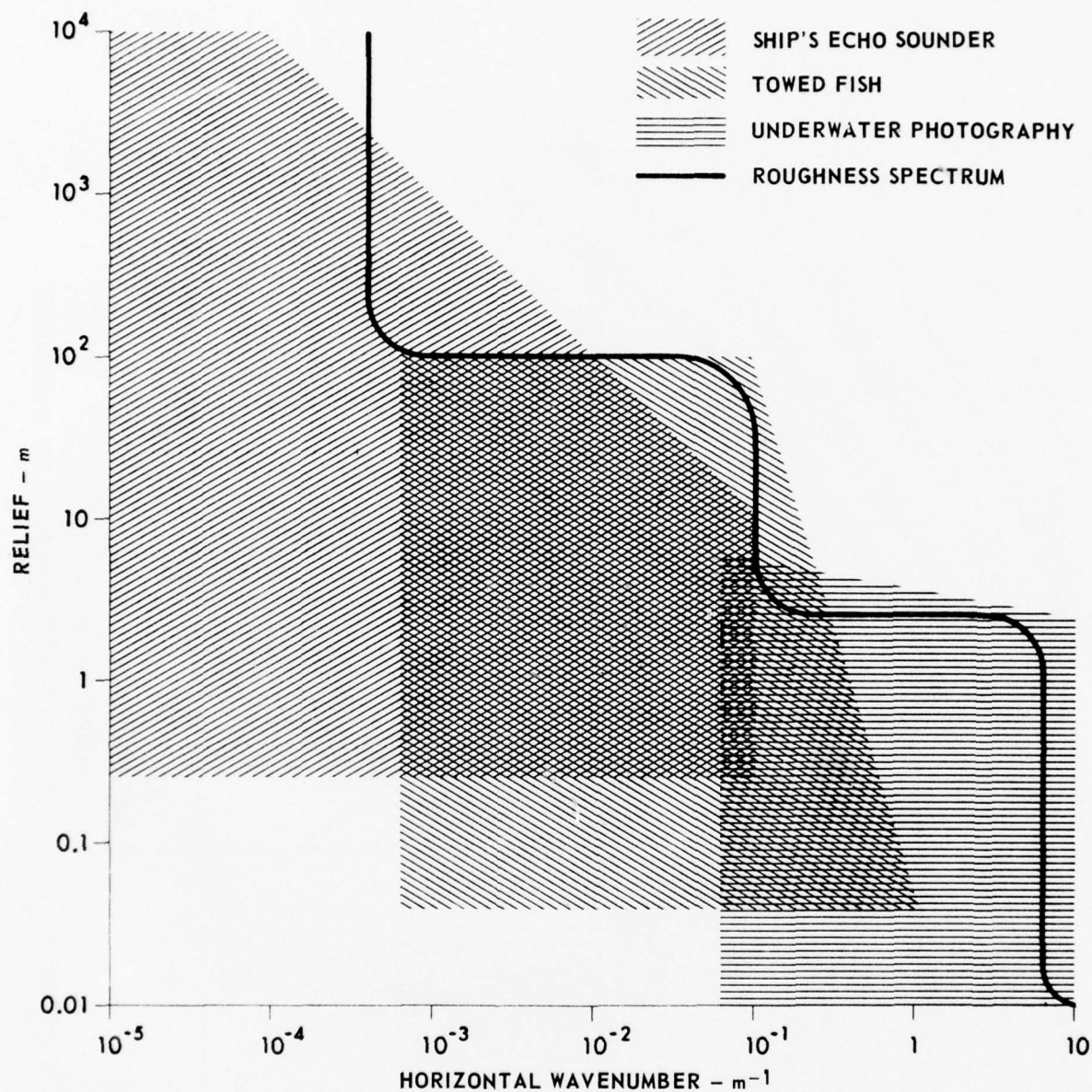
-130-

FIGURE IV-9
SPECTRUM RANGE OF SEA FLOOR ROUGHNESS AND RESOLUTION
CAPABILITIES OF MEASUREMENT TECHNIQUES

ARL - UT
AS-77-279
KEH - DR
3 -22 -77

(Adapted from Akal[25])

HEIGHT ABOVE MEAN DEPTH (m)
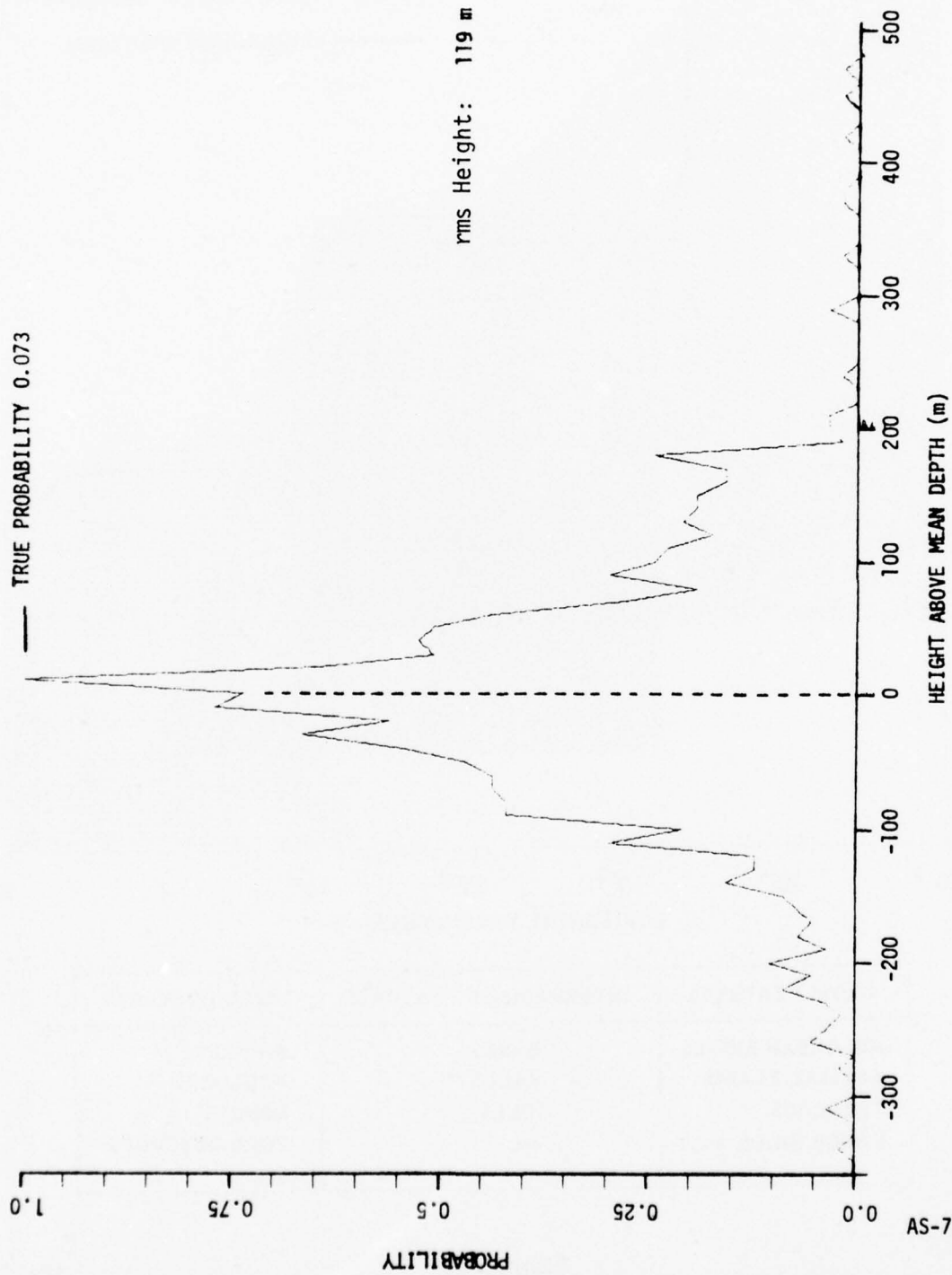
FIGURE IV-10

RELATIVE PROBABILITY DENSITY OF HEIGHTS ABOVE MEAN DEPTH FOR CHURCH ANCHOR
BASELINE TRACK FROM SITE B TO SITE C

rms Height: 119 m

TRUE PROBABILITY 0.073

PROBABILITY

AS-77-289

132
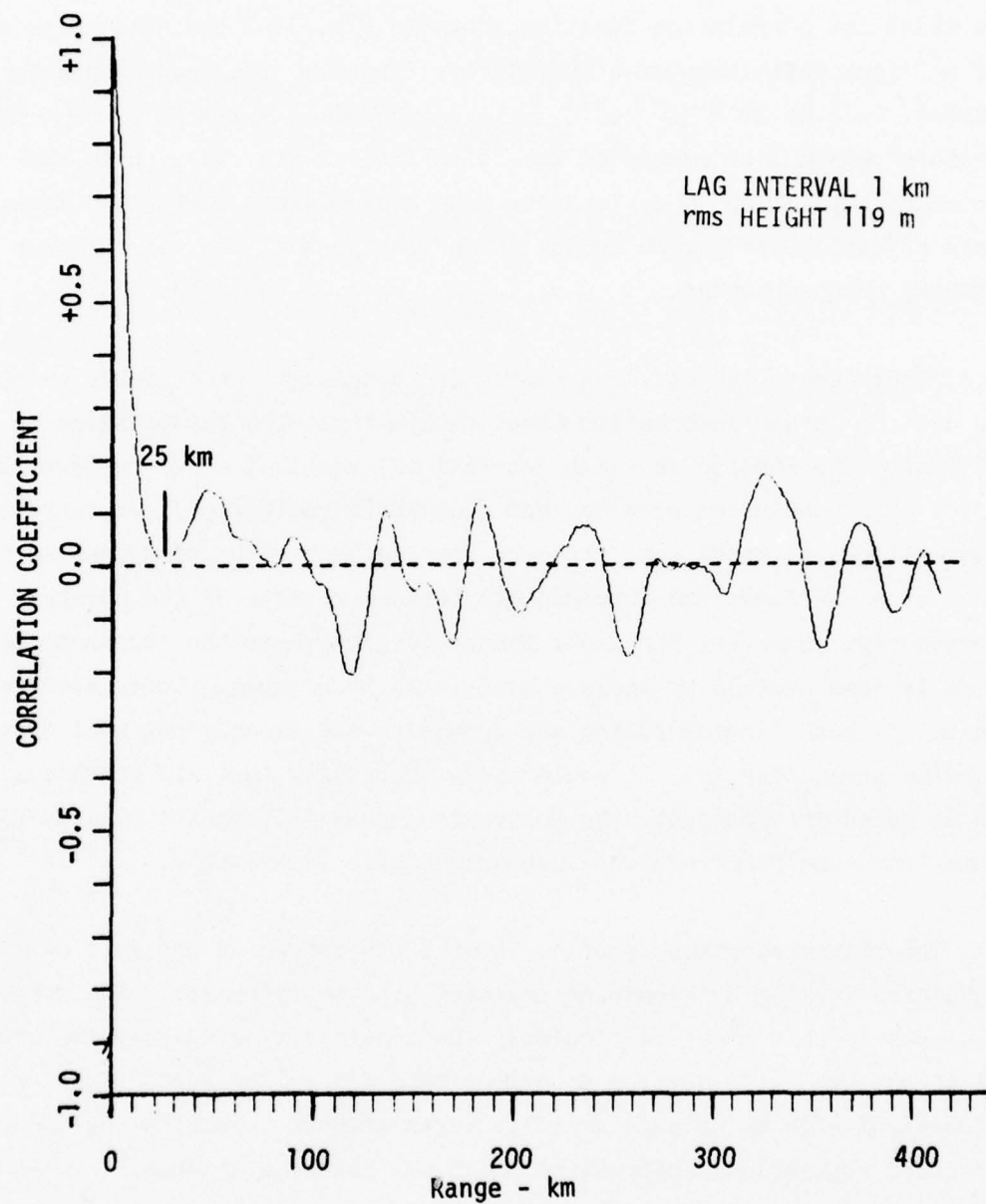
FIGURE IV-11

CORRELATION COEFFICIENT OF WATER DEPTHS versus RANGE
ALONG CHURCH ANCHOR BASELINE FROM SITE B

133

at which the correlation function shown in Fig. IV-2 has decayed to a value of e^{-1} (one definition of a correlation length). The resulting wave number, $2\pi/6.25$ km $\cong 10^{-3}$ m^{-1}, and height, 120 m, leads to an "average feature" which lies nearly on the solid line of Fig. IV-9, near the boundary separating large features from intermediate features. Thus, this abyssal hills region is one which lies just at the outer bounds of the sloping bottom problem.

There are a variety of acoustic and nonacoustic techniques which can be used to obtain information about bathymetry. The shaded areas in Fig. IV-9 show the domains in which conventional vertical echo sounders, deep towed high resolution systems, and underwater photography are operative. Conventional vertical echo sounders, having beamwidths of approximately $10°$, span the large and intermediate feature regions of the spectrum adequately. However, the small feature region where the roughness problem lies is inaccessible by these conventional techniques. Underwater photography is both time consuming and expensive and clearly not well adapted to wide area coverage. It would seem, therefore, that, if roughness is to be taken into account, the bottom roughness information will have to come from some other source, such as acoustic experiments.

The bottom roughness problem is thus one for which one gets no intuitive feeling by examining ordinary bathymetry charts. The goal of research in this area, particularly the sensitivity studies being conducted at ARL:UT, is to develop an approximate method for accounting for the acoustical effects of such small features without requiring the use of detailed statistical information which may not be available.

This effort is based on the use of a smoothed boundary condition applied to the mean (flat) surface. Initial work suggests that this approach can be turned into a well-defined, useful method for obtaining roughness effects in which one can have high confidence.

Although it is by no means clear that any results from rough surface

scattering theory can be used to provide boundary conditions in a propagation model, it is nevertheless useful to examine one case of rough surface scattering. Under reasonably general circumstances it can be shown that the intensity of the coherent scattered field, I_s, can be given in terms of the field reflected from a plane surface of the same material, I_p, by the expression $I_s = \sigma_{coh} I_p$, where σ_{coh} is the coherent scattering coefficient. Figure IV-12 shows an example of the comparison of computed coherent scattering coefficients with measurements made at ARL:UT. These data have been reported by Boyd and Deavenport.[3] The Rayleigh parameter g is defined as $4k^2 h^2 \sin^2 \theta$, where k is the acoustic wave number, h the rms height, and θ the grazing angle. It will be observed that, for small roughness (small g), both theoretical predictions converge on the data and agreement is good. For the range $0 \leq g \leq 1.5$ the scattering can be expected to be primarily coherent and theoretical prediction of the scattering coefficient will be good. It is just this regime which is important in the low (and very low) frequency bottom interaction problem. For example, at 100 Hz a feature 1 m high will produce a Rayleigh parameter value less than 0.70. Such a feature with a mean length of 6 m will lie near the center of small roughness regime of Fig. IV-9.
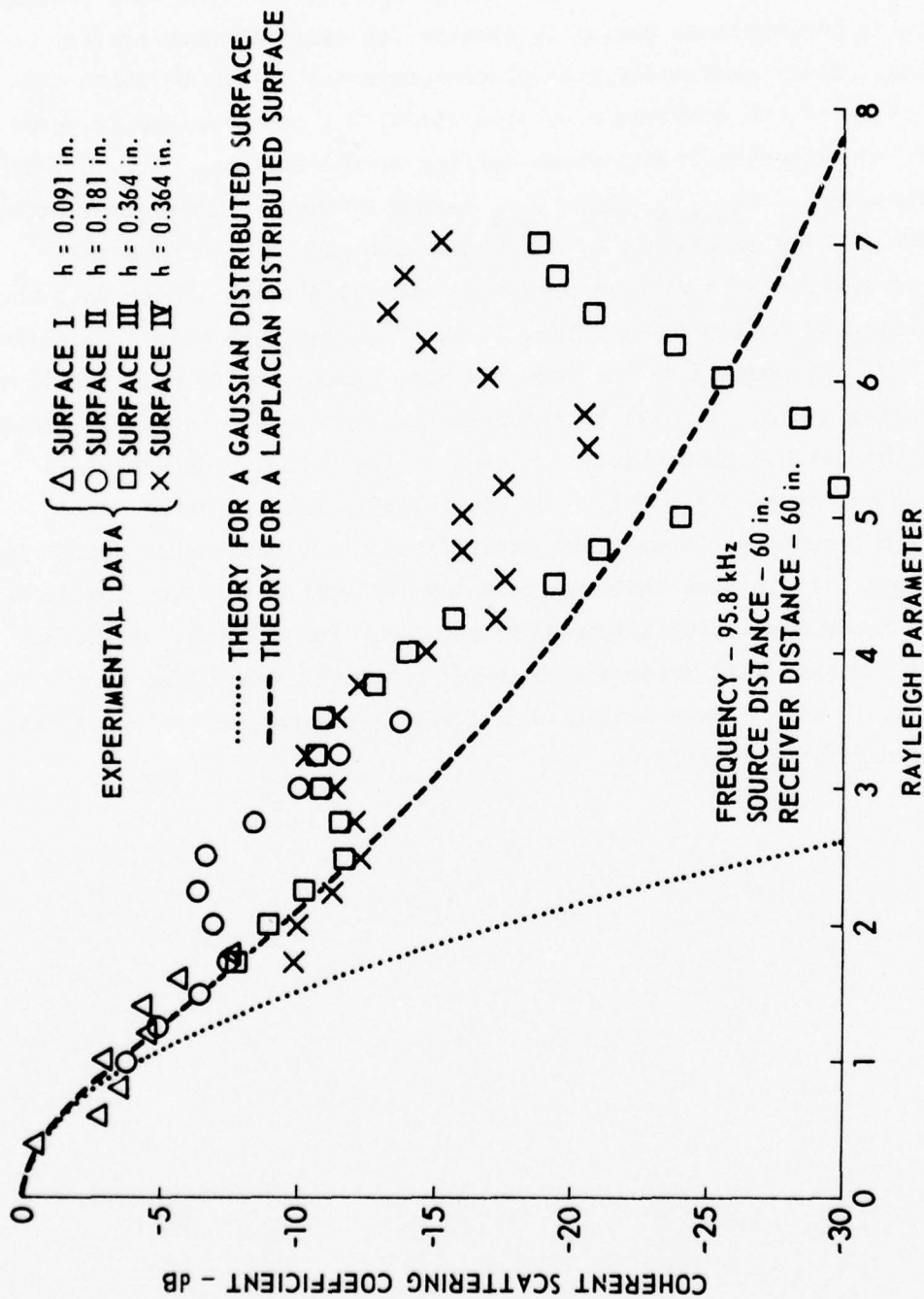
FIGURE IV-12

COMPARISON OF THE EXPERIMENTAL AND THEORETICAL SPECULAR
COHERENT SCATTERING SURFACES FOR ALL FOUR SURFACES

References - Chapter IV

1. K. E. Hawker, A. L. Anderson, K. C. Focke, and T. L. Foreman, "Initial Phase of a Study of the Bottom Interaction of Low Frequency Underwater Sound", Applied Research Laboratories Technical Report No. 76-14 (ARL-TR-76-14), Applied Research Laboratories, The University of Texas at Austin, 6 April 1976.

2. C. S. Clay, and W. K. Leong, "Acoustic Estimates of the Topography and Roughness Spectrum of the Sea Floor Southwest of the Iberian Peninsula", Physics of Sound in Marine Sediments, L. D. Hampton (ed.), (Plenum Press, New York, 1974).

3. M. L. Boyd, and R. L. Deavenport, "Forward and Specular Scattering from a Rough Surface: Theory and Experiment", J. Acoust. Soc. Am. 53, 791 (1973).

V. ANALYTICAL TECHNIQUES FOR DETERMINING SUBBOTTOM VELOCITY PROFILES IN UNCONSOLIDATED SEDIMENTS

The purpose of this chapter is to discuss and summarize research previously released in an ARL:UT technical report by Rutherford.[1] The purpose of this work was to describe and summarize different analytical methods for determining velocity profiles in unconsolidated sediments from experimental data. This work was by no means exhaustive; its intent was to assemble in one place those methods which would be most useful to underwater sound propagation modelers and best suited to the types of data to which they usually have access.

There are different ways of obtaining information about the velocity structure of the subbottom. In shallow water, divers with probes can take samples of the upper few meters of sediment for later laboratory analysis. A somewhat deeper probing of the sediment structure is possible with sediment coring apparatus deployed from a research vessel. The cores thus obtained may be analyzed in the laboratory or the velocity profile of the sediment may be measured in situ with a device such as the ARL:UT Compressional Wave Profilometer,[2] which can be attached to a corer. These direct methods are limited by the depths that a corer can probe, roughly 30 m. The only other direct methods involve the analysis, either in situ or laboratory, of drilling cores. This method, which is very useful in many acoustic studies, relies on well cores which are often widely spaced and must be supplemented with other methods.

The methods addressed in the abovementioned report are indirect, acoustical techniques, which more often than not provide the only way of estimating the velocity structures of the unconsolidated sediments to the depths required by underwater propagation modelers. These indirect methods are concerned only with the unconsolidated sediments, although some of the methods can be and are used in seismic profiling. Seismological methods such as those involving lateral and shear waves were not discussed in the report. The report was primarily intended to serve the needs of those

-139-

PRECEDING PAGE BLANK-NOT FILMED

working in the field of underwater sound propagation modeling who have little knowledge of the techniques for extracting subbottom velocity information which is necessary input for their models.

The remaining sections of this chapter will summarize the different methods that were discussed and detailed in the abovementioned report. The intent of these methods is to extract information concerning sound speed gradients, layering structure, and layer velocities from experimental data, primarily wide angle profiling data.

The summary in the following sections of this chapter deals with the different methods in the order they were discussed in the original report. The different analytical techniques treated are the reflected arrival methods, the $V(t)$ method, and the refracted arrival methods. In the original report, the treatment of each method comprised an entire chapter. In the following, the discussion of the analytical methods will be dramatically condensed. Each method will be briefly described, the results of any examples will be quoted, and one example showing the connection between the reflected arrival methods and the $V(t)$ method will be included.

A. Reflected Arrival Methods

The first analytical techniques treated are the reflected arrival methods. These methods are most useful when wide angle subbottom profiling data which exhibit a sediment layering structure are analyzed. The purpose of the reflected arrival methods is to determine the sound velocities and thickness of subbottom sediment layers from travel time curves obtained from wide angle profiling.

There are two basic types of reflected arrival methods, the $T^2(X)$ methods [3,4,5,6] and the ray parameter methods.[7] In the derivation of both of these methods, it is necessary to make certain simplifying assumptions about the velocity structure of the layers being analyzed so that tractable mathematical results may be obtained. The validity of these simplifying

assumptions ultimately determines how well the $T^2(X)$ and the ray parameter methods perform.

1.   The $T^2(X)$ Method[3,4,5,6]

The three $T^2(X)$ methods are the reduced time-reduced distance method, the short range method, and Durbaum's method. The methods are based on the fact that the relationship between the travel time of a ray reflecting in a single isovelocity layer and the range attained while the ray is traveling through that layer is a hyperbolic one given by

$$T^2(X) = T^2(0) + \frac{1}{C_1^2} X^2 \quad .$$

The quantity denoted by C_1 is the isovelocity speed of sound in the layer and $T(0)$ is the vertical two-way time through the layer. The linear relationship between $T^2(X)$ and X^2 for the isovelocity layer allows C_1 and $T(0)$ to be obtained graphically if the travel-time curve (T versus X) of arrivals reflecting in the layer is known.

When the $T^2(X)$ methods are applied to wide angle profiling data, the layers exhibited by the profiling data are assumed to be isovelocity. This isovelocity assumption allows one to analyze travel-time curves of subbottom layers by subtracting the effects of the overlying layers such that a one-layer problem remains. When this is done, the velocity of sound and layer thickness in a subbottom layer may be obtained in the same manner that one would use for the single layer case.

The isovelocity assumption necessary in the derivation of the $T^2(X)$ methods has two major effects. First, when the $T^2(X)$ methods are applied to nonisovelocity situations, the sound velocities obtained are interpreted as interval velocities, which are the time averaged sound speeds through the layer. Second, the $T^2(X)$ methods cannot be applied to situations in which the ratio of the thickness of the overlying layers to that of the subbottom layers being analyzed is greater than about 15:1.

This problem arises because the absolute error introduced by the isovelocity assumption in overlying layers is magnified, in the layer being analyzed, by the ratio of the thickness of the overlying layers to the thickness of the layer in question. When this ratio exceeds about 15:1, the $T^2(X)$ methods can no longer be relied upon to give accurate results.

In the text of the abovementioned report the reduced time-reduced distance method and the small range method are illustrated with examples. Both of these methods are used to find the layer velocity in a 200 m thick sediment layer underlying a 500 m thick water layer (thickness ratio 2.5:1). The reduced time-reduced distance method determined a layer velocity of 1539 m/sec and the small range method yielded 1575 m/sec. The standard value calculated from equations derived in the report was 1561 m/sec, which yielded percentage differences of 1.4 and 0.89, respectively.

2. The Ray Parameter Method[7]

The ray parameter method, which is the second of the reflected arrival methods, is fundamentally different from the $T^2(X)$ methods, although it also analyzes travel-time data of reflected arrivals. The ray parameter method is unique in that water or sediment layers overlying the layer to be analyzed are irrelevant to the solution; thus, simplifying assumptions about the velocity structure above the layer in question need not be made. The only simplifying assumption made is that the layer being analyzed is isovelocity. This has the effect of allowing the ray parameter method to be used in layers that are thinner than could be handled by the $T^2(X)$ methods.

The ray parameter method is so named because it compares the ray paths of the same ray parameter which have reflected off the top and bottom of the layer in question. The ray parameter is defined by $p = \cos \theta (z)/c(z)$ and is calculated from travel-time data by evaluating the derivative of a travel-time curve, i.e., $p = dT/dx$. Two different types of ray parameter methods are discussed in the report, the normal method and the thin

layer approximation.[7] Both methods calculate the sound velocity and thickness of a particular layer by matching the derivatives of travel-time curves. The thin layer approximation incorporates a graphical technique which alleviates instabilities associated with thin layers so that thickness ratios of up to 250:1 may be handled.

An example of the ray parameter method is considered in the text of the abovementioned report. The results will be summarized here. The thin layer approximation of the ray parameter method was used on a 50 m subbottom layer having a constant sound speed gradient underlying a 5000 m thick layer (thickness ratio 100:1). The thin layer approximation calculated a layer thickness of 49 m and an interval velocity of 1549 m/sec. This interval velocity compared favorably with the value calculated from an equation derived for a layer having a linear velocity profile (1565 m/sec).

B. The V(t) Method[8,9]

The next technique discussed is a method whereby velocity measurements obtained by reflected arrival methods may be analyzed to construct a velocity profile throughout the sediment layers. As stated earlier, the reflected arrival methods determine a layer velocity under the isovelocity assumption, a condition which is rarely met in the physical world. For this reason, the velocities calculated by the reflected arrival methods are interpreted as interval velocities which are assumed to be the time averaged sound velocity in a particular layer or interval.

The V(t) method is a method which analyzes the depth variation of interval velocities to obtain velocity gradients and layer thicknesses throughout the sediment layer structure. The method is based on a velocity function which is formed by fitting the layer or interval velocities to a polynomial in t, the one-way vertical travel time to the time midpoint of the various layers in the sediment structure. Once the velocity function is known, a gradient function and a depth function which specify the gradient

-143-

and depth as a function of t may easily be determined.

The V(t) method is implemented by fitting the interval velocities to a continuous third order polynomial in t, the one-way travel time to the layer midpoints, i.e.,

$$V(t) = A + Bt + Ct^2 + Dt^3 \quad .$$

The depth as a function of t (depth function) is obtained by integrating V(t) to obtain

$$H(t) = \int V(t)dt = At + \frac{1}{2} Bt^2 + \frac{1}{3} Ct^3 + \frac{1}{4} Dt^4 \quad .$$

The velocity function may be manipulated in the following way to give a gradient function, g(t).

$$g(t) = \frac{dV(t)}{dH(t)} = \frac{dV(t)/dt}{dH(t)/dt} = \frac{dV(t)/dt}{V(t)}$$

$$g(t) = \frac{B + 2Ct + 3Dt^2}{A + Bt + Ct^2 + Dt^3} \quad .$$

The gradient and depth functions may then be combined to yield the gradient as a function of depth.

The main limitations of the V(t) method are associated with errors in the interval velocities and velocity discontinuities. In the text of the report which this chapter summarizes, these effects are examined and shown to be significant in some situations. In particular, an example involving velocity discontinuities predicted layer gradients that were in error by an average of 30% as opposed to average differences of 1% when velocity discontinuities were absent.

As an example relating the reflected arrival methods and the V(t) method,

-144-

consider the case of four subbottom layers underlying a 5000 m water layer
having a bilinear profile. Table V-1 lists the parameters of the sub-
bottom layers and the water layer. The subbottom profile of this example
has gradient discontinuities across the layer interfaces but the sound
velocities are continuous.

Figure V-1 depicts the computer generated T-X curves for the example.
Since the thickness ratios are large, the ray parameter method, using the
thin layer approximation, was employed to determine the interval velocities,
layer thicknesses, and vertical travel times. These values are listed
in Table V-2. For comparison, the actual layer thicknesses and the calcu-
lated layer velocities are included in parentheses.

Before applying the $V(t)$ method, one needs to form a set of values
for the interval velocity versus one-way travel time to the midpoints, in
time, of the four subbottom layers. These values are listed in Table V-3.
The one-way times are referenced to the interface between the water and the
first subbottom layer, i.e., t=0 refers to the top of the first subbottom
layer.

The velocity-time values are next used as input to the polynomial
fitting procedure. In this example, the values of instantaneous velocity
at the top of the first layer, i.e., t=0, are assumed to be known and are
included in the fitting procedure. One output of this procedure is the
velocity as a function of depth. A plot of this function is pictured in
Fig. V-2. The vertical bars in Fig. V-2 denote typical uncertainties of
±100 m/sec in the interval velocities. From the values of velocity, depth,
and gradient as a function of t, it is possible to reconstruct the sub-
bottom profile. The velocity profile determined in this manner for the
present example is listed in Table V-4. Again, the correct values are
listed in parenthesis.

TABLE V-I

WATER PROFILE

Depth (m)	Sound Velocity (m/sec)
0	1500
1280	1487
5000	1550

SUBBOTTOM PROFILE

Subbottom Layer No.	Thickness (m)	Constant Gradient (sec^{-1})	Initial Sound Velocity (m/sec)
1	100	.5	1550
2	100	1.0	1600
3	100	1.5	1700
4	100	2.0	1850
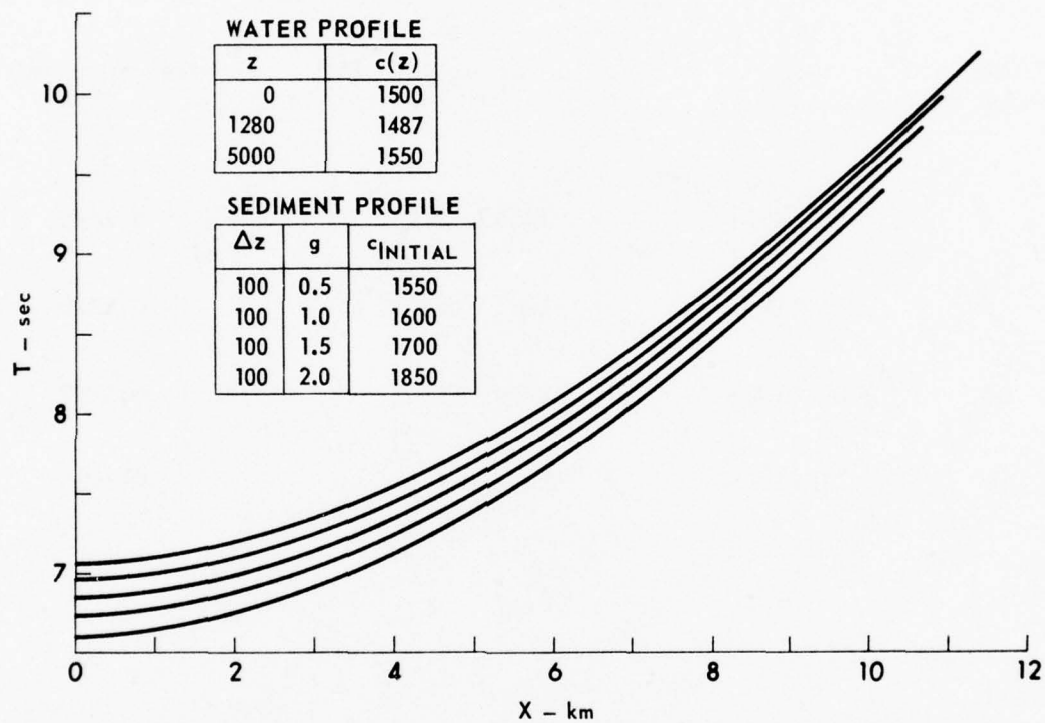
FIGURE Ⅴ-1
TRAVEL TIME CURVES FOR A THICK WATER LAYER
OVERLYING FOUR THIN SEDIMENT LAYERS

TABLE V-2

LAYER PARAMETERS CALCULATED BY THE THIN LAYER
APPROXIMATION OF THE RAY PARAMETER METHOD

Subbottom Layer No.	ΔZ (m)	Interval Velocity (m/sec)	2-Way Vertical Travel Time (sec)
1	99 (100)	1560 (1575)	0.1270
2	101 (100)	1660 (1650)	0.1212
3	100 (100)	1779 (1774)	0.1127
4	101 (100)	1957 (1949)	0.1027

TABLE V-3

INTERVAL VELOCITY AS A FUNCTION OF ONE-WAY TIME

Interval Velocity (m/sec)	One-Way Time to Midpoint of Layer (sec)
1560	0.03175
1660	0.09381
1779	0.15228
1957	0.20613
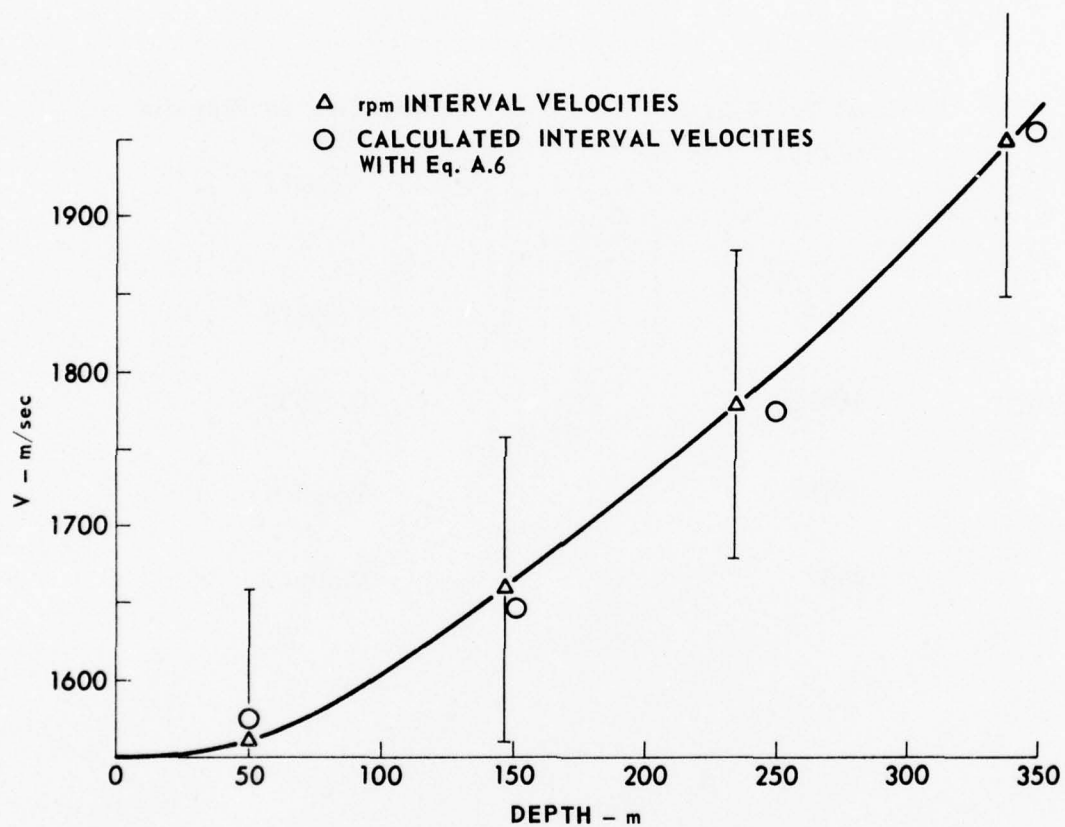
FIGURE V-2
SUBBOTTOM VELOCITY PROFILE OBTAINED BY V(t) METHOD

TABLE V-4

VELOCITY PROFILE RECONSTRUCTED FROM V(t) METHOD

Subbottom Layer No.	Thickness (m)	Gradient (sec^{-1})	Initial Sound Velocity (m/sec)
1	99.7 (100)	0.5 (0.5)	1550 (1550)
2	95.2 (100)	1.1 (1.0)	1602 (1600)
3	77.0 (100)	1.5 (1.5)	1716 (1700)
4	129.0 (100)	1.8 (2.0)	1862 (1850)

C. The Refracted Arrival Methods

The last methods developed are the refracted arrival methods, Dicus'
method[10] and Hanna's method.[11] These methods differ from the reflected
arrival methods in that the effects of shallow refracted arrival methods
in that the effects of shallow refracted arrivals instead of reflected
arrivals are analyzed; also, these methods explicitly assume that a gra-
dient exists in the sediment layer. It is expected that both of these
methods would most successfully be applied to thick, single sediment layers.
The term refracted arrival should not be confused with arrivals resulting
from lateral or interface waves; it means those arrivals that are returned
from the sediment layer by virtue of a turning point arising because of a
velocity gradient.

Dicus' method is a graphical method which deals with the time differences
of the refracted arrivals and the arrivals that attain the same receiver
position via one bottom reflection. The method is derived assuming a
pseudolinear sediment velocity profile and yields the gradient at the top
of the sediment layer and the ratio of velocities at the water sediment
interface by a graphical solution of the following equation

$$\left(\frac{3\Delta\tau}{2}\right)^{2/3} = \frac{-1}{\beta^{2/3}}\left\{\left(\frac{C_o}{C_w}\right)^2 \cos^2\theta_w + 1\right\} \quad .$$

The quantity $\Delta\tau$ is the difference in travel time of the reflected and
refracted arrivals, C_o/C_w is the ratio of the sound velocities at the
water-sediment interface, θ_w is the bottom angle of the reflected arrival,
and β is the gradient at the top of the sediment layer.

In an example, Dicus' method was applied to a single sediment layer
with a constant gradient of 1 $\sec^{-1}$ having a velocity ratio at the water-
sediment interface of 1.0333. Dicus' method calculated a velocity ratio
of 1.0358 and a gradient at the top of the layer of 0.99 $\sec^{-1}$, which
correspond to differences of 0.24% and 1%, respectively.

Finally, a completely different method by Hanna is considered. This technique yields the same output as Dicus' method by an analysis of the nulls in propagation loss curves which arise because of the interference produced by refracted arrivals. This method also models the sediment with a pseudolinear velocity profile.

Hanna's technique proposes to determine sediment velocity and gradient information from the interference structure exhibited by the transmission loss curve for a bottomed receiver over the range of the direct arrival. The range is restricted in this manner because outside the range of the direct arrival, multibounce ray paths further complicate the transmission loss by adding more interference structure.

If there were no energy being returned from the bottom, the interference structure of the transmission loss should be accounted for quite well by the Lloyd's Mirror effect. (The Lloyd's Mirror effect is most noticeable when a shallow source is used and results from the interference of ray paths that are upgoing and downgoing at the source.) When energy is allowed to refract or reflect back into the water column, the transmission loss curve will show added interference structure. Hanna's method proposes to identify interference nulls in transmission loss curves that arise because of refracted energy and to determine velocity and gradient information from the positions of these nulls.

References - Chapter V

1. S. R. Rutherford, "Analytical Techniques for Determining Subbottom Velocity Profiles in Unconsolidated Sediments", Applied Research Laboratories Technical Report No. 76-58 (ARL-TR-76-58), The University of Texas at Austin, 21 December 1976.

2. D. J. Shirley and A. L. Anderson, "In Situ Measurement of Marine Sediment Acoustical Properties During Coring In Deep Water", IEEE Trans. Geo. Elect. GE-13(4), 163-168 (1975).

3. C. H. Dix, "Seismic Velocities from Surface Measurements", Geophysics 20, 68-86 (1955).

4. G. L. Maynard, G. H. Sutton, D. M. Hussong, and L. W. Kroenke, "The Seismic Wide Angle Reflection Method in the Study of Ocean Sediment Velocity Structure", from Physics of Sound in Marine Sediments, L. Hampton (ed.), (Plenum Press, New York, 1974).

5. H. Durbaum, "Zur Bestimmung von Wellengeschwindigkeiten aus Reflexionsseismischen Messungen", Geophys. Prospecting 2, 151-167 (1954).

6. C. S. Clay and P. A. Rona, "Studies of Seismic Reflections from Thin Layers on the Ocean Bottom in the Western North Atlantic", J. Geophys. Res. 70, 855-869 (1965).

7. G. M. Bryan, "Sonobuoy Measurements in Thin Layers", from Physics of Sound in Marine Sediments, L. Hampton (ed.), (Plenum Press, New York, 1974).

8. R. J. Houtz, J. Ewing, and X. LePichon, "Velocity of Deep-Sea Sediments from Sonobuoy Data", J. Geophys. Res. 73, 2615-2641 (1968).

9. R. E. Houtz, "Preliminary Study of Global Sediment Sound Velocities from Sonobuoy Data", from Physics of Sound in Marine Sediments, L. Hampton (ed.), (Plenum Press, New York, 1974).

10. R. L. Dicus, "Preliminary Investigations of the Ocean Bottom Impulse Response at Low Frequencies, "NAVOCEANO Technical Note, TN6130-4-76, 1976.

11. J. S. Hanna, "Short-Range Transmission Loss and the Evidence for Bottom-Refracted Energy", J. Acoust. Soc. Am. 53, 1686-1690 (1973).

VI.   SUPPORT WORK

This chapter contains a brief summary of modeling efforts conducted at ARL:UT, under this contract, in support of the bottom interaction acoustic studies. This summary consists of three sections devoted to (1) normal mode model, (2) an update of the bottom loss model, and (3) an update of the ray trace model. All three models discussed in this chapter were developed at ARL:UT in the bottom interaction program to solve specific bottom interaction problems.

A.   A Normal Mode Model

A parallel shooting technique together with numerical integration is used to solve the depth separated wave equation. The model is restricted to low frequencies and a horizontally stratified deep ocean but allows arbitrary sound speed profiles with a detailed bottom description. Initial estimates for the first eigenvalue are obtained using harmonic oscillator eigenvalues. Estimates for the nth eigenvalues are obtained from the ray theory cycle distance using the (n-1)st eigenvalue, and the eigenvalue spacing of the (n-1)st and (n-2)nd eigenvalues. The secant method is then used to improve the eigenvalue estimates. Integration of the depth separated equation is done toward the axis from each of the boundaries and is matched at the sound channel axis, thus eliminating much of the numerical instability that is associated with some modes. In addition, group velocities are computed by evaluating an integral rather than by direct numerical differentiation. This method of computing group velocities gains in both speed and accuracy relative to differential methods.

Auxiliary programs compute and plot propagation loss (fully coherent and incoherent mode sums) as well as the modes and sound speed profiles, ray and mode cycle distances, phase and group velocities, and other useful quantities. Software is under development to permit the use of multisensor 2-dimensional receiving arrays.

Considerable attention has been paid to producing a noninteractive
mode model which is relatively fast and has sufficient accuracy to permit
computation of propagation loss to long ranges. Execution time of present
versions of this model are approximately 3 to 5 sec per mode on a CDC 3200
computer. This time includes the time to compute the mode at each of the
several thousand depth points in the mesh. Each entire mode as well as
eigenvalue, group velocity, mode attenuation, etc., is written on a magnetic
tape for later use.

A version of this model is complete and is in daily use. Further
refinements are being made, particularly to ensure stability of solution
and complete noninteractiveness. A report describing in detail the
characteristics, advantages, and limitations of this model is in prepara-
tion and will be issued during the next contract year (FY 77).[1]

B. Updates of the Bottom Loss Model (BOTLOSS)

A previous report, Hawker et al.,[2] contains a brief description of a
plane wave bottom reflection loss model based on numerical solution of the
wave equation (program BOTLOSS). Subsequently, a detailed technical report
on the model, Hawker and Foreman,[2] was issued which described its mathemati-
cal underpinnings, computational methods, and research applications. Since
the report was released, BOTLOSS has undergone further revisions. Most
of these changes were implemented to reduce program run time and to provide
more flexible input/output options. These routine modifications will not
be described here because they pertain only to the details of running the
program. However, there have also been more substantive changes which
affect the representation of the bottom sediments in the model. These
alterations are the subject of this section.

1. Background

Consider the model ocean bottom of Fig. VI-1; the bottom consists
of horizontally stratified inhomogeneous fluid sediment layers overlaying
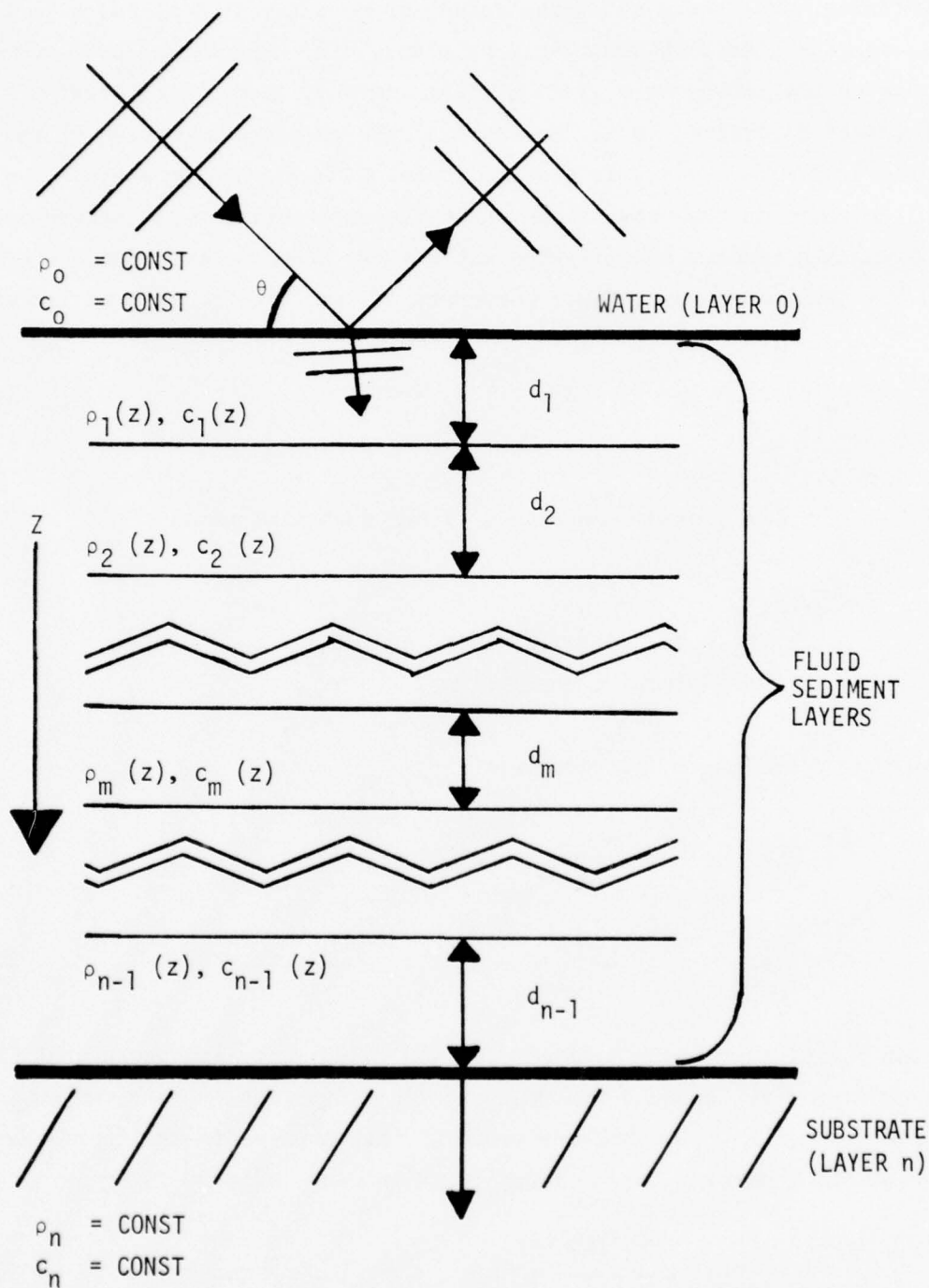
FIGURE VI-1

LAYER NUMBERING CONVENTION

AS-76-142

159

an infinite homogeneous substrate which may be a fluid, a solid, a perfect
reflector, or a perfect absorber. If plane, time harmonic acoustic waves
inpinge on the bottom at a given grazing angle θ, then the reflection
coefficient is defined to be the ratio of the pressure amplitude of the
upgoing (reflected) waves to the amplitude of the downgoing waves. The
total pressure in the water is given by the superposition of the upgoing
and downgoing waves. Assuming the water to be homogeneous and nonattenuating,
then the time independent depth component of pressure, p_o, may be expressed
as

$$p_o(z) = A_o(e^{i\kappa_o z} + R\, e^{-i\kappa_o z}), \text{ where} \qquad (1)$$

z is depth,

A_o is the pressure amplitude of the downgoing wave,

$\kappa_o = \omega/c_o \sin\theta$,

ω is $2\pi f$,

c_o is the sound speed in water, and

R is the reflection coefficient.

Evaluating p_o and dp_o/dz at z=0 gives

$$R = \frac{1-\delta}{1+\delta} \quad , \qquad (2)$$

$$\delta = \frac{p_o{}'(0)}{p_o(0)} \; \frac{1}{i\kappa_o} \quad . \qquad (3)$$

One can therefore compute R given p(0) and p'(0). To find these quantities
BOTLOSS must first compute the pressure field numerically over the entire
interval from the top of the substrate to the water-sediment interface.
The equation governing the pressure field in each sediment layer is

$$p_j{}''(z) - \frac{p_j{}'(z)}{p_j(z)} \; p_j{}'(z) + \kappa_j{}^2(z)\, p_j(z) = 0 \quad , \qquad (4)$$

$$\kappa_j^2(z) = k_j^2(z) - k_o^2 \cos^2 \theta \quad , \tag{5}$$

$$k_j(z) = \frac{\omega}{c_j(z)} + i\alpha_j(z) \quad , \tag{6}$$

where $\alpha_j(z)$ is attenuation, $\rho_j(z)$ is density, and $c_j(z)$ is sound speed. At each fluid sediment layer interface we have the boundary conditions

$$p_j = p_{j+1} \quad , \tag{7}$$

$$\frac{p_j'}{\rho_j} = \frac{p'_{j+1}}{\rho_{j+1}} \quad . \tag{8}$$

If the substrate is a fluid or solid, one can calculate the pressure at the bottom of the adjacent fluid layer up to a constant using given values of substrate density, sound speed, shear wave speed, and shear and compressional attenuations. The calculation is greatly simplified if the substrate is a perfect absorber or reflector. The undetermined constant turns out to be an amplitude coefficient whose exact value is related only to the pressure field normalization. BOTLOSS is not concerned with the normalization; thus this coefficient is set arbitrarily to unity. BOTLOSS proceeds to compute the pressure field by solving the differential Eq. (4) with layer interface conditions (7) and (8) and initial values given at the sediment-substrate interface by using a standard numerical routine. When the solution is complete, the values of $p_o'(0)$ and $p_o(0)$ are known and the program can immediately calculate R by Eqs. (2) and (3).

2. Liberalization of Sediment Profile Descriptions

Note that the pressure field Eq. (4) calls for the evaluation of the profile functions $p_j(z)$, $p_j'(z)$, $c_j(z)$, and $\alpha_j(z)$. BOTLOSS permits the user to select analytic profile functions appropriate to his needs for

-161-

each layer from among a set of available functions. The repertoire of
available functions has been expanded slightly and now includes

$$
\rho_j(z) = \begin{cases}
\rho_j(0) \text{ (constant density)} \\[1em]
\rho_j(0) \, gz \text{ (constant density gradient)} \\[1em]
\rho_j(0) \, e^{\beta z} \text{ (exponential density profile)}
\end{cases}
$$

$$
c_j(z) = \begin{cases}
c_j(0) \text{ (constant sound speed)} \\[1em]
c_j(0) + gz \text{ (constant sound speed gradient)} \\[1em]
c_j(0)/\sqrt{1+\beta z} \text{ (pseudolinear sound speed profile)} \\[1em]
c_j(0)/\sqrt{1+A^2(e^{-\beta z}-1)} \text{ (modified exponential sound speed} \\
\qquad\qquad\qquad\qquad\qquad\qquad\qquad \text{profile)}
\end{cases}
$$

$$
\alpha_j(z) = \begin{cases}
\alpha_j(0) \text{ (constant attenuation)} \\[1em]
\alpha_j(0) + gz \text{ (constant attenuation gradient)} \\[1em]
\alpha_j(0)/\sqrt{1+\beta z} \text{ (pseudolinear attenuation profile)} \\[1em]
\alpha_j(0)/\sqrt{1+A^2(e^{-\beta z}-1)} \text{ (modified exponential attenuation} \\
\qquad\qquad\qquad\qquad\qquad\qquad\qquad \text{profile)} \\[1em]
\alpha_j(0) \, c_j(0)/c_j(z) \text{ (sound speed linked attenuation profile,}
\end{cases}
$$

where A, β, and g are constant parameters. The modified exponential profile
functions have an extra parameter which causes the profile gradient to
decrease at great depths, in accordance with some measured data.

These particular choices of profile functions were made largely because considerable research has been done in the past using them. Typically, these functions were used because they lead to exact solutions or simple approximations in the analysis of bottom loss effects. It is expected that these functions will change in the future, particularly in response to new information about measured profiles.

It should be noted that establishing the attenuation function $\alpha(z)$ in its own right, instead of linking the attenuation to the sound speed profile, represents a considerable departure from previous practice. This development is the subject of the next section.

3. Uncoupling the Attenuation from the Sound Speed

In most published reflection coefficient models and in earlier versions of BOTLOSS, the complex wave number, k, has been written as

$$k(z) = \left\{ \frac{\omega}{c(0)} + i\alpha(0) \right\} \frac{c(0)}{c(z)} \quad . \tag{9}$$

The attenuation as a function of depth is thus implicitly defined to be inversely proportional to the sound speed

$$\alpha(z) = \alpha(0)\frac{c(0)}{c(z)} \quad . \tag{10}$$

The sound speed and attenuation have traditionally been coupled in this fashion because, for certain assumed forms of (real) $c(z)$, one can find analytical solutions to the wave equation and, by linking attenuation to sound speed as in Eq. (10), one may introduce attenuation effects into the solution without making the analysis more difficult.

Program BOTLOSS, however, solves the wave equation numerically; thus, there is no need to write $k(z)$ in a form which renders the wave equation analytically tractable. The current version of BOTLOSS, therefore, has

$$k(z) = \omega/c(z) + i\alpha(z) \quad , \tag{11}$$

where $c(z)$ and $\alpha(z)$ are independent of each other. The numerical integration algorithm is largely indifferent to the exact forms of $c(z)$ and $\alpha(z)$ from the standpoint of execution time and accuracy; thus the user is free to choose them to be as physically realistic as possible. At present, BOTLOSS is equipped to handle constant, linear, pseudolinear, modified exponential attenuation profiles and sound speed linked attenuation profiles. This repertoire will almost certainly change as more information becomes available concerning actual variations of attenuation with depth.

Some preliminary studies have shown that, for certain types of very thick sediments, the implicit attenuation function of Eq. (9) is inadequate; this results in bottom loss predictions which differ markedly from predictions obtained using Eq. (10) and $\alpha(z)$ chosen to fit measured attenuation profiles (see Chapter II. B).

4. Reduction in Program Run Time

An aspect of the numerical integration approach used in BOTLOSS is its relatively slow speed, which limits use of the program to sediments no thicker than about 100 wavelengths for reasonable execution times. Most of the run time is spent in the numerical solution of the differential equation. Some of the factors which influence integration time are discussed in the technical report on the model. However, the difficulty is essentially that both the pressure and its derivative are rapidly varying functions of depth and therefore the numerical integrator is forced to take very small steps in order to control errors. It was hoped that the rapid variation of the wave function could be removed by writing the solution as a sum or product or other suitable combination of an analytical approximation, and, a slowly varying corrector which could be found numerically. For example, one might write

-164-

$$p(z) = p_{JWKB}(z) \, T(z) \quad , \quad\quad (12)$$

where $p(z)$ is the desired exact solution, $p_{JWRB}(z)$ is the JWKB approximation to the solution, and $T(z)$ is a numerically determined corrector. Introducing this expression into the wave equation produces a new, nonlinear differential equation with solution T, which is (it is hoped) slowly varying. Several such schemes were examined but, so far, these attempts have been only partially successful. Typically, whenever the behavior of $p(z)$ was approximately exponential, the numerical integration was greatly accelerated because the integrator could take much larger steps; however, the problems of integrating in oscillatory portions of the field remained. Roughly speaking, the reason for the failures in the oscillatory regions was that the approximate solution contained errors in both the magnitude and phase of oscillation; although these errors were usually small, the corrector could not compensate for both of them simultaneously. These schemes based on the JWKB approximation were abandoned after a short investigation but they may merit a closer look, especially since any successful techniques which are developed will likely be applicable to a much broader range of problems.

A modification of this approach which holds considerable promise is to use in place of the JWKB term an asymoptotic approximation due to Langer.[4] The utility of this approach in acoustic normal mode calculations has already been investigated at this laboratory by Mitchell.[5] It is anticipated that, when a clear need arises for significantly decreasing the execution time of the program, this method will be implemented.

C. Developments in Acoustic Ray Theory Programs

The final report for 1975 on the bottom interaction study,[2] sponsored by NAVELEX, Code 320, includes a description of a computer program developed at ARL:UT; this program numerically locates eigenrays (rays connecting a source and receiver) and prints their travel times, launch angles, bottom reflection angles, and other ray path information. This program, RANGER BP,

has a limited capacity to find eigenrays which travel through ocean bottom sediments. By providing a detailed path history of each eigenray arriving at a given receiver, RANGER BP has aided in understanding and predicting the effects of multipath arrivals. Its capacity to trace rays through the bottom made it useful in the investigation of acoustic techniques for probing the bottom to determine such sediment properties as sound speed and layer thickness.

Since 1975, ray theory modeling capability at ARL:UT has been upgraded and expanded to include several programs, collectively referred to as RANGER. The most important development has been the added ability to compute the acoustic pressure contribution of each eigenray to the total pressure at a receiver.

All programs in the RANGER package assume a range invariant, horizontally stratified ocean acoustic environment. The sound speed profile is approximated by piecewise linear segments, for which analytical expressions are available for computing travel time, path length, horizontal distance (range), and range derivatives as functions of the ray "launch angle." These geometric ray path quantities permit calculation of the ray pressure at the receiver within the limits of the ray theory approximations.

The computational methods used in RANGER are discussed in detail in a separate report (Foreman[6]). The descriptions of the programs currently in the RANGER package are summarized below with emphasis on their applications to the bottom interaction study.

RANGER BL - Computes and plots propagation loss as a function of range. Intensities are calculated by locating eigenrays and summing their individual contributions until the total intensity begins to converge, whereupon the search for additional eigenrays is discontinued. Both incoherent and fully coherent intensity summations are performed. Tables of bottom loss and phase as functions of grazing angle are used to account for bottom interactions. (No rays are traced through the sediment in this version.)

The ability to fully account for phase interference effects has been crucial in accounting for some effects observed with receivers in close proximity to each other or to the ocean surface or bottom.

RANGER MP - Prints an account of the ray path history of each eigenray which arrives at the receiver within a specified time interval of the earliest arrival. It predicts multipath arrival times, pressure levels, arrival angles, turning depths or surface/bottom reflection angles, phase shifts due to ray interactions with the surface or bottom or caustics, and a general description of the ray (upgoing/downgoing at the source/receiver, number of shallow and deep turning points, etc.). This program is particularly useful for identifying the ray paths which determine the multipath arrival structure in experimental data.

RANGER BP - Prints ray histories similar to RANGER MP. It has a limited capacity to trace rays through sediment layers. It can be used to predict multipath arrival times for rays which undergo only one bottom interaction. RANGER BP does not perform intensity calculations.

RAYFAM - Plots ray paths through the ocean for given launch angles.

RTHETA - Plots ray range as a function of launch angle for a given number of deep turning points (bottom reflections or deep refractions).

References - Chapter VI

1. R. G. Gonzalez and K. E. Hawker, "On the Calculation of Acoustic Normal Modes Using Numerical Integration", Applied Research Laboratories Technical Report No. 77-2 (ARL-TR-77-2), Applied Research Laboratories, The University of Texas at Austin, in preparation.

2. K. E. Hawker, A. L. Anderson, K. C. Focke, and T. L. Foreman, "Initial Phase of a Study of the Bottom Interaction of Low Frequency Underwater Sound", Applied Research Laboratories Technical Report No. 76-14 (ARL-TR-76-14), Applied Research Laboratories, The University of Texas at Austin, 6 April 1976.

3. K. E. Hawker and T. L. Foremen, "A Plane Wave Reflection Coefficient Model Based on Numerical Integration", Applied Research Laboratories Technical Report No. 76-23 (ARL-TR-76-23), Applied Research Laboratories, The University of Texas at Austin, 21 June 1976.

4. R. E. Langer, "On the Asymptotic Solutions of Ordinary Differential Equations", Trans. Am. Math. Soc. 33, 23 (1931).

5. S. K. Mitchell, "An Extension of Langer's Asymptotic Solutions with Applications to Ocean Acoustics, Applied Research Laboratories Technical Report No. 77-13 (ARL-TR-77-13), Applied Research Laboratories, The University of Texas at Austin, 1 March 1977.

6. T. L. Foreman, "Acoustic Ray Models Based on Eigenrays", Applied Research Laboratories Technical Report No. 77-1 (ARL-TR-77-1), Applied Research Laboratories, The University of Texas at Austin, 4 April 1977.

ACKNOWLEDGMENTS

During the reporting period covered this research program was directed at ARL:UT by Dr. Aubrey Anderson, now of the Naval Ocean Research and Development Activity. The directions and methodology of this research program reflect to a great extent his interests and knowledge, and although this document was itself generated without his assistance, a great deal of the success of this program is his.

The authors also wish to acknowledge the guidance and direction of Dr. Loyd Hampton and Mr. Glen Ellis, both of ARL:UT.

At various times the authors have benefited from conversations with Dr. Steve Mitchell, ARL:UT, Mr. Jack Shooter, ARL:UT, Mr. Steve Watkins, ARL:UT, and Dr. Art Williams, Brown University, who has served as a consultant to this program.

DISTRIBUTION LIST FOR
ARL-TR-77-27
UNDER CONTRACT N00039-76-C-0081

<u>Copy No.</u>

Commanding Officer
Naval Ocean Research and Development Activity
NSTL Station, MS 39520

1	Attn: LCDR G. J. Ranes (Code 500)
2	R. D. Gaul (Code 600)
3	CDR J. Paquin (Code 600)
4	CDR T. McCloskey (Code 200)
5	S. W. Marshall (Code 340)
6	H. Eppert (Code 360)
7	Hugo Bezdek (Code 460)
8	Thomas Pyle (Code 430)
9	A. L. Anderson (Code 320)
10	E. M. Stanley (Code 500)

11   Commanding Officer
Office of Naval Research
Arlington, VA 22217
Attn: J. B. Hersey (Code 102-OS)

12   Office of Naval Research
Branch Office Chicago
536 S. Clark
Chicago, IL 60605

Commanding Officer
Naval Electronic Systems Command
Department of the Navy
Washington, DC 20360

13-14	Attn: J. Sinsky, J. Cybulski (Code 320)
15	Code PME 124-30
16	Code PME-124-62

Director
Naval Research Laboratory
Department of the Navy
Washington, DC 20375

17	Attn: R. H. Ferris
18-20	B. B. Adams (Code 8160)
21	Code 2627

Copy No.

	Commander
	Naval Ocean Systems Center
	Department of the Navy
	San Diego, CA 92152
22-24	Attn: E. Tunstall (Code 531)
25	R. R. Gardner (Code 53)
26	M. A. Pederson (Code 307)
27	H. P. Bucker (Code 5311)

	Commander
	Naval Sea Systems Command
	Department of the Navy
	Washington, DC 20362
28	Attn: C. D. Smith (Code 06H1)
29	A. P. Franceschetti

	Chief of Naval Operations
	Department of the Navy
	Washington, DC 20350
30	Attn: R. S. Winokur (OP95E1)

	Chief of Naval Material
	Department of the Navy
	Washington, DC 20360
31	Attn: G. R. Spalding (Code 08T24)

	Commander
	Naval Intelligence Support Center
	4301 Suitland Road
	Washington, DC 20390
32	Attn: Code 222

	Oceanographer of the Navy
	Hoffman Building
	200 Stovall Street
	Alexandria, VA 22332
33	Attn: CDR E. Young

34	Commander
	Naval Surface Weapons Center
	White Oak Laboratory
	Silver Spring, MD 20910

35	Commander
	David M. Taylor Naval Ship Research and Development Center
	Bethesda, MD 20034

Copy No.

	Naval Oceanographic Office
	Department of the Navy
	Washington, DC 20373
36	Attn: W. H. Geddes
	Commander
	Naval Air Development Center
	Department of the Navy
	Warminster, PA 18974
37	Attn: P. Van Schuyler (Code 2052)
38	C. L. Bartberger
39	P. Haas

Commander
New London Laboratory
Naval Underwater Systems Center
Department of the Navy
New London, CT 06320
40   Attn: F. R. DiNapoli
41   R. Martin

42   Assistant Director
Ocean Control DDR&E
Room 3D, 1048 Pentagon
Washington, DC 20301

OASN (R,E & S)
Room 4D, 745 Pentagon
Washington, DC 20301
43   Attn: G. A. Cann

Advance Research Project Agency
Acoustic Research Center
Moffett Field, CA 94035
44   Attn: T. Kooij

Superintendent
Naval Postgraduate School
Monterey, CA 93940
45   Attn: Library

Commanding Officer
Naval Air Systems Command
Department of the Navy
Washington, DC 20360
46   Attn: CDR J. Messegee (Code PMA-264)

Dist. List for ARL-TR-77-27 under Cont. N00039-76-C-0081, Cont'd

Copy No.

47-48	Commanding Officer and Director Defense Documentation Center Defense Services Administration Cameron Station, Building 5 5010 Duke Street Alexandria, VA 22314
	Arthur D. Little, Inc. Acron Park Cambridge, MA 02140
49	Attn: G. Raisbeck
	Woods Hole Oceanographic Institution 86-96 Water Street Woods Hole, MA 02543
50	Attn: E. E. Hays
51	G. Frisk
	Science Applications, Inc. 8400 Westpark Drive McLean, VA 22101
52	Attn: J. Hanna
53	C. Spofford
	Pennsylvania State University Applied Research Laboratory P. O. Box 30 State College, PA 16801
54	Attn: S. McDaniel
	Underwater Systems, Inc. World Building 8121 Georgia Avenue Silver Spring, MD 20910
55	Attn: M. S. Weinstein
	University of California, San Diego Marine Physical Laboratory of the Scripps Institution of Oceanography San Diego, CA 92132
56	Attn: V. Anderson
	Tracor, Inc. 1601 Research Boulevard Rockville, MD 20850
57	Attn: J. Gottwald
58	A. Wittenborn

176

Copy No.

              Bell Telephone Laboratories, Inc.
              Whippany Road
              Whippany, NJ 07981
59   Attn: S. A. Kramer

              Planning Systems Incorporated
              7900 Westpark Drive, Suite 507
              McLean, VA 22101
60   Attn: L. Solomon

              TRW, Inc.
              TRW Defense & Space Systems Group
              Washington Operations
              7600 Colshire Drive
              McLean, VA 22101
61   Attn: R. T. Brown

              Xonics, Inc.
              6837 Hayvenhurst Avenue
              Van Nuys, CA 91406
62   Attn: J. Wilson

              SUTRON Corporation
              Suite 700
              1923 North Lynn Street
              Arlington, VA 22209
63   Attn: C. Dabney

              Daubin Systems Corporation
              104 Crandon Boulevard
              Key Biscayne, FL 33149
64   Attn: S. Daubin

65   A. O. Williams, Jr.
              Dept. of Physics
              Brown University
              Providence, RI 02912

              Defense Scientific Establishment
              HMNZ Dockyard
              Devonport, Auckland
              New Zealand
66   Attn: K. M. Guthrie
67   R. N. Denham

Dist. List for ARL-TR-77-27 under Cont. N00039-76-C-0081, Cont'd

Copy No.

	University of Auckland Physics Department Auckland, New Zealand
68	Attn: A. C. Kibblewhite
69	G. Bold

	The Catholic University of America 6220 Michigan Avenue NE Washington, DC 20017
70	Attn: H. M. Uberall

	TRACOR, Inc. 1601 Research Boulevard Rockville, MD 20850
71	Attn: R. J. Urick

	Geophysical and Polar Research Center Department of Geology and Geophysics The University of Wisconsin Madison, WI 53700
72	Attn: C. S. Clay

73   D. C. Stickler
      Courant Institute
      251 Mercer Street
      New York, NY 10012

74   Glen E. Ellis, ARL:UT

75   Terry L. Foreman, ARL:UT

76   Ruth Gonzalez, ARL:UT

77   Loyd D. Hampton, ARL:UT

78   Kenneth E. Hawker, ARL:UT

79   John Lemmon, ARL:UT

80   Stephen K. Mitchell, ARL:UT

81   Susan Payne, ARL:UT

82   Steve Rutherford, ARL:UT

83   Jack A. Shooter, ARL:UT

84   Chris Tindle, ARL:UT

Dist. List for ARL-TR-77-27 under Cont. N00039-76-C-0081, Cont'd

Copy No.

85	Donna Venable, ARL:UT
86	Paul Vidmar, ARL:UT
87	Reuben H. Wallace, ARL:UT
88	Steven L. Watkins, ARL:UT
89	Library, ARL:UT
90-110	Reserve, ARL:UT